LEVEL III

AD

AD-E400 320

CONTRACTOR REPORT ARLCD-CR-79009

ACCIDENTAL EXPLOSIONS AND EFFECTS OF BLAST LEAKAGE INTO STRUCTURES

KENNETH KAPLAN
SCIENTIFIC SERVICE, INC.
REDWOOD CITY, CALIFORNIA

PAUL D. PRICE
PROJECT LEADER
ARRADCOM

JUNE 1979

US ARMY ARMAMENT RESEARCH AND DEVELOPMENT COMMAND
LARGE CALIBER
WEAPON SYSTEMS LABORATORY
DOVER, NEW JERSEY

UNCLASSIFIED

SECURITY CLASSIFICATION OF THIS PAGE (When Data Entered)

REPORT DOCUMENTATION PAGE	READ INSTRUCTIONS BEFORE COMPLETING FORM
1. REPORT NUMBER: Contractor Report ARLCD-CR-79009	2. GOVT ACCESSION NO. / 3. RECIPIENT'S CATALOG NUMBER
4. TITLE (and Subtitle): ACCIDENTAL EXPLOSIONS AND EFFECTS OF BLAST LEAKAGE INTO STRUCTURES	5. TYPE OF REPORT & PERIOD COVERED: Final
	6. PERFORMING ORG. REPORT NUMBER
7. AUTHOR(s): Kenneth Kaplan, Scientific Service, Inc. P.D. Price, Project Leader, ARRADCOM	8. CONTRACT OR GRANT NUMBER(s): DAAK10-77-C-0011
9. PERFORMING ORGANIZATION NAME AND ADDRESS: Scientific Service, Inc. 1536 Maple Street Redwood City, CA 94063	10. PROGRAM ELEMENT, PROJECT, TASK AREA & WORK UNIT NUMBERS: MMT: 5774291
11. CONTROLLING OFFICE NAME AND ADDRESS: ARRADCOM, TSD STINFO (DRDAR-TSS) Dover, NJ 07801	12. REPORT DATE: June 1979 13. NUMBER OF PAGES: 153
14. MONITORING AGENCY NAME & ADDRESS (if different from Controlling Office): ARRADCOM, LCWSL Manufacturing Technology Division (DRDAR-LCM-SP) Dover, NJ 07801	15. SECURITY CLASS. (of this report): Unclassified 15a. DECLASSIFICATION/DOWNGRADING SCHEDULE
16. DISTRIBUTION STATEMENT (of this Report): Approved for public release; distribution unlimited.	
17. DISTRIBUTION STATEMENT (of the abstract entered in Block 20, if different from Report)	
18. SUPPLEMENTARY NOTES: This project was accomplished as part of the U.S. Army's Manufacturing Methods and Technology Program. The primary objective of this program is to develop, on a timely basis, manufacturing processes, techniques, and equipment for use in production of Army materiel.	
19. KEY WORDS (Continue on reverse side if necessary and identify by block number): Blast overpressures; Accidental explosions; Personnel protection; Blast leakage pressure; MMT - Ammunition	

20. ABSTRACT (Continue on reverse side if necessary and identify by block number)

The effects of openings in structures struck by blast waves from accidental explosions are of two types: those that alter loadings used for design of the basic structures; and those that subject interior elements to loadings. Basic design loadings on structures with openings such as windows and doorways can differ substantially from what they would be on closed structures. Interior spaces are affected both by the portion of the blast wave that enters through openings, spreads out, and reflects from all interior surfaces, and

DD FORM 1 JAN 73 1473 EDITION OF 1 NOV 65 IS OBSOLETE

UNCLASSIFIED

SECURITY CLASSIFICATION OF THIS PAGE (When Data Entered)

20. ABSTRACT (continued)

by high-velocity jets that can form later due to blast-caused pressure differences between the exterior and interior. Methods of determining the effect of these loads are presented.

ACKNOWLEDGEMENTS

Some of the concepts in this report, especially in the area of net loading, owe their present form to discussions with A.B. Willoughby, a most knowedgeable and incisive commentator in this general area. Similarly, in the area of jet flow, discussions with John A. Rempel, author of Ref. 40, were most productive. The editorial suggestions and analysis of Evelyn P. Kaplan must also be gratefully acknowledged. Paul Price of U.S. Army Armament Research and Development Command, the designated Control Project Officer, and Norval Dobbs, of Amman and Whitney in New York, provided the guidance needed to properly delimit the scope of the effort, most necessary when dealing with such broad subject matter.

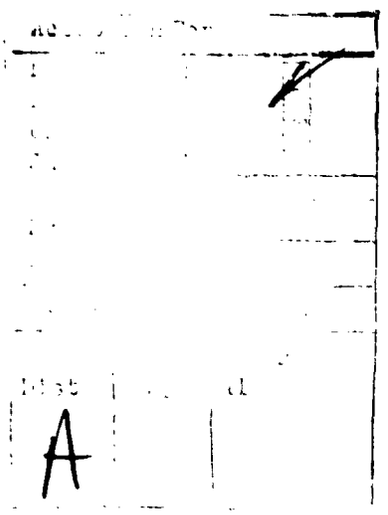

SUMMARY

The effects of openings in structures struck by blast waves from accidental explosions are of two types: those that alter loadings used for design of the basic structures; and those that subject interior elements to loadings.

Basic design loadings on structures with openings such as windows and doorways can differ substantially from what they would be on closed structures. Even without considering secondary reflections of the shock wave that enters the structures, for example, net front wall and side wall impulses can be reduced by one half or more, and rear wall loadings can actually reverse in direction. Subsequent shock wave reflections can create even greater changes by imposing outward-directed forces on the walls after the blast wave itself has passed the structure. Basic design loadings can also change even when exterior walls are not affected by interior phenomena (which can occur, for example, when a doorway opens on a hallway rather than on a room whose exterior wall is exposed to the blast wave). In those cases, clearing times are shortened from what they would be on closed structures.

Interior spaces are affected both by the portion of the blast wave that enters through openings, spreads out, and reflects from all interior surfaces, and by high-velocity jets that can form later due to blast-caused pressure differences between the exterior and interior. On interior elements, such as walls, forces due to shock wave reflections will tend to be larger than those due to jet flow, though the two will not occur at the same time, and jet forces can be applied over a more limited area than can shock wave forces. On elements or objects that are quickly immersed in

the flow behind a shock wave, the dominant force is that due to drag or to flow past the object. Until shock wave pressures are quite high, drag forces created by jet flow are much larger than those created by the flow immediately behind the shock front. Small objects that are not fixed can attain relatively high velocities due to this flow.

A final effect of flow through an opening is that of "filling", in which the overall interior and exterior pressures essentially equalize. The times required for this phenomenon to occur are such that it should not be of importance with accidental explosions of interest here, except when interior volumes are quite small compared with the openings through which filling would occur.

TABLE OF CONTENTS

Table of Contents (contd)

LIST OF TABLES

LIST OF FIGURES

List of Figures (contd)

List of Figures (contd)

INTRODUCTION

The possibility of a very rapid, even explosive, accidental energy release at any facility in which explosives or propellants are manufactured, loaded into shells, bombs, missiles and the like, or even just stored can never be discounted. Such incidents have taken place ever since materials in which detonation or deflagration waves can be sustained were first employed in commerce, industry, and by the military.

Both the materials involved in these accidents and their geometry have varied widely, but a common characteristic of them all is the formation of a pressure pulse in the air around the source. This pulse is created by the piston-like action of the rapidly expanding hot gases to which the original material is converted.* The pulse propagates away from the source at speeds greater than the speed of sound in the ambient air.

At some distance from the source, virtually all such pulses—whatever the source material and whatever its geometry—will be characterized by an initial extremely rapid rise in pressure (a shock front) followed by a much slower pressure decay to and somewhat below ambient air pressure before the pulse finally passes the point of observation.** In these shock or blast waves, the maximum initial peak overpressure (pressure above ambient) is about 8,000 psi (55 MPa) at the surface of an explosive

---

* High velocity missiles can also be created, but this report deals solely with the pressure pulse.

** The phrase "...much slower pressure decay..." can be misleading. For example, the entire positive pressure pulse duration, at a point 100 ft from a TNT source weighing 1,000 lbs is only about 20 ms.

source like TNT, and decreases to zero with distance at a non-linear rate dependent on charge size and to some extent on the nature of the source and its geometry.

This report deals primarily with structures located where initial peak blast overpressures from accidental explosions range from about 20 psi to 1 psi (≈ 140 - 7 kPa). Structures in such locations — especially at higher overpressures — must be specifically designed to withstand the forces imposed on them by blast waves, and a large portion of the comprehensive manual "Structures to Resist the Effects of Accidental Explosions" (Ref. 1) is devoted to methods for preparing these designs.

In the manual, however, design loadings on exterior walls and roofs are those for a structure without any opening (i.e., windows, doors, and vents). Openings are only considered for their role in allowing overall interior pressures to increase by permitting air flow into a structure and then only because these interior pressures can affect personnel.

And yet, the dynamic response to blast of many structural elements can be changed substantially if pressures on them are altered as a result of the passage of a blast wave through an opening. Blast wave passage through an interior space can also subject objects in that space to damaging forces. Finally, blast-created high pressure outside an opening (such as a vent) can create very high flow velocities through the vent and thus subject ducts behind the vent to high flow forces.

The existence of these effects (collectively termed blast leakage effects) has long been recognized, but they have not yet been incorporated into general methods for designing structures. This is largely because much relevant information was derived from tests with nuclear or other exotic, extended, or irregular sources and requires adaptation to be incorporated into a general design method. Furthermore, much of the information appears in publications that are long out of print.

Because of the potential importance of leakage effects in the design

of structures located near explosive or propellant sources, the U.S. Army Armament Research and Development Command retained the services of Scientific Service, Inc. to bring together, analyze, and correlate already available information, and — without conducting any new tests — to prepare material that could be used for structural design. To be included was a review of the effects of explosive source geometry and character. This is the final report on that project.

It is divided into two main parts, with the first — Accidental Explosions and Closed Structures — essentially setting the stage for the second, which deals specifically with effects of openings. The first part discusses the basic elements of accidental explosions — the blast waves they create and the effects of the different potential explosive sources (also termed donors) namely, effects of donor quantity, type, and materials (Section I-1). This part also briefly reviews techniques currently in use for determining design forces on closed structures; that is, structures with no openings (Section I-2).

The second part of the report contains six sections. Section II-1 describes in general terms what happens when a blast (or shock) wave strikes a structure with openings. Section II-2 presents methods for determining how openings affect design loadings on exterior faces of structures assuming there are no counterforces from interior sources. The next two sections deal with interior phenomena: Section II-3 with shock waves; and Section II-4 with air flow created by shock-structure interaction. In the last two sections, design loadings are again discussed, with Section II-5 dealing with interior loadings alone, and Section II-6 with net design loadings; that is, the difference between exterior and interior loadings.

Conclusions and recommendations immediately follow the main part of the report. The Appendix contains examples illustrating use of the techniques developed for determining loadings due to accidental explosions.

Part I

ACCIDENTAL EXPLOSIONS AND CLOSED STRUCTURES

Section I-1
BLAST WAVES AND DONOR CHARACTERISTICS

BLAST WAVES

For structural design, the most important characteristics of a blast pulse are its peak overpressure and its positive overpressure impulse (i.e., the area under a plot of overpressure vs time to the time at which the pulse decays to ambient pressure). For explosions of TNT, and for values of peak overpressure* up to about 200 psi (= 1.4 MPa), the relationship between pressure, P, and time, t, given by Kinney in Ref. 2 (similar to Brode's in Ref. 3) is:**

$$P = P_{so}\left[1 - (t/t_o)\right] e^{-\alpha t/t_o} \qquad (1)$$

where P_{so} = peak pressure in the pulse

t_o = positive pulse duration

α is a non-dimensional constant with values of

$\alpha = 1$ for $0 \leq P_{so} \leq 20$ psi (140 kPa)

$\alpha = 0.57\, Y_{so}^{0.65}$ for $P_{so} > 20$ psi (140 kPa)

$Y_{so} = (P_{so} + P_o)/P_o$

P_o = ambient pressure.

---

* For convenience when referring to blast waves, the term "pressure" will be used in place of overpressure.

** Impulse from Eq 1 is given by:

$$i_s = P_{so}t_o[(1/\alpha) - (1/\alpha^2)(1 - e^{-\alpha})] \qquad (1a)$$

which, for P_{so} of $\leq$ 20 psi (140 kPa) equals $(\underline{0.37})P_{so}t_o$, and for P_{so} of 200 psi (1.4 MPa) equals $(\underline{0.22})P_{so}t_o$. For a truly triangular pulse, impulse would be $(\underline{0.5})\, P_{so}t_o$.

For design convenience, the pressure pulse given by Eq 1 is replaced by an equivalent triangular pulse having the same peak pressure and the same impulse and with a fictitious duration given by:

$$t_{of} = 2i_s/P_{so} \qquad (2)$$

where i_s = impulse, i.e., $\int_0^{t_o} P\,dt$

Fig. 1 contains normalized pressure vs time plots (pressure as a fraction of peak pressure vs time as a fraction of positive pulse duration) for peak pressures, P_{so}, of 0-20 psi (0-140 kPa) and 200 psi (= 1.4 MPa). Equivalent pulses for the two pressures are also shown.

DONOR CHARACTERISTICS

The blast waves from standard high explosives such as TNT—when in a concentrated source such as a sphere in free air or a hemisphere on the surface—are well defined; however, the same generally cannot be said of accidental explosions of other explosive materials. There is always uncertainty with regard to the fraction of the total donor material contributing to the explosion, the geometry of such material, the influence of surrounding inert materials, and for many materials, their inherent explosive properties. Yet, these factors— quantity, type, and geometry of donor materials affect the blast pulse to which a structure can be exposed. In the following, the influence of donor characteristics on blast waves is briefly discussed.

Donor Quantities - Scaling Rules

Numerous tests with high explosive charges ranging in weight from a few grams to thousands of pounds, and even nuclear sources with yields ranging from sub-kiloton to megatons, have long confirmed expressions relating peak pressure, impulse, and time, with charge weight (or energy release) derivable on the basis of dimensional considerations alone. Broadly, these relationships indicate that at some distance from two compact charges (i.e., spheres, hemispheres, cubes, etc.) of the same material but of different weights:*

- peak pressures will be essentially the same at the same values of scaled distances $d/W^{1/3}$
- scaled time, $t/W^{1/3}$, will be essentially the same at the same values of $d/W^{1/3}$
- scaled impulse, $i/W^{1/3}$, will be essentially the same at the same values of $d/W^{1/3}$

} (3)

where d = the distance from the charge

W = the charge weight.

* The relationships apply strictly to charges exploded at equal ambient pressure P_o. Sachs, however, in Ref. 4, showed that they could be generalized to apply to different ambient pressures as well by replacing charge W with an equivalent charge weight (W/P_o) in all cases.

Normal variability in explosive material from batch to batch, and even within the same batch, accounts for some departure from these general scaling rules; blast anomalies such as those shown in Fig. 2 (from Ref. 5) account for others. Still, the relationships are generally accurate and widely used, as in Ref. 6, where they provide the basis of tabulated values of acceptable distances from different quantities of explosives (Quantity-Distance relationships) for various activities.

Fig. 3 shows curves relating peak pressure P_{so}, scaled duration $t_o/W^{1/3}$, and scaled impulse $i_s/W^{1/3}$ to scaled distance $d/W^{1/3}$ from a hemispherical charge of TNT on the surface (from Ref. 1).

Donor Materials

The variety of possible donor materials is almost endless. Ref. 7 lists over 100 explosives of military interest; there are scores of solid propellants which can detonate; a wide variety of explosive liquid combinations can be created by mixing various oxidizers such as liquid oxygen and liquid fluorine (see others in Ref. 6) with liquid fuels and other substances; and new explosive materials in a variety of forms (such as aqueous gelled slurry explosives, Ref. 8) are continually being developed.

At sufficient distances from the most common sources fabricated in a relatively compact shape such as a sphere or hemisphere, the blast waves will resemble those shown in Fig. 1.

While the most common explosives are of relatively high density, (about 1.6 and 1.8 gm/cm^3; TNT's density is about 1.65 gm/cm^3), Wilton's unpublished data (Ref. 9) indicate that explosives with densities as low as 0.31 gm/cm^3 will yield similar results. For example, the curves of peak pressure and impulse in Fig. 4 from 55-gm hemispheres of low density nitroguanidine and high density C-4 are similar in shape.

Such simple relationships cannot be assumed for all explosives,

however. For example, in Ref. 10*, a particular propellant in a particular cylindrical configuration is shown to give both higher and lower peak overpressure blast waves, when compared to a TNT hemisphere on the ground.

As another example, in Ref. 11 Strehlow indicates that peak pressures from very low density explosives (gases) will not scale as high explosives do but that impulse will.

Thus, while Eq 1 and Fig. 3 will apply to many potential explosive accidents, if the source material involved is not a conventional high explosive, other relationships among peak pressure, impulse, distance and time must be employed.

Donor Geometry

Perhaps the most difficult problem to deal with in predicting blast characteristics from accidental explosions is that of source geometry. While compact sources would not be uncommon, they may also be barricaded, that is, very close to substantial barriers, or contained, as in a steel-arch earth-covered magazine. They may consist of a single explosion, or multiple explosions, not necessarily simultaneous. Sources that are not compact may be essentially in a line or they may cover a considerable area and thus resemble a cylindrical source with a very small length (or height) to diameter ratio (L/D). Some extreme examples of the latter type of source involving gaseous materials are given by Strehlow in Ref. 12: after spillage of liquid petroleum gas in 1962 at New Berlin, N.Y., the vapor cloud covered 200,000 ft^2 (18,600 m^2) and was 80 ft (24 m) deep before it exploded (L/D ≈ 0.16). After an accidental opening of a gate valve on an isobutylene tank in 1967 at Lake Charles, LA, a vapor cloud eventually

* In Ref. 10, Petes notes that, whatever the configuration of a source, its blast output is usually compared to that from a sphere or hemisphere of TNT. He maintains that this can be misleading.

formed which also covered about 200,000 ft^2 (18,600 m^2) and was about 20 ft (6 m) deep before it exploded (L/D = 0.04). Finally, following the burst of a 40-year old pipeline carrying propane gas in 1968 at Fort Hudson, MO, the vapor cloud eventually covered some 10 acres (40,500 m^2) before it exploded. (No cloud height was given.)

An extreme example of a line source explosion involving more conventional explosive sources occurred in 1944 at Port Chicago, CA with the explosion of the ship E.A. Bryan which contained some 1,800 tons (1.6×10^6 kg) of high explosives. A similar extreme example of a source covering a large area, which also involved multiple explosions, occurred in 1926 at Lake Denmark, N.J. when explosions propagated from one storage magazine to another, eventually involving some 800 tons (7.3×10^5 kg).

Some of the problems with these geometric effects can be resolved quite simply. For example, a number of investigators (Refs. 13, 14, 15) have observed that barricades have little influence on a blast wave at the overpressure ranges of interest in this report. That is, both peak pressures and impulse from barricaded charges are essentially the same as they would be from unbarricaded charges. (At some ranges, impulse is actually greater with a barricade than without one.)

Other geometric effect problems cannot be solved so easily. In tests with explosives stored in arched and covered magazines, for example, Zaker (Ref. 16) showed that far-field peak pressures and impulses scaled generally as in Fig. 3 (though higher values of equivalent weight for impulse indicated that pressure decay with time would be slower than that given by Eq 1). Closer to the magazines, however, Sound in full-scale tests (Ref. 17) and Kingery and Coulter (Ref. 18) in model scale tests showed that while scaling as given in Eq 3 held quite well (over a range of charge weights of 125,000 lb), pressure-distance relationships differed substantially from those in Fig. 3 and differed among themselves, depending on whether measurements were made at locations along a normal to the axis

of the magazine, in line with the axis closer to the headwall, or in line with the axis closer to the earth-covered rear of the magazine.

As noted in Ref. 1 multiple explosions, if close enough together in time, can give rise to a shock wave characteristic of a single source weighing the same as the multiple source. (See, for example, Ref. 19.) This is especially true at lower pressures. With more widely spaced explosives, the waves from two or more sources can partially merge, giving rise to a blast wave with multiple peaks, or even to a series of separate shock waves. Since the time of publication of Ref. 1, the problem has been extensively studied (Refs. 20, 21) and some criteria have been developed for determining whether single partially merged or multiple pulses will occur. If partially merged or multiple shock waves are incident on a structure, the loading of that structure will, of course, differ considerably from the kind of loading that would arise from a single merged pulse with characteristics such as those given in Eq 1.

Line charges, or charges that are very long compared to their width, will generate pulses that resemble those in Fig. 1 only qualitatively, and will actually follow a different relationship between peak pressure and distance from the charge than that in Fig. 3. Characteristics of the pressure pulses from a truly linear charge (i.e., one of infinite length) will not scale as the cube root of the charge weight, but rather as the square root (Ref. 22). If the length-to-width ratio is large enough, this cylindrical character of the shock wave will persist to low values of overpressure. The blast wave from the ship explosion at Port Chicago displayed cylindrical characteristics to great distances (see Fig. 5 from Ref. 23).

Finally, the length-to-diameter ratio of an essentially cylindrical charge with its axis vertical can also have a significant effect on pressure pulse produced by the charge. This can be seen in Fig. 6 from Wilton's unpublished data (Ref. 9). The cylindrical charges of Comp C-4 with L/D = 3.8 were intended to provide an approximate HE simulant of liquid propellants in an upright missile, and those with an L/D = 0.1, a simulant

of conditions after the liquid propellants had spilled on the ground. The measurements were made on the ground at right angles to the charge axis. Note that at a scaled distance of about 4 ft/lb$^{1/3}$ (1.6 m/kg$^{1/3}$), peak pressure differed by a factor of 3, with the lowest value being that for L/D = 0.1; at d/W$^{1/3}$ = 10 ft/lb$^{1/3}$ (4 m/kg$^{1/3}$) they differed by about 50% and at greater distances peak pressures became almost equal from all charges. Impulses followed a different pattern, however, being a factor of 2 different at d/W$^{1/3}$ = 4 ft/lb$^{1/3}$ (1.6 m/kg$^{1/3}$), (L/D = 0.1 being the lowest) virtually equal at d/W$^{1/3}$ of 10 ft/ lb$^{1/3}$ (4 m/kg$^{1/3}$), and at larger distances, impulse from the charges with small L/D ratios were greater than those with the larger ratio.

Also shown on Fig. 6 is the curve given by Petes (Ref. 10) for TNT cylinders with L/D ratio equal to 5. Except at the higher pressures, it closely matches the Wilton curve for L/D = 3.

As before, the fact that peak pressures and impulses for the two cylinders behave differently as a function of distance either compared with each other or compared with the standard surface burst curve indicates that the simple relationships given in Eq 1 will not hold. Peak pressures are close, but at a scaled distance of about 4 ft/lb$^{1/3}$ (1.6 m/kg$^{1/3}$) from the pancake-like charge, the shock wave from the cylinder has a much steeper decay of pressure with time than that from a hemispherical charge.

Summary

From the foregoing it is concluded that

- At the distances of primary interest for this report (peak overpressures less than 20 psi (140 kPa)) all non-conventional explosive sources considered generate blast waves generally similar in character to those from conventional spherical or hemispherical TNT charges, in that they have a sharp-fronted shock front and a faster than linear decay of pressure to ambient values. Thus, existing experimental

information on the modification in loadings on buildings due to various openings obtained from any such sources should be generally applicable to accidental explosions.

- For certain types of sources and source geometries, however, the pulse shapes differ substantially from those for TNT. Thus, for these sources, it should be recognized that special techniques will be required to determine loadings on buildings.

Section I-2
CLOSED STRUCTURES

INTERACTION PROCESSES

When a shock wave encounters an object—such as a building—partially blocking its path, a number of different interactions take place, some of which, for a structure with no openings, are illustrated in the plan view of Fig. 7.

If the shock wave path is nearly perpendicular to the wall (the angle of incidence is small), "regular" reflection takes place and a single reflected wave is formed. If the shock wave strikes the wall at a glancing angle (angle of incidence is large), a "Mach" reflection occurs, and a three-shock configuration forms with one shock (the Mach stem) being almost straight and propagating essentially parallel to the wall. A rarefaction wave forms at the edge of the structure and propagates down the wall, relieving pressures against it.

While this is going on, the remainder of the shock wave traverses the roof, possibly forming low pressure rotating flow; i.e., vortices, at the leading edges of the building. Finally, the wave diffracts on to the back face of the structure, both over the roof and around the edges, creating upstream propagating rarefaction waves and again possibly forming vortices. This diffracted wave subjects the back face to pressure loadings.

Absent the effects of vortices, the structural faces on which reflection occurs will experience higher initial loadings than the pressure in the incident wave; those faces generally parallel to the direction of shock wave propagation (the roof in Fig. 7) and those on which diffraction

occurs will experience initial pressures below incident values.

For purposes of this report, an angle of incidence of zero will be assumed, mainly because this assumption generally leads to maximum—worst case—loadings. Details of the interactions that can take place on front walls, roofs (and side walls), and back walls are shown graphically in Figs. 8 and 9, from an analysis of Schlieren photographs of shock interactions with blocks made by Bleakney almost 30 years ago (Ref. 24). Incident shock wave strength was about 1.9. In both Fig. 8A, taken 15 μs after the shock wave struck the block, and Fig. 8B, taken 30 μs later, the rarefaction wave proceeding down the front face can clearly be seen. In both plots, the head of the rarefaction wave is at reflected pressure, and its tail at the edge of the opening is essentially at incident pressure. (A vortex is clearly forming at the block corner.) Pressures above the block near its front face remained close to incident values, despite the high pressure wave propagation above the block from the corner.

The process of diffraction on to a back face is shown in Fig. 9. In Fig. 9A the process has just started, almost independent of front face effects which have not yet propagated across the block. The head of the wave proceeding down the wall is close to ambient pressure; the head of that proceeding into the shock from the corner is at incident shock pressure. Fig. 9B depicts conditions just before reflection occurs at the base of the block. Clearly, a strong vortex has already formed. Outside the region of the vortex, however, pressures along the wall are uniformly almost at ambient levels.

Later interaction processes will become even more complex, as all the shock waves, rarefaction waves, and vortices just described encounter each other and create more waves which propagate up and down along the structure's face and across its roof.

Very broadly, the effects of these complex processes are to reduce overall pressures on front faces (those first encountered by the shock wave) to just above incident values; and to raise pressures on the roofs and other walls to just below incident values.

LOADINGS USED FOR DESIGN

It has been normal practice, in structural design, to ignore transient loadings due to these complex interactions and to replace them with far more simplified loading-time relationships. The practice is generally justified because natural periods of many structures and structural elements are far greater than the very rapid pressure changes brought on by intersecting shock and rarefaction waves.

A set of such simplified loading (pressure) vs time relationships for long duration waves was derived in Ref. 25 for the case shown in Fig. 7; that is, for a wave striking a structure at angles of incidence greater than zero. It accounts for both Mach and regular reflection, and maximum pressures on "front" walls occur only after the shock has traversed that wall.

Another set of such curves also for very long duration waves, but for zero angle of incidence is given in Ref. 26. (The curves in Ref. 25 and 26 were actually derived for blast from nuclear weapons.) This set of curves resembles those shown in Fig. 10 (from Ref. 1), which were derived for use with relatively short duration blast waves. In Fig. 10, on the front face of a structure, high reflected pressure loadings are assumed to occur instantaneously over the entire face. Then, if the shock wave is long enough, the loading pressures are assumed to decrease linearly with time to a value of $P_s + C_D q$,* where P_s is the pressure in the incident wave (i.e., the blast pressures that would exist at the location

---

* Fig. 32 contains plots of various shock wave parameters, derivable from those in Fig. 3 and used in Fig. 10. These include: q = dynamic pressure, U = shock velocity, P_r = peak reflected pressure. Other structural and shock wave terms used in Fig. 10 are illustrated in the inset on Fig. 11. See Ref. 1 for values of i_r = peak reflected impulse.

in the absence of the structure), q is the dynamic pressure in the incident wave, and C_d is the front face drag coefficient taken as equal to 1. The time for this decrease to occur is known as the clearing time, and in Ref. 1 (as well as many other sources) front face clearing time is given as:

$$t_c = 3\ S/U \qquad (4)$$

where S = the height or half width of the face, whichever is lesser

U = the shock front (not shock flow) velocity.

Front face pressure is then assumed to decay linearly with time to zero at a time equal to the positive duration of the shock wave. In Fig. 10A, the dashed line connecting the pressure, P_r, with the time, t_r, represents the loading pulse counterpart of the equivalent triangular shock wave pulses shown in Fig. 1. It has a fictitious duration of $t_r = 2\ i_r/P_r$, where i_r and P_r are peak reflected impulse and pressure respectively. If the area of this triangular pulse is smaller than that of the solid curve (i.e., if the triangular impulse is the smaller), the implication is that the incident pulse is too short for clearing phenomena to have a significant effect. In that case, the triangular pulse is used for design purposes.

On the roof and side walls of a structure, the loading patterns are based on the assumption that the wave on these faces is the unmodified incident shock wave. Pressure builds up linearly with time to a maximum value which depends, in part, on whether the span being considered is parallel with or perpendicular to the shock front. The maximum also includes a factor, $C_D q$, in which q is again incident wave dynamic pressure, and C_D is a drag coefficient, with a value ranging from -0.6 for $0 \leq P_{so} \leq 35$ psi (240 kPa) to -0.2 for $P_{so} = 120$ psi (2,800 kPa). (If the span direction is perpendicular to the wave front, as might occur on a roof, the maximum value also includes a factor dependent on shock wave length to span length given in Fig. 11.) Pressure is then assumed to decay linearly with time, essentially until the wave leaves the structure.

Finally, on the back face of a closed structure, pressure is assumed to build up linearly with time to a value dependent, both on the ratio of shock wave length to span length, and on $C_D q$, where values of C_D are the same as those for the roof and side walls. The time for this buildup is taken as the time for the shock wave to traverse the distance, s, defined in the same way as for the front face. Thereafter, pressure is again assumed to decay linearly with time essentially until the shock wave leaves the back face.*

---

* The basic difference between the loading pulses shown in Fig. 10 and those for nuclear weapons given in Ref. 26 are: in the latter, the final pressure decay to zero follows the modified exponential form of Eq 1; the maximum pressures on roof, side walls, and back wall are identically $P_s = P_s(t) + C_D q$ (the shock wave length being very much longer than the span length); and values for roof and side wall drag coefficients differ from those in Ref. 1.

Part II

EFFECTS OF OPENINGS

Section II-1
GENERAL DESCRIPTION

An opening (a window, doorway, vent,etc.) in any wall struck by a shock wave causes additional interactions which can change the exterior loading patterns from those shown in Fig. 10 and subject the interior to loadings as well.

EXTERIOR EFFECTS

Immediately after a blast wave strikes the front face of a structure, rarefaction waves form at the edges of any opening in the face. These are generated by the difference between incident shock pressures in the area of the opening, and reflected pressures on the wall adjacent to it. They propagate at the velocity of sound into the reflected shock region, causing a reduction in pressures on the exterior face of the wall, from their reflected values. At the same time a higher pressure pulse propagates at acoustic velocities into the area of the opening.

On the exterior of the roof and side walls of a structure, an opening again serves to reduce pressures because of the generation of rarefaction waves that propagate away from the opening along the exterior faces. Similarly, on the exterior of the rear face of a structure, an opening serves to reduce pressures which, however, are already below incident values because of diffraction effects.

INTERIOR SHOCK WAVE EFFECTS

An opening in a wall struck by a blast wave allows a portion of the wave to enter the structure creating other shock waves that can reflect and re-reflect from interior surfaces, generating rapidly changing loadings on them. An example of the types of interior interactions that can occur is shown in Fig. 12, shadowgraphs of tests in a shock tube carried out by Coulter (Ref. 27). In the sequence the shock wave first diffracts around the opening (Frames 2, 3); reflects from the side walls, generating reflected waves (Frames 4-7); and then the reflected waves interact (Frame 8). A vortex is also formed at the edge of the opening (Frames 3-7) and begins to move downstream (Frame 8). Note that the central portion of the main shock wave remained straight for some time (up through Frame 5). After that the entire main shock wave became curved.

INTERIOR FLOW EFFECTS

At some time after arrival of the shock wave at the opening, if the shock duration is long enough, and if the interior volume does not fill too quickly, a jet of high speed air will form in the opening, driven by the difference between internal and external pressures. The general characteristics of the jet are shown in Fig. 13.

Flow velocities immediately behind a shock wave can be quite high. (With a shock pressure of 5 psi, for example, flow velocity behind the shock is about 230 ft/sec.) At the same pressure levels, however, the flow velocities in the jet—and especially in its core—are far greater. If the difference between internal and external pressures is the same 5 psi (which could occur with a 5 psi, long-duration shock wave at a vent on the roof of a structure, or even at an opening on the front face of a structure if the front face area is small) jet flow core velocities would be on the order of 720 ft/sec, more than three times the shock flow velocity. If

the pressure difference were 11 psi (a little less than reflected pressure from a 5 psi blast wave), jet core velocities would be on the order of 1,000 ft/sec.

INTERIOR SHOCK WAVES IN NOMINALLY CLOSED STRUCTURES

A final effect of "openings" in one type of building which ostensibly does not contain any openings should be mentioned. During recent tests on a strengthened pre-engineered building (a steel frame building with cold rolled, ribbed, steel siding and roofing) which had no openings, pressure pulses propagating in the interior of the building, and keeping pace with the shock wave outside it, were recorded. The peaks of these waves were 30 to 40% of peak incident pressures (Ref. 28). The pulses had relatively steep fronts, though there was some rounding (Ref. 29). It is conjectured that the steel siding and roofing parted enough along seams during shock loading to provide enough open area to create such a pulse. Motion picture records confirmed that such seams did open and close repeatedly during loading, but closed again, and most remained closed, after shock wave passage.

Too little is known about the phenomenon, at present, to develop relationships that would apply to other similar situations. It is apparent, however, that the effects could be significant in particular circumstances.

Section II-2
EXTERIOR LOADINGS

This section discusses how loadings on exterior surfaces alone are modified by the presence of openings. If interior loadings can affect the design load on a structural element, Section II-6 should be consulted.

FRONT FACE

As indicated in Figs. 8 and 9, the pressures on the front face of a closed structure struck by a shock wave decrease because of rarefaction waves from roof and side walls meeting, crossing, striking solid boundaries and generating complex non-uniform loading patterns across the wall face. Exactly the same kind of interactions shown in Figs. 8 and 9 occur on the front face exterior wall as the result of an opening in the wall. Rarefaction waves form at the edges of the opening, propagate away from it, interact, reflect from nearby surfaces, and generally subject the wall to highly non-uniform loadings. The overall effect of all this process, however, is again, to reduce loadings on the exterior face of the wall from peak reflected values to values just above incident pressures.* It would appear then, that effects of openings can be combined with other effects on front faces of structures, at least during the clearing time period.

The clearing time as given by Eq 4 is essentially the time for rarefaction waves formed at the roof or side edges of a structure to travel from their origins to a major reflecting surface (the ground in the case of structure height, another rarefaction wave in the case of structure

---

* This assumes a large enough interior space that significant filling does not occur during shock passage.

width) back to their origins, and once again back to the reflecting surface.* An opening in the front face of a structure should, in essence, shorten this clearing time by providing intermediate sources of rarefaction waves; that is, sources other than the top and side edges of the front face.

A situation in which there is no doubt that clearing times will be reduced by the presence of a window opening is shown in Fig. 14A, a sketch of a structure with clerestory windows. If the strength of the window glass itself is ignored, the presence of the windows clearly shifts the origin of rarefaction waves from the roof line to the window sill, thus decreasing S in Eq 4 and shortening the clearing time.

In other cases, a window or doorway in a front surface could have a negligible effect on clearing time. In Fig. 14B, for example, a value of S equal to the height of the structure should clearly be used in Eq 4, whether the doorway in the center of the wall were present or not.

These figures emphasize the need to integrate the presence of one or more openings in the front face of a structure into the overall pattern of clearing. Such openings can, in essence, shorten either the effective building height or width (for use in Eq 4), and which effect predominates should be determined. This can be done as follows.

Referring to Fig. 15A and 15B, the overall structural width, W_s, and height, H_s, can be divided into segments of width, W_{s1}, W_{s2},... W_{sn}, and height, H_{s1}, H_{s2}, ... H_{sn}, as shown. In each segment where there is a window of height h_s, and width w_s, the "height-clearing-distance", which on a closed structure would be H_s, is decreased to $H_s' = (H_s - h_s)$. The "half-width-clearing-distance" — $W_s/2$ on a closed structure — has been decreased to $W_s'/2 = (W_s - w_s)/2$.

---

* A more logical parameter to use in Eq 4 than U, shock velocity, would be some measure of the speed of sound in a medium, since rarefaction waves propagate at the speed of sound. Newmark (Ref. 30) among others has proposed a clearing time relationship based on sound velocities.

The total effects of openings on the height clearing distance is calculated from the relationship:

$$S'_H = \frac{W_{s1}H'_{s1} + W_{s2}H'_{s2} + \cdots + W_{sn}H'_{sn}}{W_{s1} + W_{s2} + \cdots + W_{sn}}$$

$$S'_H = \left[\sum_{n=1}^{n} (W_{sn}H'_{sn})\right] \Big/ [W_s] \qquad (5a)$$

$$= A_f[1 - (A_o/A_f)] \Big/ [W_s]$$

where A_f is the total area of the front face
and A_o is the open area of the front face.

Similarly, the half-width-clearing-distance in Fig. 15A is given by

$$S'_{W/2} = \left[\sum_{n=1}^{n} (H_{sn}W'_{sn}/2)\right] \Big/ [H_s] \qquad (5b)$$

$$= A_f[1 - (A_o/A_f)] \Big/ [2H_s]$$

Note that in Eq 5a and 5b, a value of zero is assigned to the height or width of an element that is entirely open. The values of S in terms of the structure height H_s for the two simple examples of Fig. 14 are:

for Fig. 14A, $S'_H = 0.75H_s$, $S'_{W/2} = (3/2)H_s = 1.5H_s$

for Fig. 14b, $S'_H = H_s$, $S'_{W/2} = (31/16)H_s = 1.94H_s$

It should be emphasized here that if the duration of the triangular pulse in Fig. 10A ($t_r = 2i_r/P_r$) is still shorter than any of the clearing times calculated as above it should be used for design. Again, the implication is that the loading pulse is too short for clearing phenomena to have effect.

REAR FACE

The effects of openings in the rear face of a structure differ from those for openings in the front face. In the latter case, the openings served the same purpose as the edges of the structure; viz, as a source of rarefaction waves to decrease pressures from peak reflected values. On the back face of a structure, however, the edges of the face are the sources of pressure increase on the face, and the openings in the face tend to decrease that pressure. The amount of decrease is clearly related to the relative areas of openings and face. If an opening were very small relative to the area of the entire face, it would have little effect on overpressure on the face; if it were large, pressures on the remainder of the face would be essentially ambient.

If it is assumed that overall pressure varies linearly with the ratio of face area to open area, then the maximum pressure P_{mo} on the back face of a structure which contains openings would be

$$P_{mo} = P_m \left[(A_F - A_o)/A_F \right] \qquad (6)$$

where P_m is the maximum pressure on the face in the absence of openings

A_F is the total face area ignoring openings

A_o is the total area of the openings in the back face.

The time at which this pressure would be attained would still be the time required for the shock wave to traverse a distance, S, as previously defined.

ROOFS AND SIDE WALLS

The same basic reasoning as used for the back face of a structure applies to its roof and side walls; viz, the effect of any opening is to reduce the pressure to which the faces would be exposed in the absence of the openings. Whether or not it is appropriate to use a loading scheme that applies over an entire face must first be determined by the designer, however. On a side wall, for example, with the span direction parallel to the shock front, the blast wave may, if short enough, completely pass a particular element (a column, for example) before it even arrives at a distant opening. Thus, the local loading of that element would not be affected by the presence of the opening at all.

If it is appropriate to use loadings applied to an entire face, Eq 6 would give the decrease in maximum pressure on roofs or side walls due to the presence of openings in them.

LIMITATIONS

It is appropriate here to emphasize the limitations of the various design loading methods just presented, even those for closed structures. As already noted, the "clearing time" concept used for front and back faces is itself a substantial simplification of actual events, and there are differences of opinion about how these times should be calculated.

Elements of the methods which rely on experimental information are of questionable accuracy. Where Ref. 1, for example, recommends values of C_D ranging from -0.6 at low pressures to -0.2 at high pressures for roofs, side walls, and back faces, Iwanski et al. (Ref. 31) recommend a value of $C_D = 0$ for back faces, and a constant -0.6 at high pressures for roofs and side walls. In Ref. 26, values of C_D at low pressures are 50% smaller than those in Ref. 1.

Whether roofs and side walls actually experience incident pressures can also be questioned. In the tests reported in Ref. 29, recorded peak pressures on the roof of the structure were about 60% lower, and 25% higher than incident, and side wall peak pressures were consistently 20 to 25% lower than incident values.

Finally, Eqs 5 and 6 accounting for the effects of openings, while drawn inferentially from experimental data, have not been directly verified experimentally. That is, the precise geometries discussed have not been the subject of tests.

Section II-3
INTERIOR PHENOMENA: SHOCK WAVES *

GENERAL BEHAVIOR

The behavior of a shock wave downstream from an opening can be divided into three phases. An initial, plane wave, phase begins as soon as the shock wave passes into the interior. During this phase, a part of the wave proceeds as if there were no opening at all. (See, for example, Frames 1-3 in Fig. 12.) Acoustic signals from the edges of the opening have not yet arrived to "inform" that part of the wave of the existence of an opening. As the wave proceeds into the interior, it diffracts into the region shielded from the incident shock wave by the wall adjacent to the opening and rarefaction waves propagate back toward the center of the main wave. Pressures at the front of the portion of the diffracted wave proceeding along the wall adjacent to the opening are essentially zero (see Fig. 9, where the shock wave diffracts onto the back face of the block).

While the diffracted portions of the wave are sharply curved, a significant portion of the main wave remains essentially plane for some time even after the rarefaction waves have traversed the entire main wave front, though pressures along the front are no longer uniform. (See Fig. 12, Frames 4 and 5.) By the time, however, that the main wave has progressed a distance into the interior of between one and two opening widths, it is

---

* This discussion is restricted to waves striking a structure head-on; that is, to shock waves entering through an opening in the front face of a structure. For the same size opening, interior shock wave effects from this orientation are the most severe. It also deals only with the characteristics and effects of the shock wave on its initial passage through a room downstream from an opening. Some characteristics of subsequent effects (e.g., second, third, and other reflections), which are highly geometry dependent, are discussed in Section II-5.

curved along its entire front. During this intermediate (curved wave) phase, it spreads out until it encounters reflecting surfaces such as roofs or side and back walls.

The final phase only occurs if the back wall is distant from the opening, and reflections from other interior surfaces have occurred. In those cases, the shock wave again becomes essentially plane and proceeds down the axis of the room.

While shock front pressures during the initial (plane wave front) and intermediate (curved, expanding wave front) phases are continually changing, not only in the direction of wave propagation, but along the front itself, it appears that relatively simple empirical relationships can be derived which adequately describe important characteristics of the wave front. First among these are pressures along an axis from an opening; that is, along a line, normal to the plane of the opening, drawn from its center.

INITIAL AND INTERMEDIATE PHASES

Axial Pressures

Analysis - In analyzing the results of tests in a two-dimensional, shock tube geometry, Melichar (Ref. 32) indicated that the shape of wave fronts during the period we have termed the intermediate phase was approximately cylindrical, with the center of the cylindrical expansion located upstream from the opening itself.* The analogy in three-dimensional geometries would be spherical waves also expanding from a center upstream from the opening. The occurrence of spherical expansion suggests that pressure changes with distance in the direction of wave propagation might be related to similar pressure changes in the more usual case of waves expanding spherically from an explosion source. Such changes are shown in Fig. 3 (or perhaps the equivalent of Fig. 3 for bursts in free air instead of on the ground surface). These figures indicate that over the pressure range of interest (and beyond) peak shock pressures from explosive sources decrease approximately as the 3/2 power of distance from the source.

A fair amount of experimental evidence seems to confirm that, for much of the intermediate phase, shock front pressures along an axis from an opening also vary approximately as the 3/2 power of distance, with the center of expansion located about one half an opening width upstream from the opening. The derived empirical relationship between axial shock front pressure and distance is:

$$P_s/P_{so} = \left[(2\,d' + b_o)/(3\,b_o)\right]^{-1.5} \qquad (7)$$

$$\text{for } d' \geq 3b_o/2$$

where P_s = shock front pressure along the axis,

* (In essence he found that differences in velocity of propagation between high pressure and low pressure portions of the shock front could be neglected.)

P_{so} = shock front pressure in the opening,

b_o = characteristic dimension of an opening (also referred to as opening width)*

d' = distance from the opening.

Eq 7 implies that shock front pressures begin to decrease from their values at the opening only after the wave has moved into the interior a distance equal to one characteristic dimension of the opening; that is, after $d' = b_o$. This cannot be the case, however, because axial pressures actually begin to decrease from their values at the opening before $d' = b_o$. More specifically, at about the time that $d' = b_o/2$, while much of the main wave is still plane, low pressure sonic signals from the edges of the main wave proceeding along the wave front have arrived at the axis, signaling the center of the plane wave that diffraction is taking place. The effect of these signals is to decrease pressures along the axis, thus shock front pressure when $d' = b_o$ must be less than P_{so}, the pressure at the opening. Still, Fig. 12 (and other similar shadowgraphs from Ref. 27) indicate that the wave front actually achieves a spherical shape shortly after $d' = b_o$. Thus, the spherical expansion type of pressure decrease with distance (i.e., with the 3/2 power of distance) should also be expected to begin shortly after $d' = b_o$.

A relatively simple approach in which axial pressures begin to decrease when $d' = b_o/2$, but which also leads to the spherical expansion type of pressure decrease in Eq 7, when d' is somewhat greater than b_o, is given below:

For $b_o/2 \leq d' \leq 3\,b_o/2$

$$P_s/P_{so} = 0.75(d'/b_o)^{-0.4} \qquad (8)$$

For $d' > 3\,b_o/2$, Eq 7 applies.

As will be seen later, experimental measurements are consistent with Eq 8.

---

* Because openings come in many different shapes and sizes, the definition of b_o has been standardized as the diameter of a circular opening which had the same area as the actual opening A_o. Thus, $b_o = (4A_o/\pi)^{1/2}$.

If the explosive source is small enough that a significant change of shock pressures would take place over the distance d' in the absence of any structure (i.e., if free-field pressures are changing relatively rapidly in the vicinity of the structure), expressions equivalent to Eq 7, or Eq 8, can be derived which would incorporate this change. As already noted, Fig. 3 indicates that the decrease in free-field pressure with distance follows an inverse 3/2 power relationship, viz:

$$P'_s = P_{so}\left[1 + (d'/d)\right]^{-1.5} \qquad (9)$$

where d = distance from the source to the opening,

P_{so} = peak pressure at a distance d from an explosion (in this case the opening),

P'_s = peak pressure at a distance $d + d'$ from the explosion.

If the assumption that the two pressure decays — one due to spherical spreading from an explosive source, the other due to the effects of an opening — continue to have effect after a shock wave passes an opening, Eq 7 and Eq 8 can be modified by multiplying their right-hand sides by the factor $\left[1 + (d'/d)\right]^{-1.5}$. For $d' < b_o/2$, Eq 9 alone gives the change in pressure after the shock wave from a small explosive source passes an opening.

Experimental Information - Three main sources of experimental information were used to compare with predictions of axial peak pressures from Eq 7 and Eq 8:

- o A field test in which a concrete instrument shelter was exposed to blast from a 500-ton TNT source (data reported in Ref. 33; details of the experiment are in Ref. 34)
- o An extensive series of tests of small-scale structures conducted in a shock tube (Ref. 33)
- o Tests on a full-scale room conducted in a explosively driven shock tunnel (Ref. 35, 36).

Brief descriptions of the experimental arrangements follow.

o Field Test of Full-Scale Structure. During operation Prairie Flat in 1968, a standard concrete instrumentation shelter 8 ft high by 8 ft wide by 12 ft long, shown in Fig. 16A, was exposed to the blast from a 500-ton hemisphere of TNT resting on the ground surface. The doorway, 7 ft high and 2.9 ft wide, was left open, and three pressure sensors were installed in line with the doorway opening: two in the floor, 2 ft and 4 ft from the doorway; and one in the rear wall; i.e., 12 ft from the doorway. Incident pressure at the doorway was 4.7 psi.

o Shock Tube Tests of Small-Scale Structures. An extensive series of tests on small-scale structures, reported on by Coulter in 1969 (Ref. 33) were carried out principally to derive information on room filling. In some of the tests, information on shock front pressures was also sought (and in one case was derived from shock pulses shown in Ref. 33). One of the structures used was a 1:24 linear model of the full-scale instrumentation shelter described above.* A sketch of the model is shown in Fig. 16B. As with the full-scale structure, the model was equipped with gauges in the floor at 1/3 and 2/3 the distance between front and rear walls, and in the rear wall as well.

Back wall pressure (fill) records from the prototype and one of the shock tube tests are shown in Fig. 17. For the time of interest, the shock tube record is flat; the field record shows incident pressures decaying as in Fig. 1, with the positive pressure pulse being over 160 ms long. (Fig. 3 indicates that the total duration would have been about 200 ms.) The data of importance for this study are the magnitudes of the initial peaks of the pressure records (which mark the arrival of the shock front at the back wall). At later times in both prototype and model the pulses were so long that room filling and other interior shock reflections exposed the wall to higher irregular pressures.

---

* A linear scale factor of 24 is equivalent to a charge weight (or energy) scale factor of 13,824. Thus, a model charge equivalent to the 500-ton (1,000,000 lb) charge used in the field would have weighed about 72 lb.

Another small-scale structure employed by Coulter was that shown in Fig. 18. As can be seen, the structure was variable in length with gauges located in the rear walls. Three different sizes of doorways were used, though data from the smallest (which occupied only about two tenths of one percent of the front wall) were not considered in this analysis.

With these small-scale structures an especial effort was made to identify and record the first peak of the gauge record, by employing fast as well as slow oscilloscope sweeps. Typical records are shown in Fig. 19.

One final model, which is not illustrated but for which relevant information could be derived from Ref. 33 itself, was a cubical structure, 4 in. on a side, with an opening 1.245 in. high and 0.6245 in. wide. A gauge was placed in the center of the floor. The fill and input pressure traces for an input pressure of 10.7 psi, published in Ref. 33, were clear enough to identify a first peak.

o Shock Tunnel Tests on a Full-Scale Room. For many years, a shock tunnel was employed by URS Corporation to test full-scale wall panels. The facility which was converted from the tunnels of a former 16-in. coastal gun battery, was explosively driven with strands of Primacord strung the length of its compression chamber, and had a test section 8.5 ft high by 12 ft wide. Incident shock pressures of up to about 10 psi could be generated, and though the blast pulse was somewhat noisy, its duration was about 100 ms long (50 ms flattop), and significant information on structural response of walls to blast was derived. A sketch of the facility is shown in Fig. 20.

Loading study (calibration) tests, with instrumented walls designed not to fail under blast loadings, were carried out throughout the program. One loading study configuration of interest to this program was that of a room with a window shown in Fig. 21. As can be seen,

the back wall was heavily instrumented, a gauge was located in the room on a side wall, and paired gauges were placed on the exterior and interior of the front face of the wall. Details of this portion of the test progam are given by Wilton and Gabrielsen in Ref. 35; Ref. 36 by Wilton, Kaplan and Gabrielsen is a summary report of all loading study tests.

Fig. 22 shows traces (averaged by computer) from the back wall gauges. As with Coulter's work, our interest lies in the initial step of the pressure pulses which mark the arrival of the shock front at the back wall.

Data derived from these experimental sources are summarized in Table 1. Tabulated are values of d' (distance from the opening to a gauge), b_o (characteristic dimension of the opening); measured peak pressure P_s, or in the case of back wall gauges, measured peak reflected pressure P_{sr}. (Listed in the second column labeled P_s on Table 1 are calculated incident pressures at the location of the back walls which would result in the measured reflected pressures.) Incident pressures P_{so} are also shown, as well as the ratio P_s/P_{so}.

Comparison of Analysis with Experiment - The experimental data from Table 1 are plotted on Fig. 23, along with curves from the empirical expressions Eq 7 and Eq 8. The ordinate and abscissa of Fig. 23 are, respectively, normalized axial shock front pressures (the ratio of pressure in the interior P_s to pressure at the opening P_{so}) and normalized distance (the ratio of distance into the interior d' to the characteristic dimension of the opening b_o).

The data plotted on Fig. 23 cover a considerable range of incident pressure levels (from 1 to 10 psi), and a considerable range of relative distances (from d'/b_o = 0.78 to 7.3). Not shown on the figure or in Table 1 is the fact that the range of relative opening area (area of the opening relative to the area of the face) is also quite large; viz, from about 1%

to over 30%. Over these ranges, the agreement of experimental data with the simplified prediction relationships of Eq 7 and Eq 8 appears satisfactory.

Off-Axis Pressures

It has already been noted that during the intermediate phase of shock wave behavior, when the wave is spreading out from an opening with a generally spherical shape, shock front pressures vary along the wave front, from axial values given by Eq 7 to initial values of zero at the intersection of the wave front with the interior surface of the front wall.*

At any point on a wave front, the decrease in pressure from its axial value clearly should be some function of the angle between the axis itself and a line from the center of the spherical expansion to the point. In the absence of a detailed analysis, a linear dependence on this angle will be assumed. Thus, for the geometry shown in Fig. 24, predicted values of pressure at any point along a wave front, $P_{s\theta}$, are related to axial pressures, P_s, by:

$$P_{s\theta} = P_s\left[(90 - \theta)/90\right] \qquad (11)$$

with θ in deg, and where

$$\tan \theta = W/\left[L + (b_o/2)\right]$$

W = perpendicular distance from the point of interest to the axis

L = the perpendicular distance from the point of interest to the surface containing the opening.

P_s in Eq 11 is the value along the axis from Eq 7 at a distance of $R = W/\sin\theta$ from the center of expansion, or a distance $d' = R - (b_o/2)$ from the opening.

* Pressures along the wave front gradually equalize so that if a wave can propagate far enough, without encountering any reflecting surface, it will resemble in all respects the spherically expanding, uniform pressure waves of Fig. 3. This would not occur, however, until the opening could, in essence, be considered a point source. For the conditions of interest in this report, the non-uniformity of pressure along the front as described above is appropriate.

In the absence of information that will allow off-axis front pressures to be determined during the initial (plane wave) phase of shock behavior, it is recommended that for $0 < d' \leq b_o/2$, P_s should be taken as equal to P_{so} at the opening. For $b_o/2 < d' \leq 3\, b_o/2$, the effects of the angle θ should be gradually increased until Eq 11 holds. This requires that Eq 11 be replaced by

$$P_{s\theta} = P_s\left[(90 - \theta)/90\right]^{[(d'/b_o) - (1/2)]} \qquad (11a)$$

Shock Front Pressures on Interior Surfaces

Side Walls, Roofs, etc. - During the initial phase of shock wave behavior, relatively little spreading occurs. If side walls (or a roof) are encountered by a shock wave while it is in this phase, little error should result in assuming that the pressures on the wall are little different than those given by Eq 8.

During the intermediate phase, Eq 11 provides a basis for determining shock front pressures on interior surfaces, either real or imaginary,* with which the expanding shock wave interacts. As noted in Section I-2, the shock wave reflection process depends, in part, on the angle of incidence, defined as the angle between a normal to the shock wave, and a normal to the reflecting surface. With large angles of incidence (the shock front being nearly perpendicular to the reflecting surface), Mach — or

* A real surface would be represented by a side wall, for example. An imaginary surface would be represented by a plane midway between two openings, which — from the standpoint of shock behavior — serves the same function as a solid reflecting surface. This is illustrated in Fig. 25, on the left side of which is shown shock wave behavior between two openings, and on the right side, shock wave reflection from a solid wall. The plane midway between the openings is termed a plane of symmetry.

three-shock—reflection takes place, with a shock termed a Mach stem propagating parallel to the surface. With small angles of incidence (the shock front being nearly parallel to the reflecting surface, regular—or two-shock—reflection takes place. The angle θ as defined in Eq 11 and Fig. 24 is the complement of the angle of incidence.

The pressure in the reflected wave is also dependent on the strength of the incident wave. At low incident overpressures, in most of the regular reflection region reflected pressures will be about twice incident, while Mach stem pressures can range from zero to some three times incident pressure. At higher incident pressures, regular reflected pressures increase relative to incident pressures (the relationship is given by Eq 10). In the Mach region, the angles of incidence at which particular relative reflected pressures occur tend to decrease with an increase in incident pressure.

Ref. 1 contains a plot of reflected pressure coefficients (ratio of reflected to incident pressures) vs angle of incidence, with the relationship in the Mach reflection region being highly approximate. Ref. 26 provides a more detailed plot of such coefficients. In light of the uncertainties about the value of pressure actually incident on a reflecting surface from a shock wave expanding from an opening, and the fact that the shock front itself might not be too well defined, a still simpler version than that in Ref. 1 is proposed for this report. In this version, shown in Fig. 26, the sloping line represents the Mach reflection region,* the horizontal line with a value of two represents the regular reflection region.

---

* The slope of the Mach reflection line in Fig. 26 is a compromise between those in Ref. 26 for weak shock waves (slopes are steeper), and strong shock waves (slopes are shallower). If better values of reflection coefficients in the Mach reflection region than those in Fig. 26 are desired, refer to Ref. 26. In the regular reflection region, better values can be derived from Eq 10.

Combining Fig. 26 with Eq 11, pressures at a reflecting surface, such as a side wall, are:

$$\left.\begin{aligned} &\text{For } 0 \le \theta \le 20^\circ \\ &\qquad P_{sr} = P_s[0.1\theta]\,[(90 - \theta)/90] \\ &\text{and for } \theta > 20^\circ \\ &\qquad P_{sr} = 2P_s[(90 - \theta)/90] \end{aligned}\right\} \qquad (12)$$

with θ again in degrees.

As can be seen in Fig. 21, the shock tunnel tests of a full-size room incorporated a side wall gauge (Gauge No. 10) inside the room. The type of traces recorded by that gauge (averaged over a number of tests) is shown in Fig. 27 for a test with an incident pressure of about 3.3 psi. Except for those from a pulse with an incident shock pressure of 1 psi (which had a rounded front when it arrived at the window wall), all the traces were characterized by a relatively slow pressure rise (indicating that the wave front was not sharp) to an initial peak, then a fall to a lower "plateau" value. The relative difference between peak and plateau values increased with increase in incident pressure. At a time of 17 to 20 ms, about the time required for waves reflected from the back wall to arrive at the measuring station, the plateaus ended and pressures again rose.

In the shock tunnel tests, b_o = 5.2 ft, W = 6 ft, and L = 5.6 ft, from which a value of θ of 36.2°, and a value of (d'/b_o) = 1.46 can be derived. From Eq 7, axial pressures in the interacting wave fronts are $P_s = 0.65\ P_{so}$, and from Eq 11, shock front pressures at the side wall before reflection are $P_{s\theta} = 0.60\ P_s = 0.39\ P_{so}$. With θ = 36.2 deg, regular reflection occurs, and reflected pressures are $P_{sr} = 2\ P_{s\theta} = 0.78\ P_{so}$.

In Table 2, predicted and measured values (both peak and plateau) of reflected pressure on the side wall of the room shown in Fig. 21 (12 ft wide with a window occupying about 20% of its front face area) are tabulated. They are plotted on Fig. 28 as a function of incident pressure.

It appears that, for waves expanding from a relatively large opening, Eq 12 closely predicts the peak pressures at side wall gauges over the entire incident pressure range. Plateau pressures are also closely predicted for incident pressures up to about 3 psi. At higher incident values, however, the reflected plateau values are much lower than either measured or predicted peak values.

It should be noted here that times of arrival of an expanding shock wave at a point on the interior of a side wall will always be greater than the time of arrival of the incident wave at the same point on the exterior of the wall. For shock waves with incident pressures of about 2 psi or less, the ratio of arrival times (after the wave reaches the front face of the structure) at exterior and interior points is approximately equal to the ratio of distance travelled by the waves outside and inside the buildings. Referring to Fig. 24, if points ① and ② are on side walls, the ratio of exterior to interior arrival times at the two points would be $\left[L_1/(L_1 + W_1)^{\frac{1}{2}}\right]$ and $\left[L_2/(L_2 + W_2)^{\frac{1}{2}}\right]$.

After the spherical expansion phase is over and, in a long building, the shock wave has become plane again, pressures along the wave front (and thus shock front pressures on side walls) are uniform. Their values are discussed under "Final Phase Loadings".

Rear Walls - When a shock wave that has passed through an opening arrives at the interior face of a wall opposite the opening, regular reflection occurs. Reflected shock front pressures on the wall are from Eq 10 with $P_{s\theta}$ from Eq 11, using P_s from Eq 7 or Eq 8. Table 1 and Fig. 23 indicate that this approach provides rear wall pressures in fair agreement with experimental data. (This is because Eq 10 was used to derive incident pressures equivalent to measured reflected pressures, and the derived incident values compared favorably with those from the curve of Fig. 23; i.e., with values from Eq 7 or Eq 8.)

FINAL PHASE PRESSURES

At some time after the spreading (intermediate) phase is over, and waves have reflected from side walls, etc., a plane wave should form and, if the structure is long enough, propagate down its length. It should be weaker (i.e., have a lower peak pressure) than the wave at the opening because it occupies a greater area. It should also be a shock wave because all positive pressure pulses (other than weak sound waves) are basically unstable and tend to "shock up" with distance. (See, for example, Ref. 38.) Thus, both the plane wave at the opening and that within the building should behave according to the Rankine-Hugoniot relationships governing shock wave behavior.

Assuming conservation of momentum through the window opening and past a downstream section of the interior, and constancy of shock duration, shock front pressures at the two sections should be related by

$$\left[P_s^2/(7P_o + P_s)\right] = A_r\left[P_{so}^2/(7P_o + P_{so})\right] \qquad (13)$$

where P_s = peak pressure downstream from opening
P_{so} = peak pressure in the opening
P_o = ambient pressure
and A_r = area ratio = A_o/A_d
A_o = area of the opening
A_d = area of the downstream section.

Within an accuracy of about 10%, for $P_{so} \approx 10$ psi, Eq 13 implies the following simple relationship

$$P_s \approx A_r^{\frac{1}{2}} P_{so} \qquad (14)$$

For waves from small explosive sources, the right-hand side of Eq 14 should be multiplied by $\left[1 + (d'/d)\right]^{-1.5}$

Because of the complexity of the processes leading to the formation of the plane shock wave within the interior of a structure, it is difficult to say when it can be said to form. At the time the axial pressures from Eq 7 (i.e., during the intermediate phase) equal plane front wave pressures from Eq 14, reflected side wall pressures from Eq 12 are between 30 and 60% higher than axial pressures, depending on the value of the area ratio A_r. A reasonable (though still arbitrary) guideline is that plane waves may be assumed to exist when side wall reflected pressures from Eq 12 are the same as plane wave pressures from Eq 14. This occurs at about 1.5 times the distance from the opening that axial and plane wave pressures become equal. With this assumption, the limit value of distance from the opening d'_ℓ marking the transition from intermediate (spreading) to final (plane wave) phases(from Eq 7 and Eq 14) is:

$$d'_\ell = (0.75\ b_o)(3A_r^{-1/3} - 1) \qquad (15)$$

Fig. 29 in which shock wave shapes based on Eq 15 have been drawn for two different ratios of window opening to downstream areas suggests that a somewhat larger limit might be appropriate since the incident waves still have significant curvature. Use of this limit is conservative, however, since plane wave pressures beyond d_ℓ will be higher than axial pressures from Eq 7 and side wall pressures from Eq 12.

The pressures given by Eq 14 will be experienced on side walls and roofs. On rear walls, reflected pressures should be determined by substituting P_s from Eq 14 into Eq 10.

SHOCK WAVE PRESSURES - SUMMARY AND SIMPLIFIED GRAPH

Values of axial shock front pressure, P_s, in terms of pressure at the opening, and distance from the opening, d', in terms of b_o (opening width) during the three phases of shock wave behavior are summarized below. (The first two entries describe conditions during the initial phase.)

INTERIOR SHOCK FRONT PRESSURES
ALONG AN AXIS FROM THE CENTER OF AN OPENING

Relative Distance d'/b_o	Relative Pressure P_s/P_{so}	Source (Eq)
$0 \leq d'/b_o \leq 1/2$	1	
$1/2 < d'/b_o \leq 3/2$	$0.75(d'/b_o)^{-0.4}$	(8)
$3/2 < d'/b_o \leq \left[(0.75)(3A_r^{-1/3} - 1)\right]$	$\left[(2d' + b_o)/3b_o\right]^{-1.5}$	(15), (7)
$d'/b_o > \left[(0.75)(3A_r^{-1/3} - 1)\right]$	$(A_r)^{\frac{1}{2}}$	(15), (14)

b_o = opening width
d' = distance into interior along the axis
A_r = area of the opening divided by area of an interior section
P_{so} = incident peak shock pressure at the window.

For small explosive sources, the values of P_s/P_{so} should be multiplied by $\left[1 + (d'/d)\right]^{-1.5}$ where d is the distance from an explosive source to the opening.

Off-axis shock front pressures during the intermediate (spreading) phase may be derived from:

$$P_{s\theta} = P_s[(90 - \theta)/90] \qquad (11)$$

in which θ (in degrees) is as shown in Fig. 24.

Reflected shock front pressures at a side wall (or roof) during the intermediate phase are:

for $0 \leq \theta \leq 20$ deg

$$P_{sr} = 0.1\theta P_s[(90 - \theta)/90]$$

and for $\theta > 20$ deg (12)

$$P_{sr} = 2P_s[(90 - \theta)/90]$$

Reflected shock front pressures at rear walls during the intermediate phase are given by:*

$$P_{sr} = 2P_{s\theta}(7P_o + 4P_{s\theta})/(7P_o + P_{s\theta}) \qquad (10)$$

with $P_{s\theta}$ from Eq 11.

A plot of many of the relationships just given, shown in Fig. 30, simplifies the process of predicting shock front pressures downstream from an opening. The following procedures should be followed in using Fig. 30.

I. Initial Steps Required in All Calculations

1. Calculate $(d'/b_o)_i$ at a point of interest on the axis
2. Enter graph with $(d'/b_o)_i$ and read off $(P_s/P_{so})_i$ as given by the solid curve
3. Calculate A_r and $(A_r)^{\frac{1}{2}}$
4. Enter graph with $(A_r)^{\frac{1}{2}}$, and read off value of $(d'/b_o)_c$ using the solid curve

* Eq 10 is plotted in Fig. 32.

II. Axial Pressures, P_s

A. For $A_r \geq 40\%$

5a. If $(d'/b_o)_i \leq (d'/b_o)_c$, $P_s = P_{so}(P_s/P_{so})_i$

5b. If $(d'/b_o)_i > (d'/b_o)_c$, $P_s = P_{so}(A_r)^{\frac{1}{3}}$

B. For $A_r < 40\%$

6. Multiply $(d'/b_o)_c$ by 1.5

7a. If $(d'/b_o)_i \leq 1.5(d'/b_o)_c$, $P_s = P_{so}(P_s/P_{so})_i$

7b. If $(d'/b_o)_i > 1.5(d'/b_o)_c$, $P_s = P_{so}(A_r)^{\frac{1}{3}}$

III. Off-Axis Pressures, $P_{s\theta}$

A. For $P_s = P_{so}(A_r)^{\frac{1}{3}}$

8. $P_{s\theta} = P_s = P_{so}(A_r)^{\frac{1}{3}}$

B. For $P_s = P_{so}(P_s/P_{so})_i$

9. Calculate θ (see Fig. 24)

10. For any point a distance W off the axis (see Fig. 24),

a. Calculate $(d'/b_o)_\theta = \left[W/(\sin\theta) - 0.5\right]/b_o$

b. Find P_s/P_{so} from appropriate dashed line using $(d'/b_o)_\theta$

IV. Reflected Pressures on Side Walls and Roofs, P_{sr}

A. For $P_s = P_{so}(A_r)^{\frac{1}{3}}$

11. $P_{sr} = P_s = P_{so}(A_r)^{\frac{1}{3}}$

B. For $P_s = P_{so}(P_s/P_{so})_i$

12. Calculate θ.

13. For a point on a side wall a distance W off the axis (see Fig. 24),

a. $(d'/b_o)_\theta = \left[W/(\sin \theta) - 0.5\right]/b_o$

b. Find $P_{s\theta}$ from appropriate line below solid curve using $(d'/b_o)_\theta$

c. Calculate P_{sr} from

$$0 \leq \theta \leq 20 \text{ deg}, \quad P_{sr} = 0.1\theta P_{s\theta}$$

$$\theta > 20 \text{ deg}, \quad P_{sr} = 2P_{s\theta}$$

V. Reflected Pressures on Rear Walls

With Eq 10, $P_{sr} = \left[2P(7P_o + 4P)/(7P_o + P)\right]$, (see also Fig. 32)

14. Axial values

a. For $P_s = P_{so}(A_r)^{\frac{1}{2}}$, use $P = P_s$ from step 5b or 7b

b. For $P_s = P_{so}(P_s/P_{so})_i$, use $P = P_s$ from step 5a or 7a.

15. Off-axis values

a. For $P_s = P_{so}(A_r)^{\frac{1}{2}}$, use $P = P_{s\theta} = P_{so}(A_r)^{\frac{1}{2}}$

b. For $P_s = P_{so}(P_s/P_{so})_i$, use $P = P_{s\theta}$ from step 10b.

Section II-4
INTERIOR PHENOMENA: FLOW EFFECTS

FLOW REGIMES

Air flow induced by the interaction between a shock wave and a structure with an opening stems from two different sources: flow caused by the passage of the shock front itself; and so-called jet flow which occurs later.

Flow Behind a Shock Front

In the immediately preceding material, changes in pressure at the front of a shock wave which enters a structure through an opening are discussed in some detail. In addition to causing a pressure change, passage of a shock front through a region previously undisturbed, sets the air in motion, and thus there is air flow within an interior space as soon as a shock wave passes through the opening. Velocities and forces caused by this flow will be discussed later.

Jet Flow

Characteristics - If the duration of the incident shock is long enough, and the volume of the interior relative to the area of the opening is great enough, the pressure difference between the exterior of a structure and its interior will result in the formation of a jet of air through the opening. This type of flow can take place at openings in any face of a structure and can have particular importance in connection with small openings such as vents. Flow in these kinds of jets have been studied for some time, and Abramovich (Ref. 39) has described them as shown in Fig. 31.

In the first of the three regions shown, high velocity flow that enters through an opening connecting a high pressure region (on the left) with one of lower pressure (in our case close to atmospheric pressure) begins to spread out. Velocities near the center of the jet remain at their high initial (core) values but decrease to zero at the edge of the jet. As can be seen core values are maintained for several opening diameters (≈ 4.5 b_o according to Abramovich).

The next, transition region, is about 2.2 b_o long and is marked by changing flow velocity patterns, but further downstream, in the main region, the flow has stabilized somewhat so that the change of velocity with distance normal to the axis can be described with a single relationship; viz

$$u = u_m\left[1 - (y/b)^{1.5}\right]^2 \tag{16}$$

(Note that b = jet radius, not diameter, although b_o = jet diameter at the opening.) The variable u_m is the velocity on the axis in the main region and is given by

$$u_m = u_o(6.2\ b_o/d') \tag{17}$$

where u_o is the velocity at the opening.

Flow velocity on the axis at the beginning of the main region is still quite high, being about 93% of that at the opening.

The jet half-width in the main region is given by

$$b = d' \tan\alpha \approx 0.22\ d' \tag{18}$$

When to use Jet Flow Relationships - Jet flow through an opening does not take place as soon as a shock wave arrives at the opening. At first the shock itself controls the flow, then rarefaction and reflection waves crisscross the opening causing changes and fluctuations in the flow through it. Based on an analysis of Coulter's experimental shock tube data (Ref. 27), Rempel in Ref. 40 concluded that — for long or nearly

flat-topped pulses — the time, t_j, for jet flow to establish itself (which might be called the jet clearing time) is

$$t_j = 4\, b_o/c \qquad (19)$$

where c = the speed of sound in the opening
= 1.13 ft/ms or 13.6 in./ms

For large openings (windows or doorways, etc. as opposed to vents), t_j can be relatively large compared with the durations of many of the pulses that might be caused by accidental explosions. As an example, both the concrete instrument shelter and the full-scale room with a window tested in the shock tunnel, which were discussed earlier, have values of b_o = 5 ft. Eq 19 indicates that the jet clearing times would be on the order of 18 ms. At inhabited building distance ($d = 40\, W^{1/3}$), this time exceeds the entire pulse duration from all explosives weighing less than about 100 lb. At intraline distances ($18\, W^{1/3}$ unbarricaded, $9\, W^{1/3}$ barricaded), explosives weighing less than 200 lb and 850 lb respectively are similarly completely eliminated.

With larger explosive sources, of course, jet flow can establish itself and, if the pulse is long enough, can impart significant force to any object or obstacle in its path. When jet flow effects should start to be considered is somewhat arbitrary, of course but, based on a comparative analysis of impulses from shock waves and from jet flow, the criterion adopted in this report is:

- Jet clearing time from Eq 19 should be equal to or less than 1/2 the pulse duration from Fig. 3.

For large openings, this criterion still eliminates the need to consider jet flow for most accidental explosions covered by this report. In the cases just considered, for example, (i.e., b_o = 5 ft) the explosive sources must be larger than about 700 lb at $d = 40W^{1/3}$; 1,700 lb at $d = 18W^{1/3}$; and 7,000 lb at $d = 9W^{1/3}$. With vents and other small openings, however,

the consequences of jet flow must be considered for most accidental explosions. As an example, with an 8-in.-diameter vent, $t_j \approx 2.4$ ms. The jet clearing time criterion indicates that for this size of opening, explosive sources larger than about 2 lb at $d = 40W^{1/3}$, 4 lb at $d = 18W^{1/3}$, and 16 lb at $d = 9W^{1/3}$, must be considered.

FLOW VELOCITIES

Velocity Behind a Shock Front

The velocity of the flow immediately behind the front of a shock is a function of shock pressure and is governed by the Rankine-Hugoniot relationships. Air flow velocity caused by the passage of a shock front is given by:

$$u = c_o \left\{ 5\, P_s / \left[7P_o (7P + 6P_s) \right]^{\frac{1}{2}} \right\}$$
$$= 2.135 \times 10^3 \left[P_s / (7P_o + 6P_s) \right]^{\frac{1}{2}} \qquad (20)$$

where u = flow velocity behind the shock front
P_s = shock pressure above ambient pressure
P_o = ambient pressure
c_o = the velocity of sound in ambient conditions.

In the numerical expression P_s and P_o are in psi (or other consistent units) and u is in ft/sec. Eq 20 is plotted in Fig. 32 for shock front pressures from 0.5 to 50 psi. It can be used along with Fig. 30 (or Eq 7, 8, 11, or 14 as appropriate) to determine either axial flow velocities or off-axis velocities accompanying the shock wave downstream from an opening.

Velocities in Jet Flow

Rempel's work (Ref. 40), cited earlier in connection with jet flow clearing times, was largely devoted to filling of rooms from the jet created by blast from nuclear weapons. He used basic conservation principles, quasi-steady flow, and generally employed the isentropic relationships between pressure and density changes of a perfect gas; that is,

$$\rho_1 = \rho_0(P_1/P_0)^{1/\gamma} \qquad (21a)^*$$

where ρ_1 and ρ_0 are densities at two differents states

P_1 and P_0 are <u>total</u> pressures at two different states (absolute rather than gauge pressures; i.e., psia rather than psig)

γ = the ratio of specific heats of the gas at constant pressure and volume

= 1.4 for air.

If the volume downstream from an opening is large enough that filling is not a problem (and if upstream pressures change relatively slowly), Rempel delimits two types of flow through an opening: unchoked flow in which the ratio between exterior and interior total pressures is small enough (less than about 1.9) that isentropic (i.e., frictionless and shock free) flow through the opening is possible and flow is unimpeded; and choked flow, in which the ratio between exterior and interior pressures is such that isentropic flow is not longer possible, shocks form in the opening, and mass flow through it is limited. With atmospheric pressure in the interior, the choking occurs when the total exterior pressure is 27.38 psi, or the pressure over ambient is 13.13 psi.

Convenient forms of Rempel's relationships for flow velocity, u, through an opening are:

---

* Eq 21a does not really apply to shock waves, since a shock front is not an isentropic change of state, but Rempel showed that it provides a good approximation to the pressure and density relationship for normal shock waves; viz:

$$\rho_1 = \rho_0(6P_1 + P_0)/(P_1 + 6P_0) \qquad (21b)$$

being within about 1% of Eq 21b for shock pressures of about one atmosphere (15 psi). It is within 10% for shock wave pressures as large as 50 psi. It can also be shown that the isentropic pressure-density relationship of Eq 21a provides an even better approximation to the pressure-density relationship that applies to reflected shock waves.

For $0 \leq P_1 \leq 27.83$ psia (unchoked flow)

$$u_{ju}^2 = \left[2\gamma/(\gamma - 1)\right]\left[(P_o^{1/\gamma})/\rho_o\right]\left[P_1^{(\gamma-1)/\gamma} - P_o^{(\gamma-1)/\gamma}\right]$$

or, in ft/sec,

$$u_{ju} = 1.657 \times 10^3 \left[(P + P_o)^{0.286} - 2.155\right]^{\frac{1}{2}} \qquad (22)^*$$

For $P_1 > 27.83$ psia (choked flow)

$$u_{jc}^2 = \left[2\gamma/(\gamma + 1)\right]\left[(P_o^{1/\gamma})/\rho_o\right]\left[P_1^{(\gamma-1)/\gamma}\right]$$

or, in ft/sec,

$$u_{jc} = 6.76 \times 10^2 \left[(P + P_o)^{0.143}\right] \qquad (23)^*$$

where P_1 = total pressure outside the opening
$= P + P_o$
P = pressure in excess of ambient
P_o = ambient pressure.

In the numerical forms of Eq 22 and 23, P and P_o must be in psi.

Eq 22 and 23 are also plotted in Fig. 32. As can be seen, until pressures are quite high (≈ 43 psi) jet flow velocity exceeds flow velocity behind the shock front. Note that the pressure P to be used in jet flow velocity calculations in Fig. 32 (and in Eq 22 and Eq 23) may be incident shock pressure, or reflected pressure or something in between. It is the pressure that drives the flow through the opening.

---

* Eq 22 and 23 do not include an empirical discharge coefficient of 0.7 apparently required with small models. Rempel suggests that its value may be 1.0 with full-size structures.

FORCES AND ACCELERATIONS DUE TO FLOW

Dynamic Pressures

The dynamic pressure

$$q = \rho u^2/2 \tag{24}$$

is a factor inherent in the Bernoulli equation for steady flow. It represents the additional pressure in a stream that exists because there is flow; i.e., the increase over the pressure that would exist if there were no flow. It also represents one half the momentum per unit area that flows past a particular section of a fluid per unit of time. Thus, for a body immersed in a fluid, the product of dynamic pressure and area of the object presented to the flow (and a factor dependent on the object's particular configuration) gives the force imparted to the body because of the flow. If an object or obstacle changes the momentum of the fluid, the force required to change that momentum is also a function of q.

Dynamic pressure in shock flow, from the Rankine-Hugoniot equations, is:

$$\begin{aligned} q_s &= \left[(25/14)(\rho_o a_o^2)\right]\left[P_s^2/P_o(7P_o + P_s)\right] \\ &= 2.69\ P_s^2/(7P_o + P_s) \end{aligned} \tag{25}$$

with P_s, P_o, and q_s in psi

where ρ_o = atmospheric density

a_o = atmospheric sound speed

Dynamic pressure in unchoked jet flow, in which the jet density is quite close to atmospheric density of 0.0025 slugs/ft^3 (lb-sec^2/ft^4) can be derived from Eq 22

$$q_{ju} = 23.8\left[(P + P_o)^{0.286} - 2.155\right] \tag{26}$$

Again with P_o, P, and q_{ju} in psi.

In choked jet flow, the core density changes with increase in pressure:

$$\rho_{jc} = 2.327 \times 10^{-4} (P_o + P)^{1/\gamma} \qquad (27)$$

with P_o and P in psi, and ρ_{jc} in slugs/ft^3 (lb sec^2/ft^4)

Since velocity in jet flow is a function of pressure raised to the $[(\gamma-1)/2\gamma]$ power (see Eq 23), dynamic pressure becomes a linear function of total exterior pressure

$$q_{jc} = 0.37 (P + P_o) \qquad (28)$$

with P_o, P and q_{jc} all in psi.

Values of q for both shock flow and jet flow are plotted in Fig. 32. As with flow velocities, jet flow q is very much larger than shock flow q over most of the pressure range of interest. They cross at a pressure of about 26 psi.

Forces Due to Drag

If an object quickly becomes immersed in the flow, the principal forces on it are due to drag; i.e., those forces, akin to friction, caused by the flow past the object. They are given by

$$F_D = (C_D A)q \qquad (29)$$

and impulse imparted by flow whose dynamic pressure is changing with time is

$$I = C_D A \int q \, dt \qquad (30)$$

where C_D, termed a drag coefficient, is a factor associated with the object's geometry

A is the area of the object presented to the flow.

The integral is termed dynamic pressure impulse, I_q.

Acceleration Due to Drag

The motion of an object exposed to drag forces can be determined from Newton's second law which, for an impulsive loading, can be written as

$$\Delta v = I_D/M \tag{31}$$

where Δv = change in velocity of the object
I_D = drag impulse given by Eq 30
M = object mass.

Combining Eq 30 and 31 we have

$$\Delta v = (C_D A/M) I_q \tag{32}$$

The factor $(C_D A/M) = C_A$ is called acceleration coefficient and is common to all calculations of accelerations due to drag. Values of C_A for people and various other objects are given in Table 3.

Drag accelerations are most likely to be of importance in cases where the shock wave enters a large opening behind which are movable objects. Structures with such openings are likely to be encountered at relatively low pressure levels, where drag accelerations in shock flow are negligible. (As can be seen in Fig. 32, with a shock wave pressure of 3 psi, dynamic pressure is less than 0.3 psi.) Therefore, in the remainder of this element of the report, only jet flow acceleration will be considered.

Jet Flow Accelerations - An approximate — but conservative — expression of dynamic pressure impulse due to flow in the core of the jet caused by shock waves, using the modified exponential pulse of Eq 1, is:*

$$I_{qj} = (0.4\, q_j)(t_o - t_j) \tag{33}$$

where
t_o = pulse duration from Fig. 3
t_j = the jet flow clearing time from Eq 19
q_j = the dynamic pressure at time t_j, from Fig. 32.

* (See footnote, page 57)

The pressure driving this flow is essentially that of the incident wave at time t_j. This can be taken from Fig. 1, or—more conveniently — from Fig. 33, a log-log plot of the relationship $\left[1 - (t/t_o)\right]e^{-\alpha t/t_o}$ from Eq 1. For most situations of interest, only the highest line of Fig. 33, that for a pressure range between 0 and 20 psi, need be used.

Combining Eq 32 and Eq 33, the change in velocity of an object completely engulfed in jet flow is

$$\Delta v = 57.6\ C_A q_j (t_o - t_j) \qquad (35)$$

The units of Δv are ft/sec, those of t_o and t_j are sec, those of q_j are psi and those of C_A are $ft^2/slug = ft^3/lb\ sec^2$.

While Eqs 33, 34, and 35 apply only to the core of jet flow, the same procedures can be used to determine drag accelerations on an object downstream from the end of the core and off-axis accelerations as well. In the main region of the jet (see Fig. 31) axial velocities can be determined from Eq 17, and off-axis velocities from Eq 16. In these equations u_o is the velocity in the core, which can be derived from Fig. 32. Once u_m (axial velocity) and u (off-axis velocity) have been determined, use Fig. 32 to find the pressure that will cause each velocity, and from that the dynamic pressure. Eq 35 then gives the velocity of the object.

(from page 56)

* For an opening in the front face of a structure, Eq 33 actually only applies for $t_j \geq 3\ S/U$. If t_j is significantly smaller than 3 S/U, and drag impulse is still desired, Eq 33 should be replaced with

$$I = (1/2)\ q_j(t_c - t_j) + q_c(t_{of} - t_j) \qquad (34)$$

where t_c = 3 S/U

t_{of} = duration of equivalent pulse = $2\ i_s/P_s$

i_s = impulse from Fig. 3

q_c, q_j = jet dynamic pressure at time t_c or t_j

Similar changes should be made for back wall openings if $t_j << S/U$. No changes in Eq 33 need be made for side wall or roof openings.

If the object of interest is in the transition region, it is suggested that linear interpolation between the opening and the main region be used.

Forces on Flat Surfaces

Analysis and Prediction Equations - A shock wave will interact with a flat surface in the manner discussed earlier in this report. In essence, it reflects from the surface, and a reflected wave forms and moves upstream. The surface experiences forces normal to it as long as the shock wave is in contact with it. Techniques for calculating these forces are given in Section II-3. The remainder of this section is concerned with forces due to jet flow.

The interaction of a free jet with a flat plate (or equivalent such as a wall of a duct behind a vent) differs from that of a shock wave in that the jet is redirected to flow along the plate. Force on the plate due to this redirection can be calculated from momentum considerations (see, for example, Ref. 43). In steady flow, a plate oriented normal to the direction of a jet reduces the momentum in the direction of jet flow to zero, if the plate is large enough. The force on a plate from a jet in which velocity does not vary with distance from the axis of the jet is

$$F_j = A\rho u^2 = (2A)q \tag{36}$$

where A is the area of the incident jet
ρ is the density in the jet
u is the incident jet velocity
q is the dynamic pressure of the jet

If the loading is both changing with time and of short duration (i.e., impulsive), the impulse imparted to the plate in a time t is

$$I_j = A\rho\int u^2 dt = 2A\int q\, dt \tag{37}$$

If the jet actually interacts with a configuration which reverses its

direction (rather than redirecting it by 90 deg), Eq 36 becomes

$$F_j = 2A\rho u^2 = (4A)q \qquad (38)$$

and Eq 37 will be similarly changed.

Not apparent in any of the relationships given before is an important fact that greatly simplifies the problem of predicting forces on surfaces upon which a jet like that shown in Fig. 31 impinges: the equations describing the characteristics of the jet are consistent with conservation of momentum. Since the density is about equal throughout the jet ($\rho = \rho_0$), the total momentum flux (momentum per unit of time) passing any section of the main region of the jet sketched in Fig. 31 is given by

$$\text{momentum flux} = \rho_0 \int_0^b 2\pi y u^2 dy \qquad (39)$$

in which u along the axis of the jet is given by Eq 17, and as a function of distance y from the axis by Eq 16

At the opening, the momentum flux is

$$\rho_0 \int_0^{b_0} 2\pi y u_0^2 dy = \pi b_0^2 \rho_0 u_0^2 \quad \text{or} \quad (2A_0)q_0 \qquad (40)$$

identical with Eq 39 with subscripts only changed. Substitution of Eq 16 and Eq 17 in Eq 39 and integrating gives identical results (within the accuracy of the constants used).

Thus, as long as the jet through an opening retains the characteristics of that described by Abramovich, forces and impulses on flat plates can be calculated from Eq 36 and 37, with values A_0 and q_0 substituted. If there is additional redirection back toward the origin of the jet (as might occur in a small room) forces could be somewhat larger, as shown in Eq 38 where the redirection was complete.

Since a jet through an opening from a blast takes a finite time to form, pressures driving the flow through the opening will be less than those that would be driven by peak pressures. Assuming that structure clearing is completed before the jet flow clearing is complete, force on a plate would be given by

$$F_j = 2A_o q_j \tag{41}$$

in which q_j is the dynamic pressure at the time of jet clearing. As with Eq 33, an approximate value of impulse, based on Eq 1, is:

$$I = 0.8\, A_o q_j (t_o - t_j) \tag{42}$$

These forces and impulses will be distributed over an area approximately equal to

$$A = 0.15\, d^2 \tag{43}$$

(from Eq 18).

Experimental Information - Shock Tunnel Tests - The tests on a full-scale room with a window conducted in the shock tunnel (see Fig 20 and 21) tend to confirm the applicability of this approach to forces generated by changing the direction of flow, although too much else was going on for the results to be definitive. The rear wall gauges in these tests recorded an initial step change of pressure as the initial shock wave reflected from the wall, but, as shown in Fig 22, later pressures were substantially greater than those shock front pressures. As with side wall pressures, the traces from centrally placed rear wall gauges rose to a peak at about 5 ms, then fell to minimums that occurred at between 15 to 20 ms. They then rose again to another peak at around 30 ms, and another at about 50 ms. In these tests b_o = 7.2 ft, and Eq 18 indicates that the jet flow clearing time was about 18 ms, much smaller than the flattop portions of the pulses which were on the order of 50 ms long. The total area of the window wall occupied 80% of the wall area, and gauges in the tunnel side walls upstream from

the front wall appeared to indicate that driving pressures were somewhere between reflected pressures and 80% of reflected.

The room geometry was such that flow reversal of the jet through the opening would take place, and therefore Eq 38 should apply. Table 4 lists predicted values of pressure on the rear wall due to flow reversal, using the lower value of driving pressure, and measured values from the rear wall gauges at the low point behind the first peak. It can be seen that predicted and measured values agree quite well.

Times of occurrence are generally as might be predicted (note that zero times for the traces of Fig. 28 are the times of arrival of the shock at each of the gauges). As noted earlier, however, many other things were going on. The first peak for example, probably stems from the arrival at the rear wall of the pulses reflected from the side walls (see Fig. 29). And the second peak coincides reasonably well in time with the predicted arrival times of pressure pulses that reflected from the rear wall initially, returned to the front wall, thence again to the back wall.

CHAMBER FILLING DUE TO JET FLOW

Filling, defined as the overall pressure rise in a chamber or structure due to flow into it, will not generally be a problem with accidental explosions because of the time required for the process. This can most easily be seen by noting that Kriebel (Ref. 44) has shown that filling time t_f in ms from a constant pressure blast pulse is approximately

$$t_f = V/2A \qquad (44)$$

where V is the volume of a chamber in ft^3
and A is the area in ft^2 through which filling takes place.

The equation is dimensionally inconsistent, but still useful. It indicates, for example, that with an opening of, say, 2 ft high x 3 ft wide ($A = 6\ ft^2$) and a very long duration pulse (long enough that pressure can be considered constant), a small structure 8 ft high x 10 ft wide x 10 ft long ($V = 800\ ft^3$), would have a fill time of 800/12 = 66 ms, longer than the entire duration of most of the accidental explosions of interest here.

Knowledge of the filling process can, however, aid in the design of plenum chambers, and other devices designed to mitigate the effects of jet flow. A step-wise technique for calculating fill pressures is given in Ref. 1, but the following much simpler approximate technique, based on analysis of filling relationships, should give conservative results far more quickly.

The technique is based on the observations by Rempel that over a very large range of ratios of chamber pressure to driving pressure (0.2 to 0.8), pressure rise in the chamber is almost independent of the chamber pressure and that Eq 44 itself holds approximately over a similarly wide range.

Therefore, even with a changing pressure regime outside, the role of filling should not change significantly. The pressure inside the chamber should rise to a maximum about equal to the exterior pressure,* then begin to fall as the chamber empties to the lower pressure surrounding air.

* Experimental evidence suggests that for structures with an opening in the front face (i.e., head-on shock incidence) whose area ratio A_r, (A_r = area of opening/area of face) ≥ 0.05, phenomena related to other structural dimensions can result in pressure fluctuations of up to twice fill time pressures prior to eventual filling (see Fig. 17 and 19).

Section II-5
INTERIOR DESIGN LOADINGS *

As with the exterior design loadings on solid structures discussed in Section I-2 (as well as those on structures with openings in Section II-2) loadings on interior walls, ceilings, floors, etc. that are to be used for structural design will be highly simplified. Many of the transients discussed in Section II-3 on shock waves and in Section II-4 on flow effects can safely be ignored because the duration of these transients is far shorter than the natural period of structural elements.

The interior design loadings can be of three types depending on the incident pulse duration, the size of the opening, and the dimensions and volume of the interior space downstream from the opening. Clearly, if the incident pulse duration is shorter than the jet clearing time (Eq 19, $t_J \approx 4 D_o/c$) no effects of jet flow in the interior need be considered. Interior loadings on side walls, roofs, floors and rear walls will be determined by the behavior of the shock wave in the space.

If, however, the pulse duration is long compared with the jet clearing time, internal loadings due to flow can be of importance. The flow-related loadings themselves can be of two basic types: those due to dynamic pressures, in which the direct action of the jet is important; and those due to filling phenomena, in which direct jet forces are less important than overall pressure changes within a chamber.

---

* See Section II-6 for calculation methods.

DESIGN LOADINGS DUE TO SHOCK WAVES - NO FLOW EFFECTS

General Description

A shock from an opening in a front wall will spread out as described in Section II-2. If it encounters side walls (or, with multiple openings if it encounters imaginary surfaces – see Fig. 25) it will reflect from these surfaces. If the interior is long enough compared with the distance between reflecting surfaces, it will become essentially plane. In any case, it will eventually reflect from the rear wall of the interior, and move upstream again.

With no other openings in side walls, roof, or rear wall, (and with no leakage to the outside through the walls) the strength of this upstream-directed pulse will be essentially the same as that of the plane wave pulse incident on the rear wall. This reflected wave will return to the front wall, lose some strength on reflecting from that wall, and will be redirected again toward the rear wall. Several such cycles can take place.

If side walls, roof, and rear wall contain openings, the shock wave will be further weakened during each reflection and passage. During each reflection, the peak in peak pressure of the reflected pulse can be taken as approximately equal to the ratio of opening to total area of the reflection surface; during each passage of the shock wave along a side wall, the decrease will be approximately in proportion to the total open area passed by the shock wave to the area of the shock front itself.

Initial Loadings

Described in the following material are loadings during the initial passage of the shock wave.

Front Wall Loadings - Forces on the interior of a front wall, even without any jet flow, can be significant. This is illustrated by Fig. 34, a typical example of data recorded during tests on a room with a window in the shock tunnel (see Fig. 21). Gauges G and H, on the downstream face of the window wall, recorded substantial pressures at very early times. (Gauges A and B, on the upstream face of the same wall, show only small changes from reflected values.) There is strong experimental evidence that interior loadings follow the same general pattern as followed by loadings on the back face of a block; that is, overall pressures begin to rise as soon as the shock wave passes the opening, and they stabilize a short time later. There is not enough experimental information to define precisely when stabilization occurs, but, for relatively large openings (5% and above), the available evidence (for both doorways and windows reported in Ref. 43) suggests that, with long pulses, the stabilizing time is S"/U, where S" is the distance from the edge of an opening to a nearby reflecting surface. The value of pressure when stabilizing occurs appears to depend on the area of the opening relative to the area of the face it is in.

Similar information is not available for short pulses, or for cases in which the nearest reflecting surface is far enough away that S"/U is a significant proportion of (or even greater than) the total incident loading pulse duration t_{of}. For these cases it is recommended that no interior loading pulse on a front wall be considered.

Side and Rear Wall Loadings - As can be inferred from the summary of shock wave information in Section II-3, reflections from side walls (and roofs or ceilings) of an expanding wave bring the pressure at the reflecting surface to values equal to or exceeding their values along the axis. According to the criterion adopted for plane shock formation, however, side

wall pressures themselves could be both greater and smaller than plane wave values. Accordingly, unless specific structure geometries dictate against it:

- Interior design loadings on side and rear walls from short duration pulses will be derived from plane wave values (Eq 14).

If there are openings to the exterior in side and rear walls, upon initial passage and reflection of the shock wave from the rear wall, loadings will be taken as equal to those from Eq 14 (losses and gains through the openings being assumed to be roughly balanced). In addition, unless specific structure geometries dictate against it, the interior shock wave will be assumed to keep pace with any exterior wave.

DESIGN LOADINGS DUE TO FLOW EFFECTS -- FORCES AND FILLING

With pulses, whose duration is significantly longer than the jet clearing time, forces related to jet flow must be considered in addition to the shock wave forces just discussed. The two possible types of effects (jet forces and filling) can occur together, thus structures must be analyzed for both. As far as design loadings are concerned, both types of jet forces can be used directly. Their nature has already smoothed out short period transients.

Rear Wall Loadings

For many situations that give rise to jet forces, rear wall loadings may be determined from the simple expressions, given in Eq 41 for force at time t_j, and in Eq 42 for impulse. For simplicity of calculation, a triangular pulse whose peak is F (Eq 41) and whose duration is $2I/F = 0.8(t_o - t_j)$ can be used. Note that this force need not be applied over the entire wall. Eq 18 indicates its area of application to be approximately $0.15\ d'^2$.

If the geometry is such that flow reversal takes place, Eq 41 and 42 need only be multiplied by two.

Side Wall Loadings

Use of Eq 41 and 42 for the rear wall implies that interior side wall forces are zero, since pressure in the jet along a wall past which it flows is close to ambient pressure. Forces on side walls will be generated at earlier times by the shock wave (with initial values of about twice front wall values) and at later times by a plane wave proceeding down the structure or as a result of room filling.

Front Wall Loadings

In the models employed here (see Fig. 31), there are no initial loadings on a front wall due to jet flow. At later times, flow reversal from the rear wall can cause pressure increases on the front wall, though forces from filling are much more likely to occur.

Design Loadings from Room Filling

Room filling times are given approximately by Eq 44, and room filling forces are approximately those of the incident wave at the time t_f. For relatively large openings there do seem to be mechanisms which can give rise to significant transients before filling is complete, but predicting when these occur is not yet feasible.

Section II-6
NET DESIGN LOADINGS

Where the exterior and interior surfaces of the same wall in a structure are loaded by the same shock wave, the net loadings (difference between exterior and interior loadings) can differ substantially from either one alone. The differences depend on the type of loading being experienced in each case. Methods for predicting initial shock wave, and later flow dependent, loadings are given in this section. Note before proceeding, however, that all net loadings due to interior shock wave reflections after the first will be outward directed because the exterior shock wave will have already passed the structure

INITIAL SHOCK WAVE LOADINGS

Front Wall Loadings

Early time front-face loadings, (i.e., those due to shock diffraction inside a structure and rarefaction waves propagating outside a structure) can be greatly decreased by the upstream-directed interior forces. The type of change that can occur, and its possible magnitude can be seen in Fig. 35. Fig. 35A shows average traces from shock tunnel tests in a geometry similar to that of Fig. 21, but with the rear wall removed (Ref. 45). Fig. 35B relates the size of the decrease to the window opening area, as a percent of total wall area. (A solid wall, of course, has a 0% window opening area.) As can be seen, the decrease in net loading is quite large.

The upstream-facing interior loading has two effects: it tends to reduce initial clearing times below those due to exterior effects alone (i.e., 3 S'/U from Eq 5a or 5b), and it tends to reduce all values of net pressure after initial clearing occurs as shown in Fig. 35. (Note, the

shock tunnel had no "structural" clearing time. It represented a very large — infinite — structure with many identical openings, but with no roof or side corners.) It is clear that this initial clearing time should be related in some way to relative clearing distance, though a strict linear decrease does not appear justified. In a large structure with many openings, for example, the area near the center of the structure would clear as in Fig. 35A, but areas near the edges would be essentially unaffected, because structural (edge) clearing would take place quickly.

To account for these effects in a generalized loading scheme, the following is suggested:

1) Find S" = distance from edge of opening to nearest interior reflecting surface

2) Calculate $S_r = S''/S'$; S''/U and S'/U; $\Delta t = (3S'/U) - (S''/U)$; and A_o/A_f = (opening area)/(total front wall area)

3) Find new initial clearing time $t_c'' = \left[(3S'/U) - \Delta t(S_r^{\frac{1}{2}})\right]$

4) Decrease loadings at time t_c'' from their closed structure values* by the percentage given in Fig. 35B, using $(A_o/A_f) \times 100$ as "window opening" percentage

5) Decrease loadings at time $t_c = 3S/U$ by the percentage given in step 4, and draw line to P = 0 at time t_{of}.

These steps result in a three-part front face loading pulse in place of the normal two-part pulse of Fig. 10A. As an example, with the structure in Fig. 14A, S" = S', thus $S_r = 1$. The initial clearing times would be reduced to $(3S'/U) - \Delta t = S''/U$ Because the windows occupy 25% of the wall

* Fig. 35B essentially gives the reduction in net pressures from the shock tunnel equivalent of closed structure (peak reflected) values.

area, net pressures at that time (and later) would be reduced by 40% (Fig. 35B).

Note that after these reductions in clearing times and net loading pressures are made, the area under the resultant curve should be compared with the area under the reflected impulse curve (shown dashed in Fig. 10A), and the one with the smaller area (impulse) should be used. It is unlikely, however, that the reflected impulse curve will have a lesser impulse than that constructed above.

Side Wall Loadings

If differences in arrival time can be ignored, the side wall loading pulse shown in Fig. 10B will be reduced by an identical pulse on the interior surface whose peak pressure is $P_s A_r^{\frac{1}{3}}$. Thus, the peak of the loading pulse in Fig. 10B will decrease to $P_s(1 - A_r^{\frac{1}{3}})$. Effects of openings in the side walls can be ignored during the first passage of the shock waves (gains and losses from both exterior and interior balancing). On subsequent passages, however, outward-directed forces should be derived from Eq 6.

Rear Wall Loadings

Rear wall loadings will be substantially changed, both in magnitude and direction. The maximum initial outward pressure peak will be P_r as given by Eq 10, or for low incident overpressures, approximately by 2 P_s, where P_s is either the axial pressure during the intermediate (spreading) phase, or the plane wave pressure. Again, during the first interaction, the effects of openings on shock pressures can be ignored, but on subsequent reflections, outward-directed forces should be taken from Eq 6.

NET DESIGN LOADINGS DUE TO FLOW FORCES

For structures with large openings, (that is, those not likely to be exposed to high overpressures) and especially for those narrow enough, and long enough that a plane wave can form, overall flow forces on back walls will tend to be smaller than those caused by shock wave reflections. They will, however, occur at different times. In addition, jet flow forces may be applied over a more limited area than would shock wave forces, and thus be locally more intense.

NET DESIGN LOADINGS TO DUE FILLING

Eq 44 implies that after V/2 A ms, interior and exterior pressures on a wall through which filling takes place would be essentially the same. Thus, net pressures on this surface would be essentially zero. (As noted before, there might be some substantial outward force fluctuation before the time V/2A.) Net force on other surfaces must be determined for each case.

Section II-7

CONCLUSIONS AND RECOMMENDATIONS

CONCLUSIONS

This report dealt mainly with two very different aspects of accidental explosions. Part I dealt mainly with the explosions themselves; Part II dealt principally with the ways in which openings in structures can alter explosion effects from what they would be on closed structures.

The important conclusions from Part I were that virtually all explosions generate a blast wave characterized (at distances of interest for this report) by a sharp pressure rise followed by modified exponential pressure decay to (and below) ambient pressures. Of course, all shock wave characteristics depend on the explosive used, but they can also be affected by such things as explosive density and shape. Change of shock front pressure with distance from a spherical charge, for example, will generally not be the same as that from cylindrical charges with either large or small diameter-to-length ratios.

In Part II it was shown that openings in structures, such as windows, and doorways, can not only alter loadings used to design structures, but also will allow objects within such structures to be subject to blast forces. Important factors affecting design loadings are the ratio of open to solid structural areas, and the geometry of the structures themselves. Changes of design loadings from those experienced by closed structures can be profound. In one relatively simple structure, used as an example, total initial blast wave impulse on the wall closest to the explosive (the front wall) was halved, and a later impulsive load caused by internal reflections was of about the same magnitude as the initial impulse and directed upstream. Impulse delivered to the back wall of the structure actually reversed its direction.

Internal elements can experience direct blast wave forces and may also be subject to the force of a high-velocity air jet which can form because blast-induced pressures outside the opening are higher than pressures within

the structure. The jet tends to remain more concentrated than the blast wave itself. Flow through openings also serves to "fill" a structure; that is, to raise its interior pressure until that pressure is essentially the same as exterior pressure.

RECOMMENDATIONS

1. Develop and promulgate structural design methods that incorporate effects of openings (windows, doorways, vents, etc.) on blast loadings.

The very magnitudes of some of the predicted (and observed) effects suggest that standardized design methods should include them.

2. Design and carry out an analytical and experimental program in solving blast waves that are relatively short compared with structural dimensions.

Much of the experimental information used in this report was derived from tests designed specifically to provide answers to problems associated with nuclear weapons. Some of the shock tube tests described earlier, for example, used small models of full-scale structures deployed on nuclear tests. Similarly, the "full-scale" tests in the shock tunnel with an 8½ ft x 12 ft test section were supported by civil defense agencies.

Because of this, inadequate data exist on some important blast phenomena that are size dependent. The time required for a jet to form, for example, is dependent on the dimensions of the opening. The characteristics of jets which form only after blast pressure has decayed significantly from its shock front value are not well understood.

3. Design and carry out a program to investigate the influence of windows (that is, window glass itself) on design loadings.

While very little blast pressure is needed to break a window, it takes a finite time to do so. This time can be a significant portion of the duration of a blast pulse from an accidental explosion. How this phenomenon can affect loadings described earlier in this report is conjectural.

Table 1

LISTING OF EXPERIMENTAL INFORMATION

Sta	d'	d'/b_o	Experimental Values[1] P_s or P_{sr}	→ P_s		P_{so}	P_s/P_{so}
A. From Coulter (Ref. 33)							
1. Field Structure (Ref. 34) see Fig. 16A: H 8ft x W 8 ft x L 12 ft; Entrance: H 7 ft x W 2.9 ft; b_o = 5.1 ft.							
1	4 ft	0.79	3.6			4.7	0.77
2	4 ft	1.6	3.2			4.7	0.68
3.	12 ft	2.4		5.3	2.4	4.7	0.51
2. Model of Field Structure, see Fig. 16B: H 3.92 in. x W 4 in. x L 6 in. Entrance: H 3.49 in. x W 1.45 in.; b_o = 2.54 in.							
1	2 in.	0.79	4.2			5.2	0.81
1	2 in.	0.79	3.9			5.1	0.76
2	4 in.	1.6	3.9			5.2	0.75
2	4 in.	1.6	3.5			4.7	0.74
3	6 in.	2.4		6.4	2.9	5.1	0.57
3	6 in.	2.4		6.1	2.8	5.7	0.49
3. Shock Tube Structures with Movable Rear Walls and Variable Opening Size. See Fig. 18: H 15 in. All measurements taken on rear wall.							
a) Opening[2] = H 4 in. x W 2 in.; b_o = 3.2 in.							
	4 in.	1.3		7.3[2]	3.3	4.7	0.70
	8 in.	2.5		3.1[2]	1.4	4.7	0.30
	12 in.	3.8		2.9[2]	1.3	4.7	0.28
b) Opening[2] = H 2 in. x W 1 in.; b_o = 1.6 in.							
	4 in.	2.5		2.5[2]	1.2	4.7	0.26
	8 in.	5.0		1.5[2]	0.74	4.7	0.16
	12 in.	7.5		1.2[2]	0.57	4.7	0.12

Table 1 (contd)

Sta	d'	d'/b_o	Experimental Values[1] P_s or $P_{sr} \rightarrow P_s$	P_{so}	P_s/P_{so}
4. Cubical Shock Tube Structure (no illustration) with gauge in center of floor: H, W, and L = 4 in. Opening = H 1.245 x W 0.6245 in.; b_o = 1.0 in. (Data taken from gauge trace in Ref. 33)					
-	2 in.	2	4.2	10.7	0.39
B. Room with Window in Shock Tunnel (Ref. 34, 35), see Fig. 20: H 8.5 ft x W 12 ft x L 14.5 ft. Opening = H 4.5 ft x W 4.7 ft; b_o = 5.2 ft. All measurements taken on rear wall.					
five back wall	14.5 ft	2.8	0.58[3]	0.29	1	0.29
"	"	2.8	1.2[3]	0.60	2.1	0.29
"	"	2.8	2.0[3]	0.95	3.3	0.29
"	"	2.8	2.8[3]	1.3	4.5	0.29
two back wall	"	2.8	4.0[3]	1.8	6.0	0.3

Notes: (1) Pressures P_s at the rear wall causing the measured reflected pressures P_{sr} were calculated from

$$P_{sr} = 2P_s(7P_o + 4P_s)/(7P_o + P_s) \qquad (10)$$

This expression is based on the Rankine-Hugoniot relationships (derived from conservation of mass energy and momentum) governing conditions at the front of a shock. (See, for example, Lampson, Ref. 37 and Courant and Friedrichs, Ref. 38.)*

(2) Average values from two tests with identical incident pressures.

(3) Tabulated values were derived from individual traces produced by five gauges near the middle of the back wall of the room shown in Fig. 21. The record from Gauge D-1, a gauge quite close to a side wall, was not considered.

* Most works on aerodynamics and compressible fluid flow treat shock waves because they can affect flow through nozzles and the behavior of air-foils. The references cited are relatively early works in the field.

Table 2

PREDICTED AND MEASURED SIDE WALL PRESSURES (in psi)

Incident Pressure (1)	Predicted Side Wall Pressures (2)	Measured Side Wall Pressures Initial Peak	Average Plateau
1.0	0.78	0.8	0.9
2.1	1.6	1.7	1.6
3.3	2.6	2.6	2.2
4.5	3.5	4.0	2.7
6.0	4.7	4.4	3.2

Notes: (1) From shock tunnel calibration

(2) From Eq 12 for $\theta > 20^{\circ}$.

Table 3

VALUES OF ACCELERATION COEFFICIENTS (C_DA/M)

SPECIFIC ITEMS *	$ft^2/slug = (ft^3/lb\,sec^2)$
168-lb man:	
Standing facing (and sidewise to) wind	1.67 (0.708)
Crouching facing (and sidewise to) wind	0.676 (0.547)
Prone aligned with (and perpendicular to) wind	0.203 (0.708)
Average value for tumbling man in straight, rigid position	0.966
Typical stones, 1.0 g	10.3
Typical stones, 10.0 g	4.83
Window glass fragments, 1/8 in. thick:	
1.0 g, edgewise (and broadside) to wind	15.4 (18.4)
10. g, edgewise (and broadside) to wind	10.9 (23.2)
Steel spheres, 1/4-in. diameter	2.24
Steel spheres, 1/2-in. diameter	1.12
Aluminum sphere, 1/2-in. diameter	3.36
Concrete block	0.85
GENERAL ITEMS (Approximate)	
Spheres	0.5 A/M
Cylinders:	
axis perpendicular to wind (L/D = 1)	0.6 A/M
axis perpendicular to wind (L/D = 5)	0.75 A/M
axis parallel to wind	0.2 A/M

* Largely derived from Ref. 41 and 42.

Table 4

MEASURED VALUES OF REAR WALL PRESSURES IN THE SHOCK TUNNEL ROOM, AND PREDICTED VALUES ASSUMING FLOW REVERSAL (1)

Incident Pressure	Driving Pressure (2)	Predicted Rear Wall Pressures	Measured (3) Rear Wall Pressures
1.0	1.6	1.3	1.3
2.1	3.5	2.6	2.6
3.3	5.8	4.2	3.8
4.5	8.1	5.6	5.5
6.0	11.2	7.0	7.0

Notes:

(1) All pressures in psi

(2) 80% of calculated reflected pressure

(3) At low point after first peak.

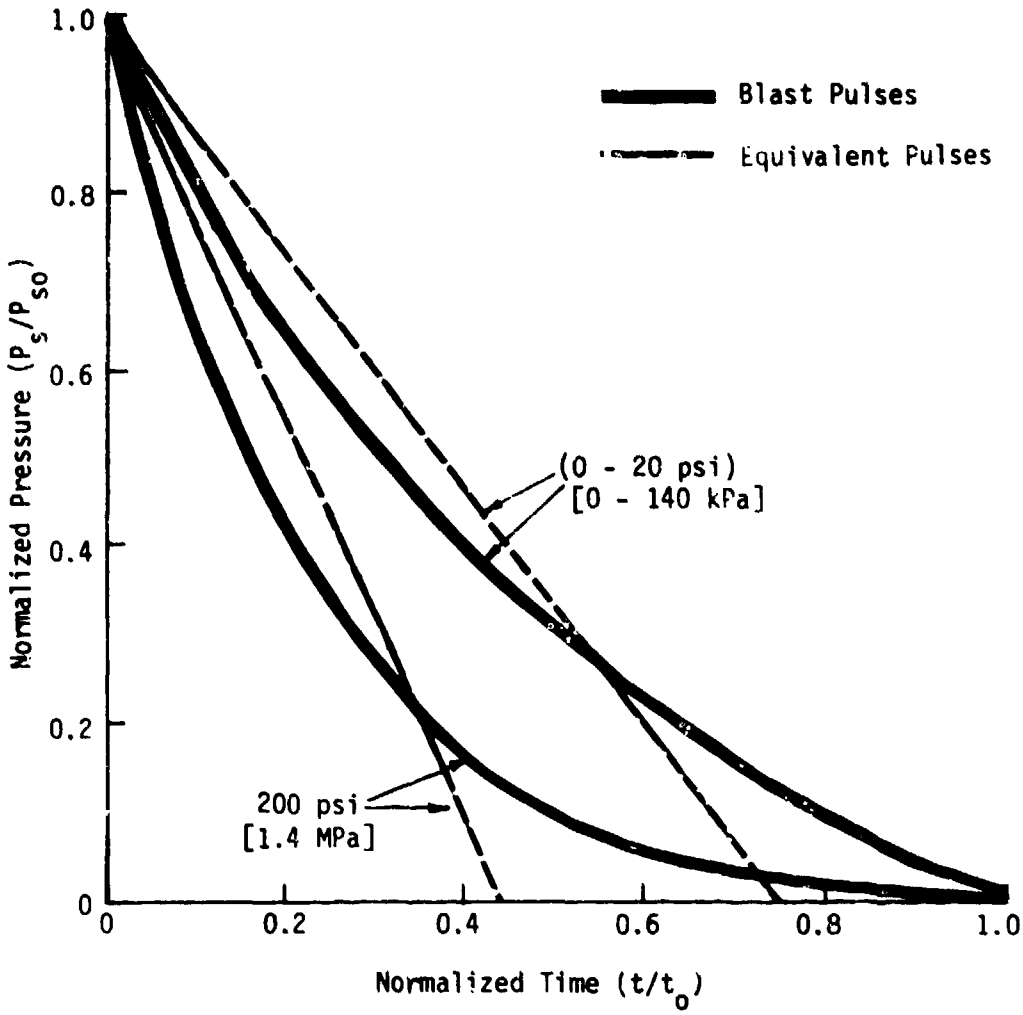

Fig. 1. Normalized Blast and Equivalent Pulses.

A. Ground View.

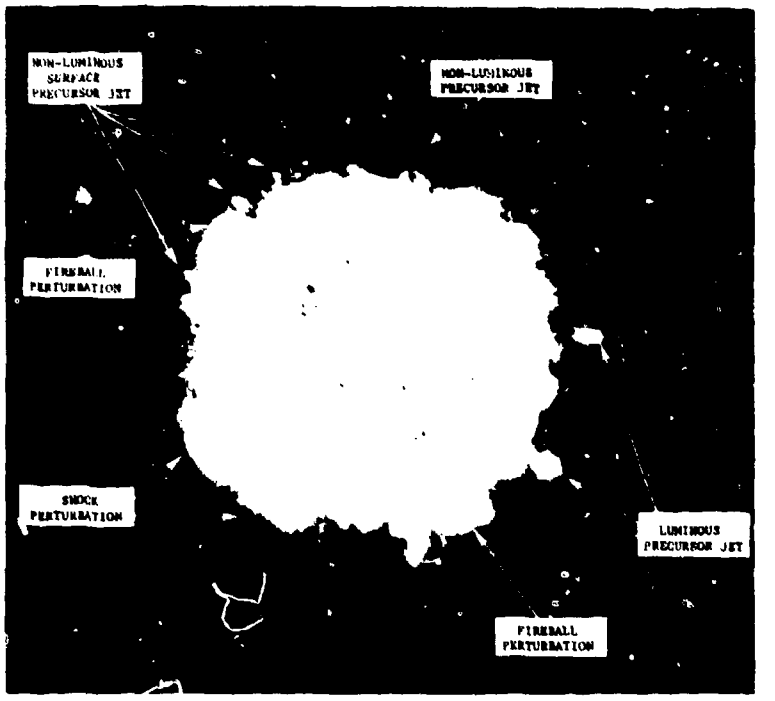

B. Aerial View.

Fig. 2. Blast Anomalies from a Burst of a 100-Ton TNT Charge, Tangent to the Ground.

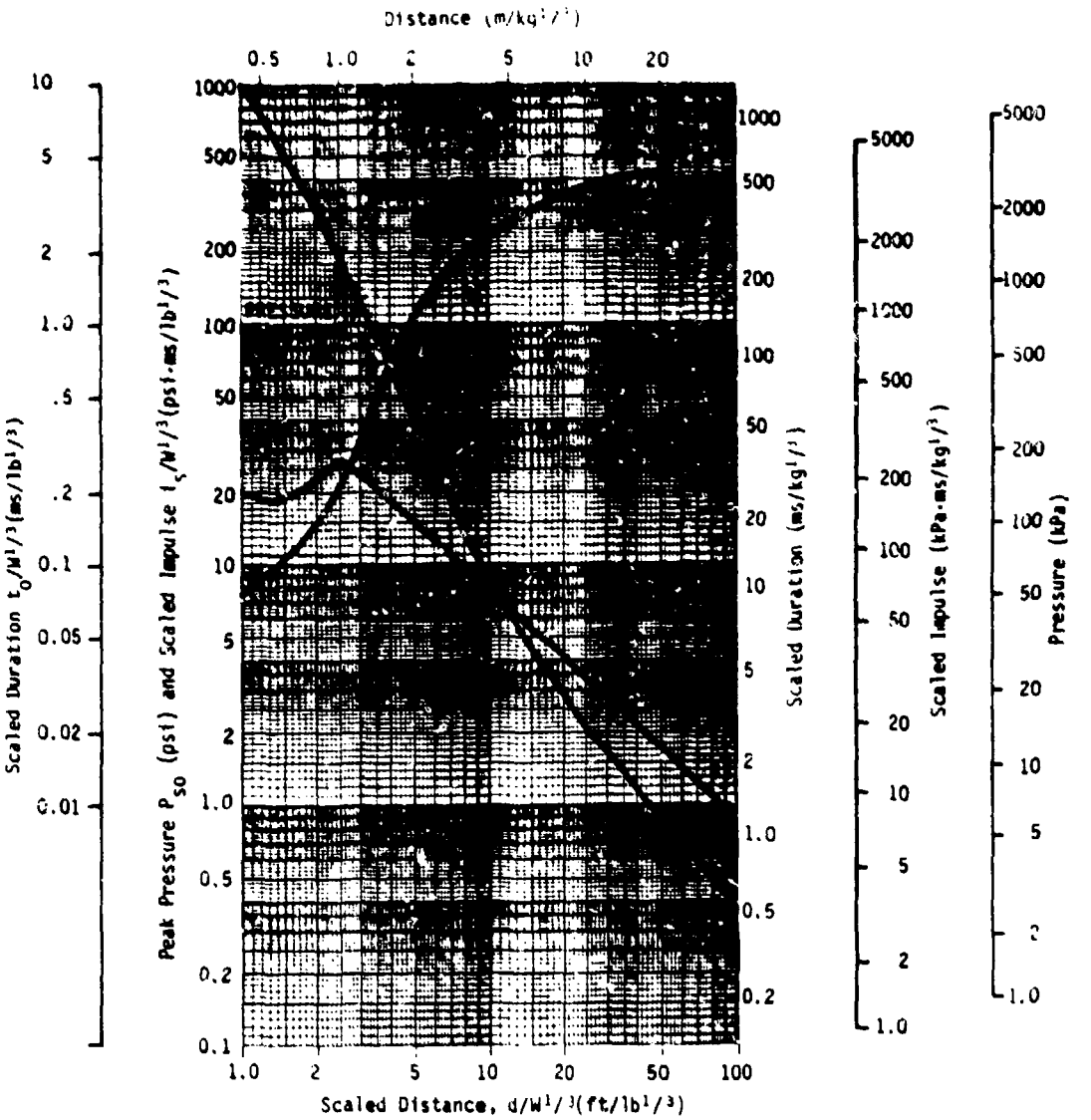

Fig. 3. Peak Positive Pressure, Scaled Positive Impulse, and Scaled Positive Duration vs Scaled Distance for Surface Bursts of Hemispherical Charges of TNT.

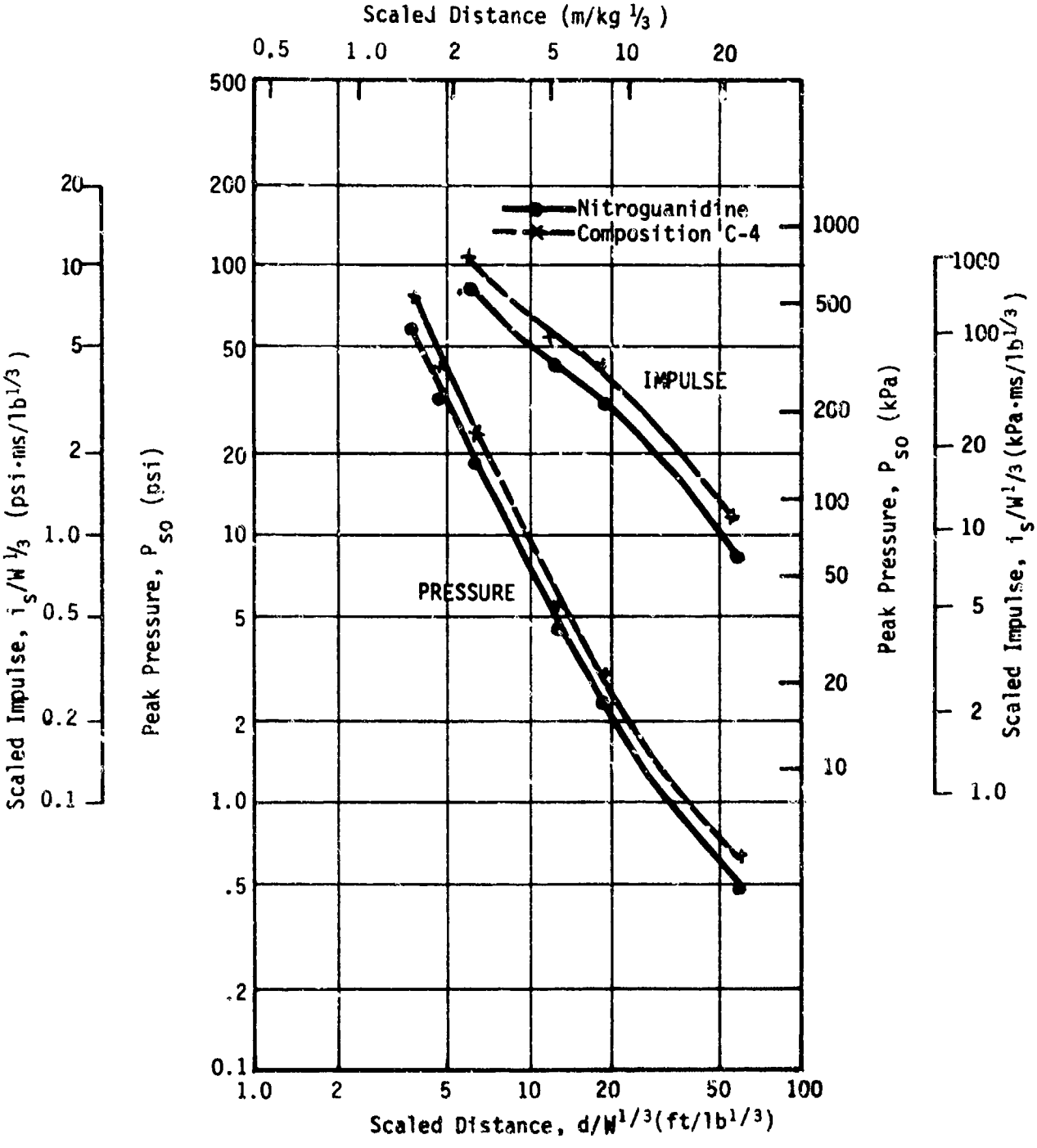

Fig. 4. Peak Pressure and Scaled Impulse vs Scaled Distance from Surface Bursts of 55 gm Hemispheres of Nitroguanidine with a Density of 0.31 gm/cm^3 and Composition C-4 with a Density of 1.6 gm/cm^3.

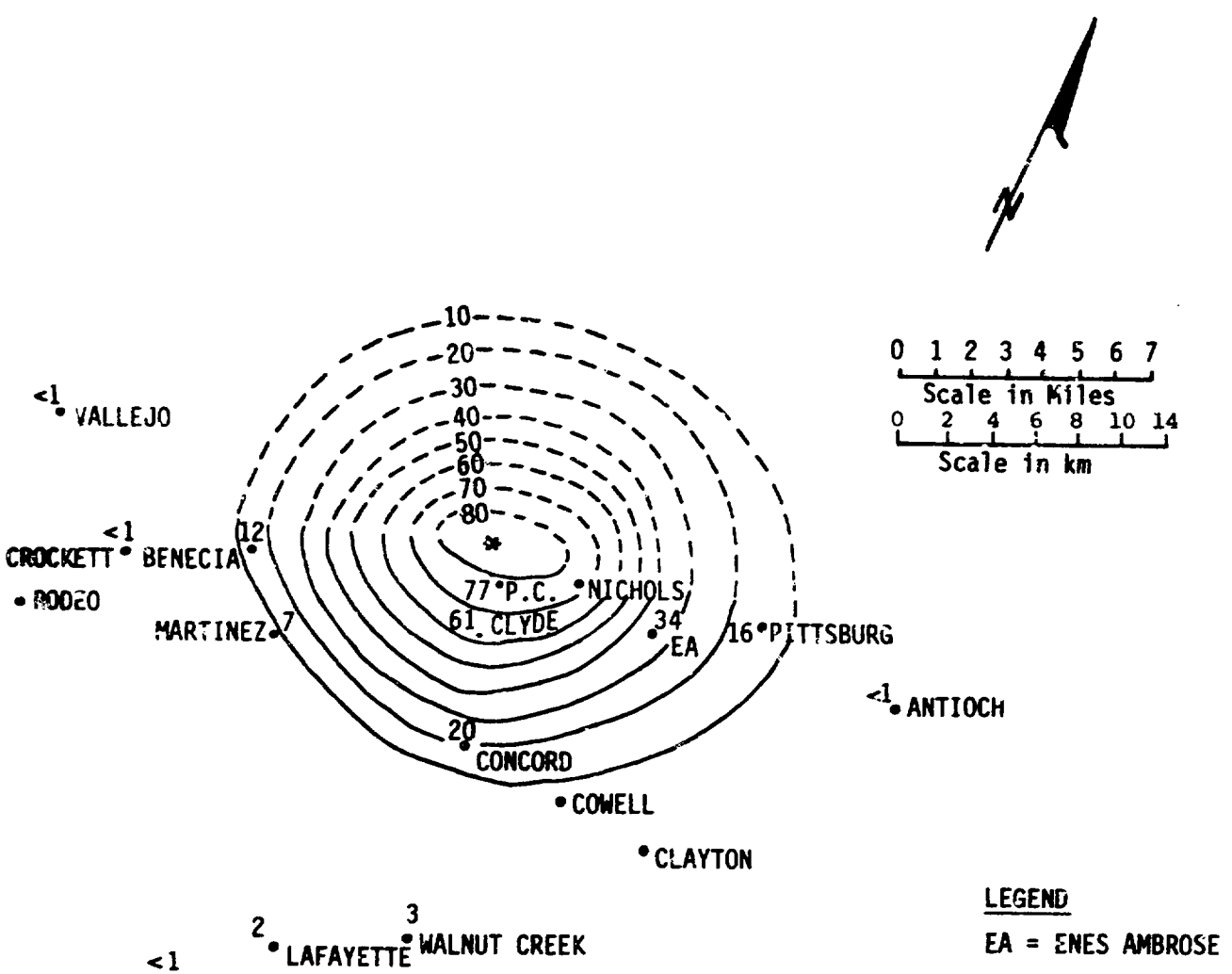

Fig. 5. Peak Pressure Contours from the Explosion of 1800 Tons (1.6 million kg) of High Explosives in a Ship at Port Chicago in 1944. Contours Derived from Window Breakage Data.

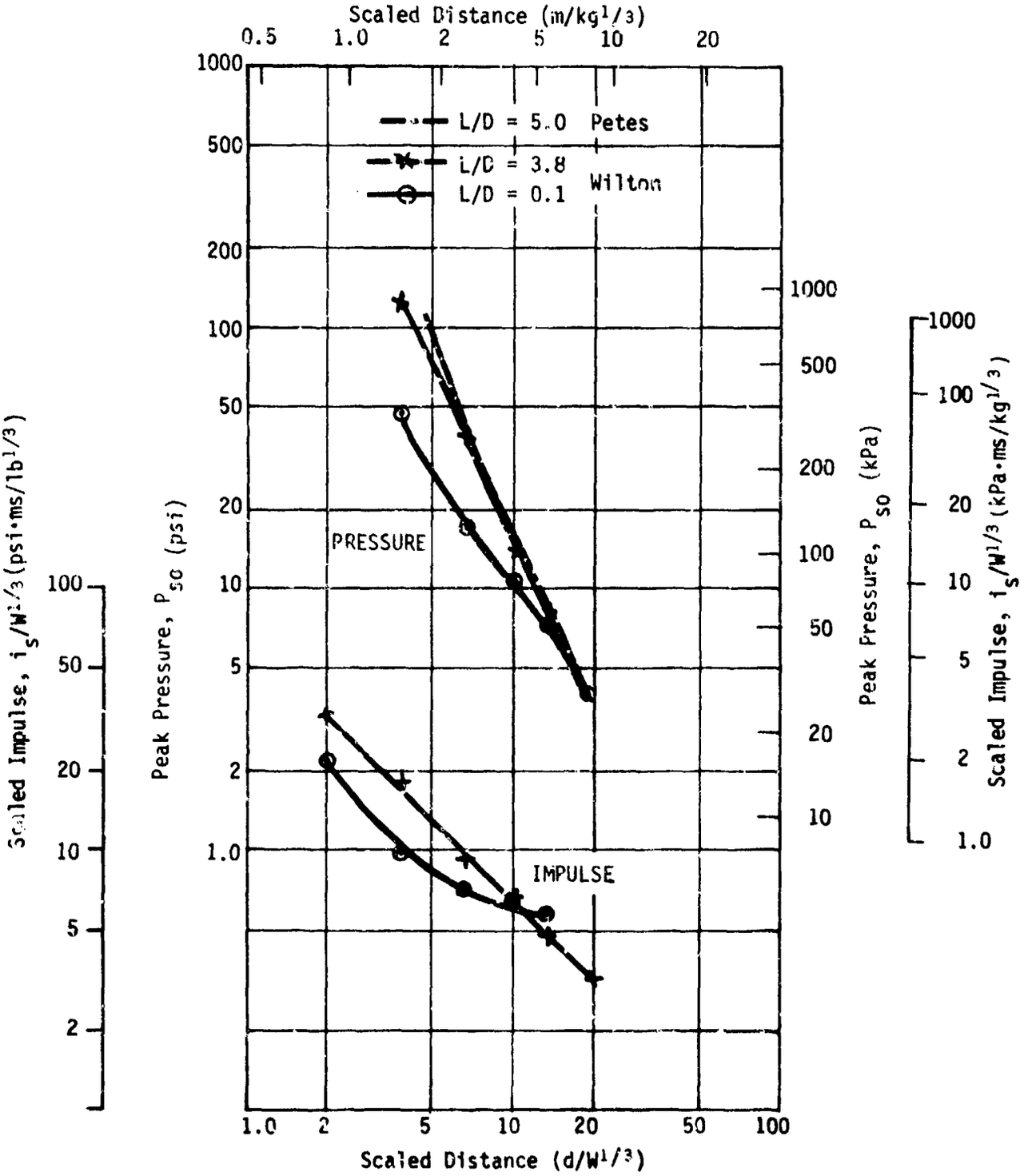

Fig. 5. Peak Pressure and Scaled Impulse vs Scaled Distance from Cylindrical Charges.
L = Axial Length of Cylinder
D = Diameter of Cylinder

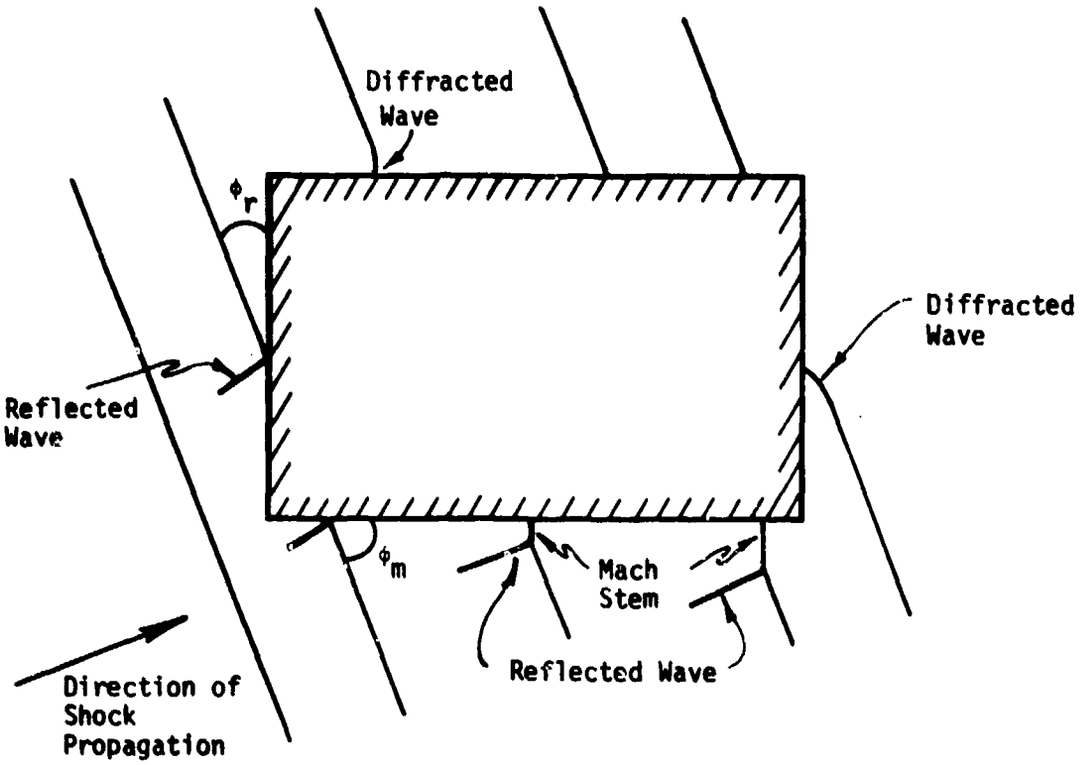

Fig. 7. Shock Wave Interactions with a Structure - Plan View

ϕ_r = Angle of Incidence for regular (two-shock) reflection

ϕ_m = Angle of Incidence for Mach (three-shock) reflection

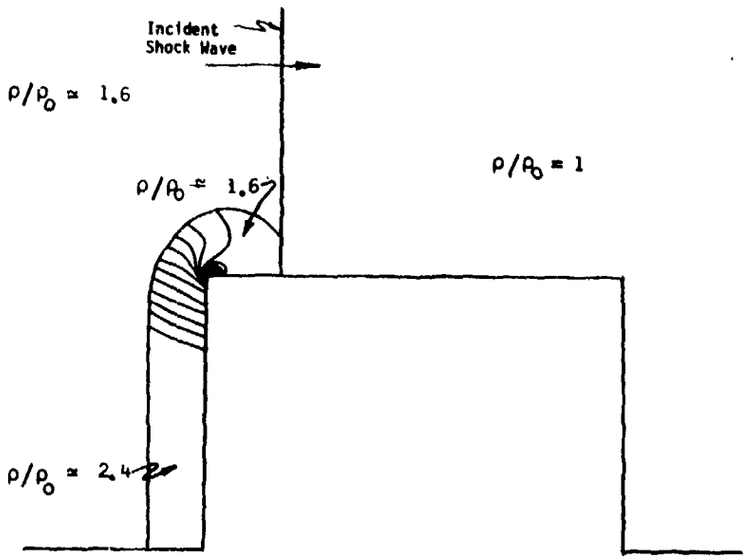

A. 15 μs After Striking Block

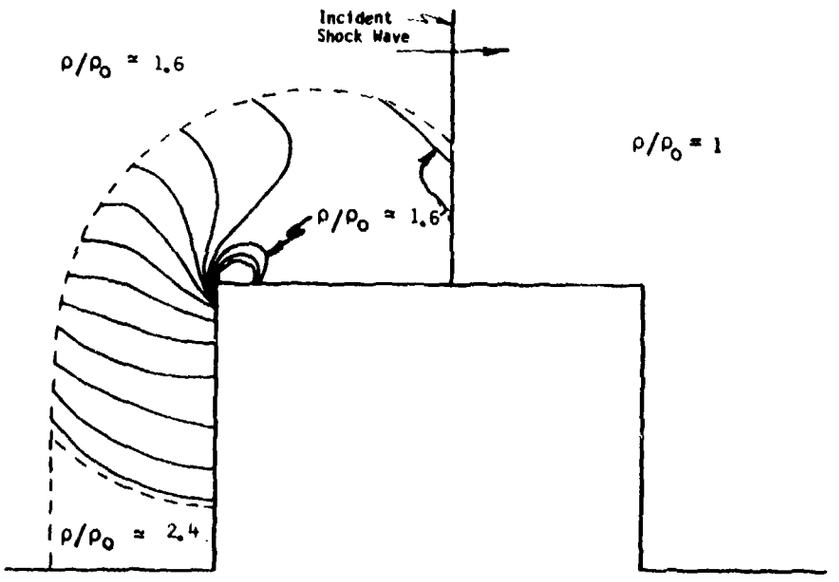

B. 45 μs After Striking Block

Fig. 8. Shock Wave Behavior at the Front Face of a Block. Isodensity Contours Behind the Shock are Shown. $\rho/\rho_0 = 1$ indicates ambient density; $\rho/\rho_0 = 1.6$ is density behind incident shock; $\rho/\rho_0 = 2.4$ is density behind reflected shock. Shock strength $\left[(P_{so} + P_o)/P_o\right] = 1.9$.

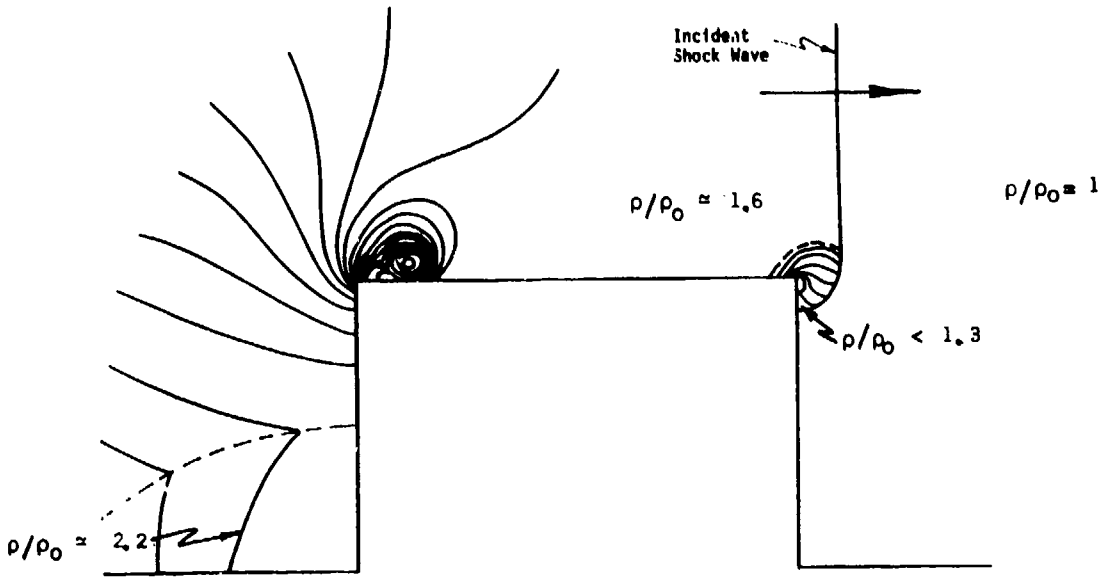

A. 90 μs After Striking Block

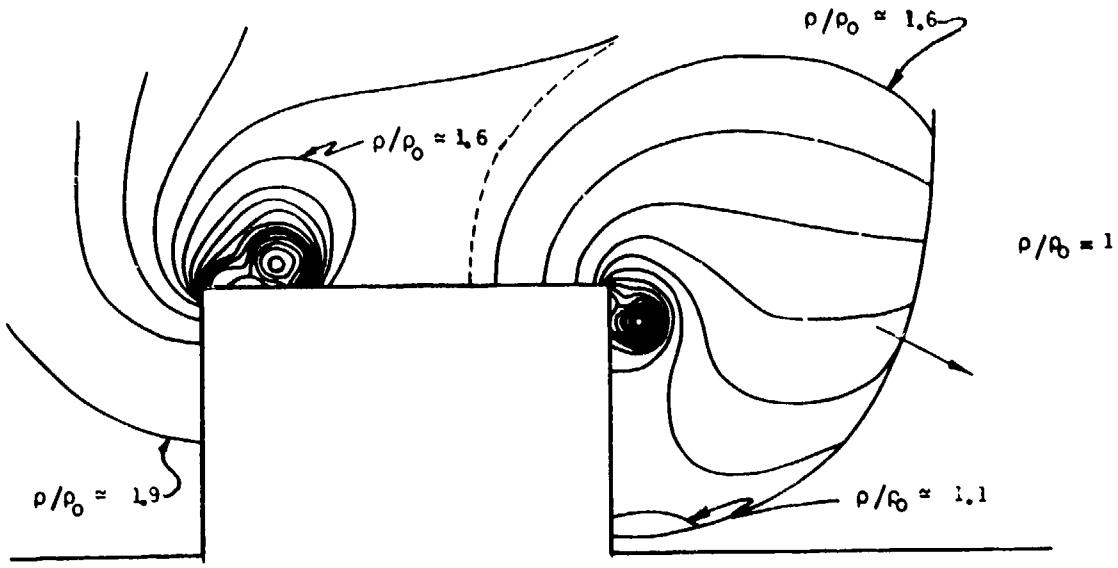

B. 149 μs After Striking Block

Fig. 9. Shock Wave Behavior at Both Front and Back Faces of a Block. Isodensity Contours are Shown. $\rho/\rho_o = 1$ indicates ambient density; $\rho/\rho_o \simeq 1.6$ is density behind incident shock; $\rho/\rho_o = 2.4$ is density behind reflected shock. Shock strength $[(P_{so} + P_o)/P_o = 1.9]$

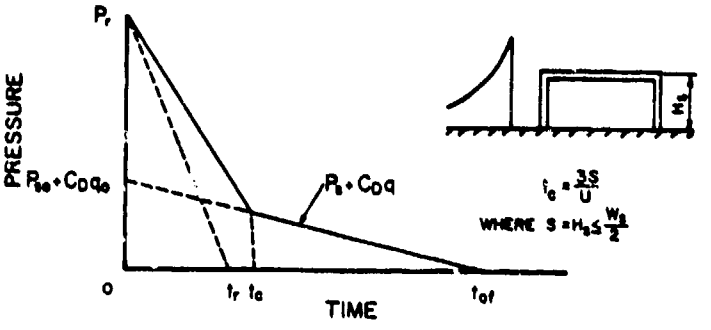

A. Front Face

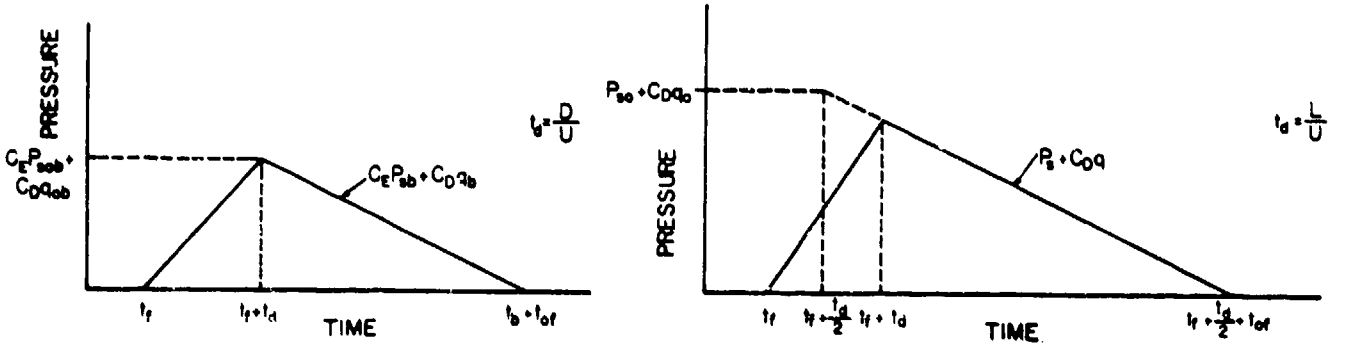

1. Perpendicular 2. Parallel

B. Roof and Side Walls - Spans Perpendicular and Parallel to Shock Front

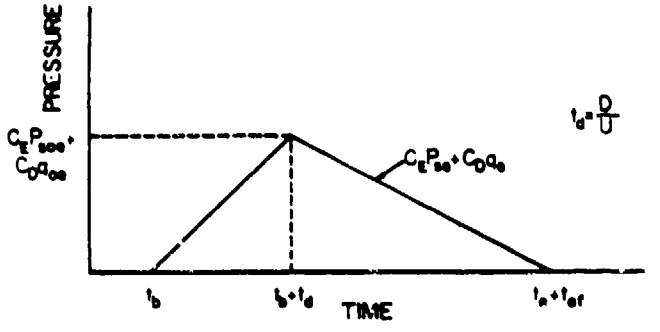

C. Back Wall

Fig. 10. Generalized Loading Patterns.

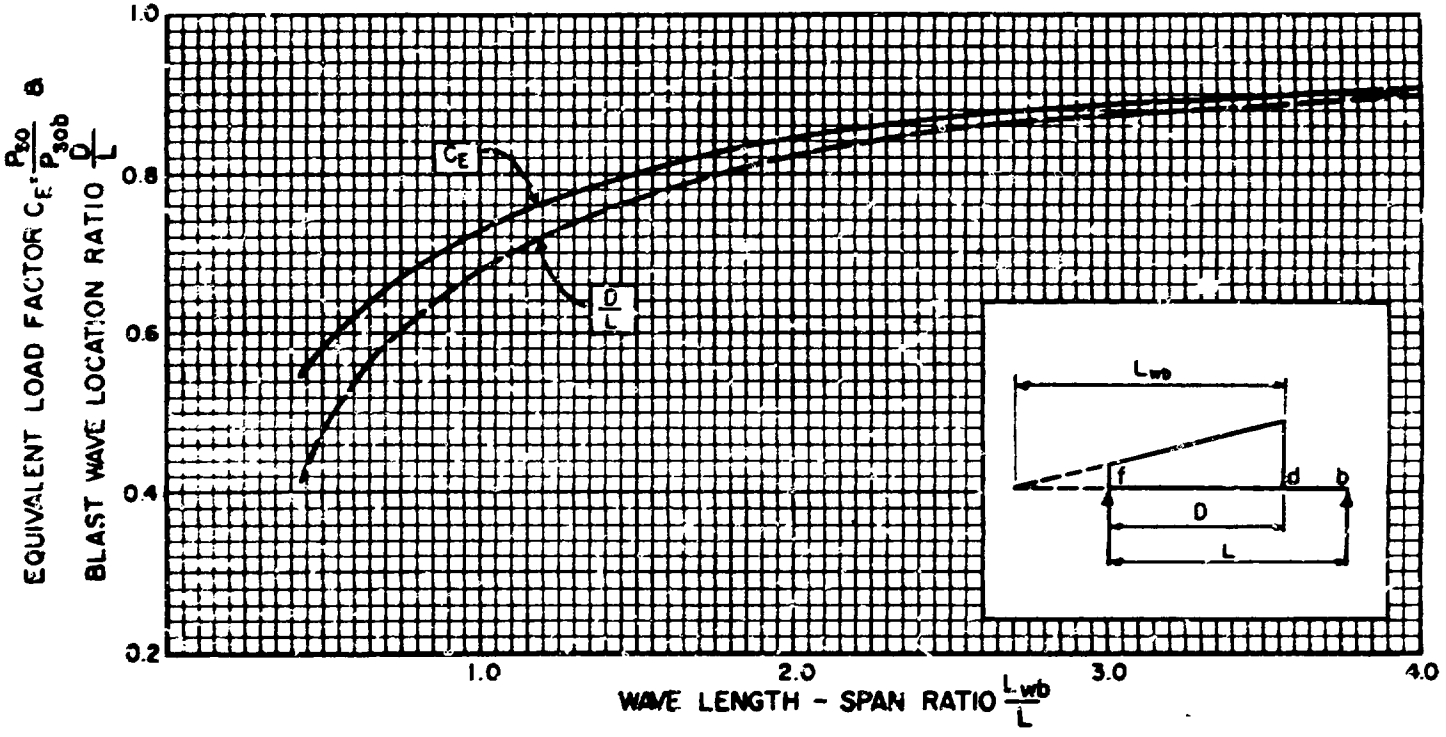

Fig. 11. Blast Wave Parameters for Use with Generalized Loading Patterns.

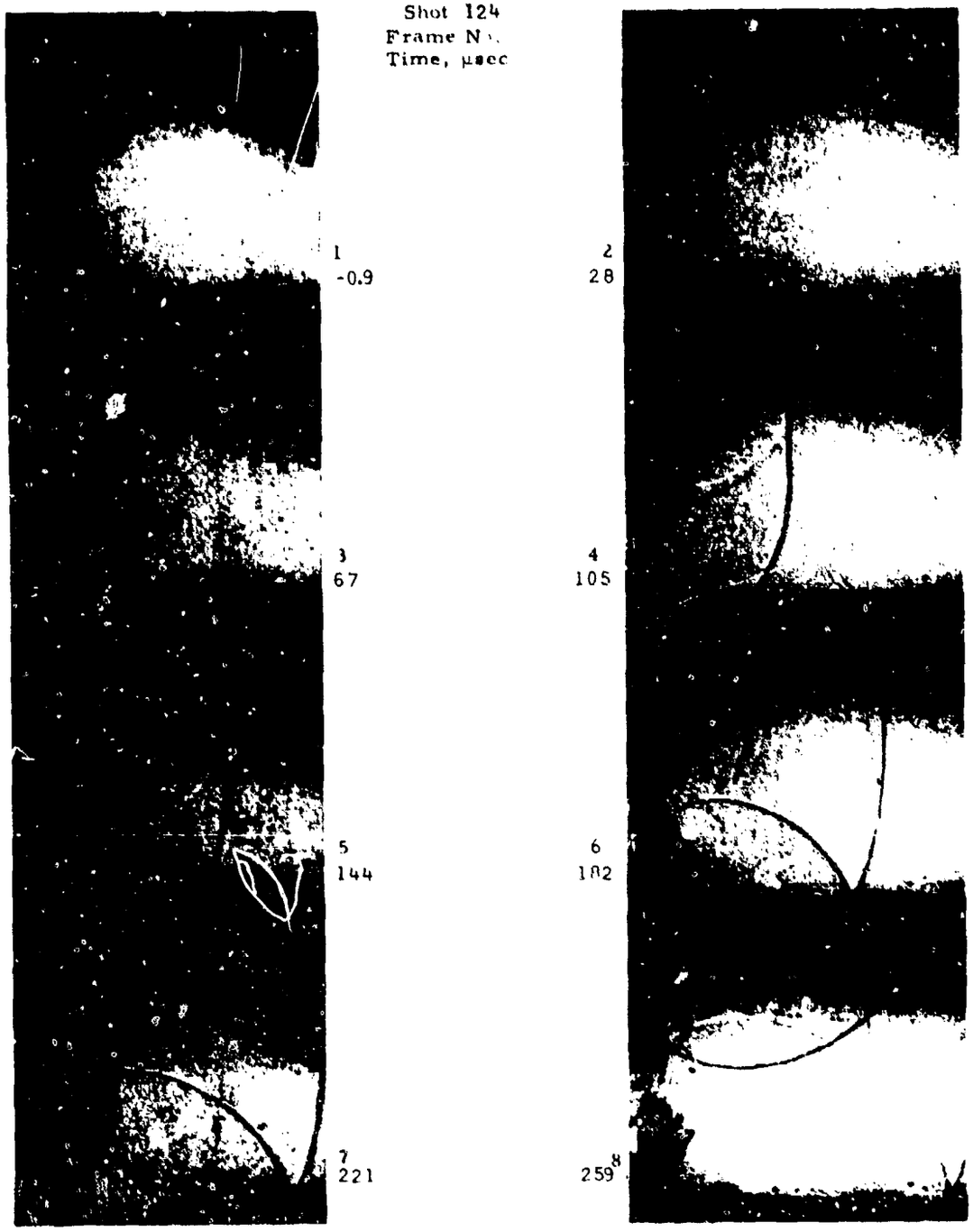

Fig. 12. Shadowgraphs of Snock Wave Entrance into a Chamber.

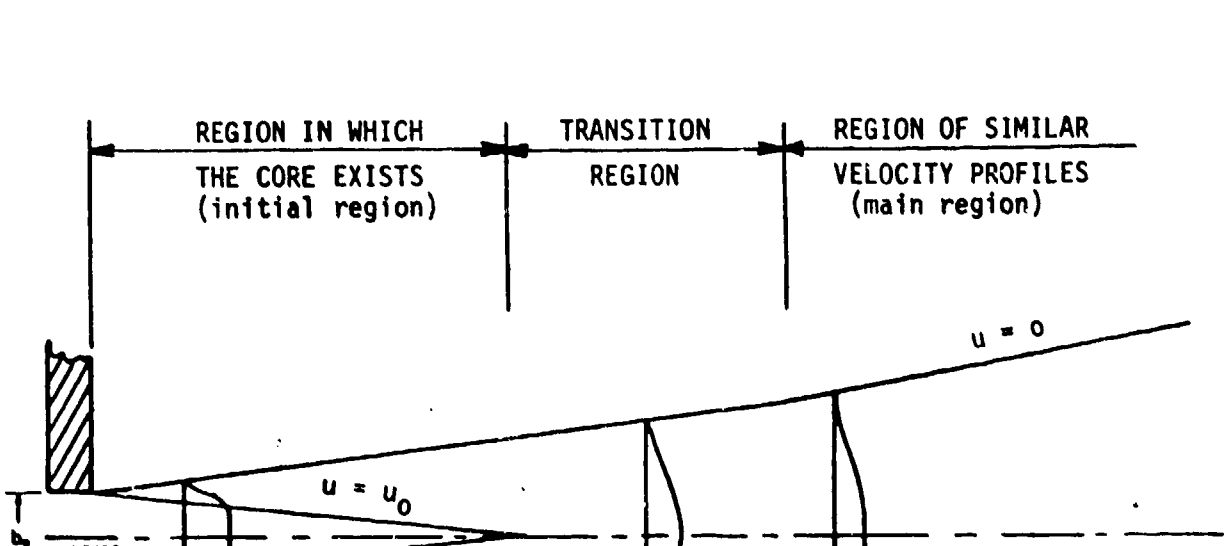

Fig. 13. Schematic of Jet Flow.

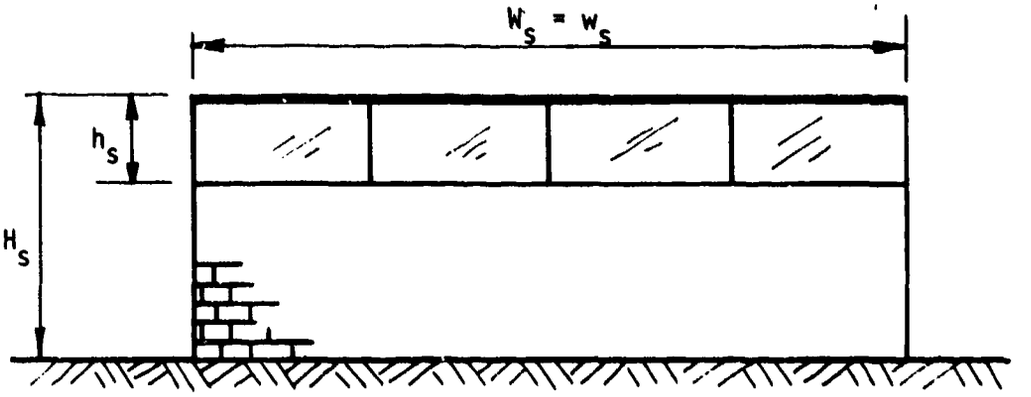

A. Clerestory Windows: $h_s = 0.25H_s$, $W_s = 3H_s$

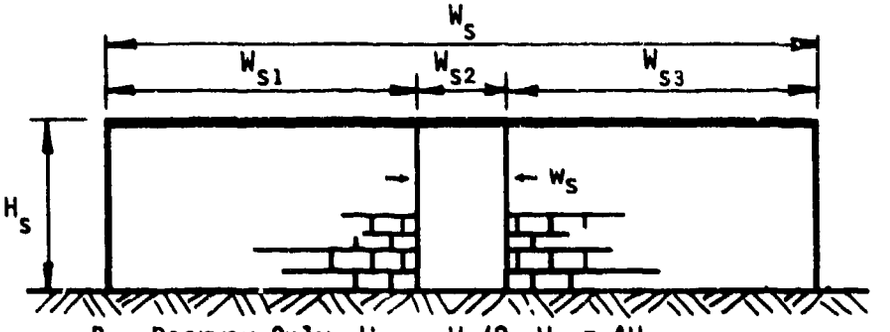

B. Doorway Only, $W_{s2} = W_s/8$, $W_s = 4H_s$

Fig. 14. Effects of Openings on the Front Face: - Single Openings

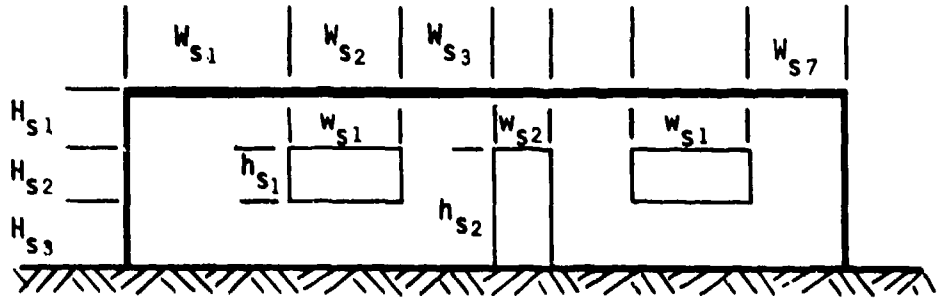

A. Single Story.

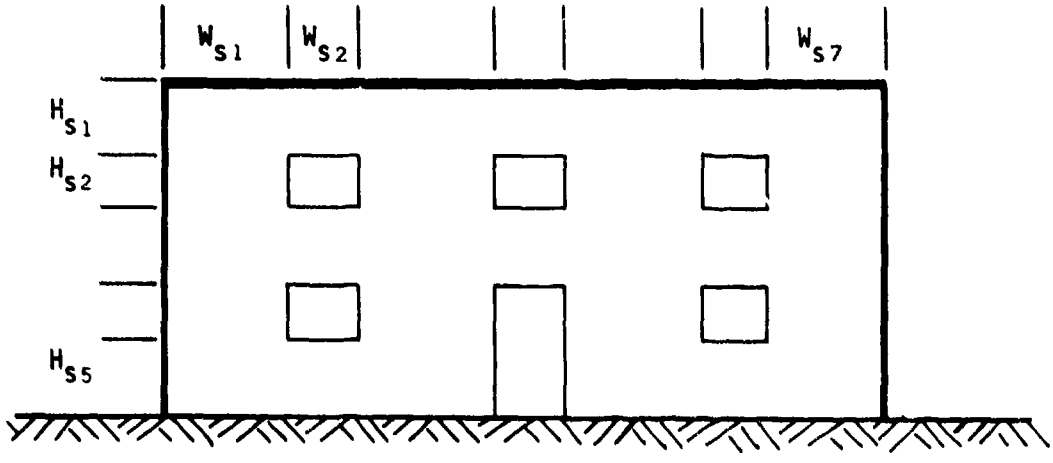

B. Two Story.

Fig. 15. Effects of Openings on the Front Face: Multiple Openings

A. Field Structure - Dimensions are 8 ft x 8 ft x 12 ft. Doorway is 2.9 ft x 7 ft.

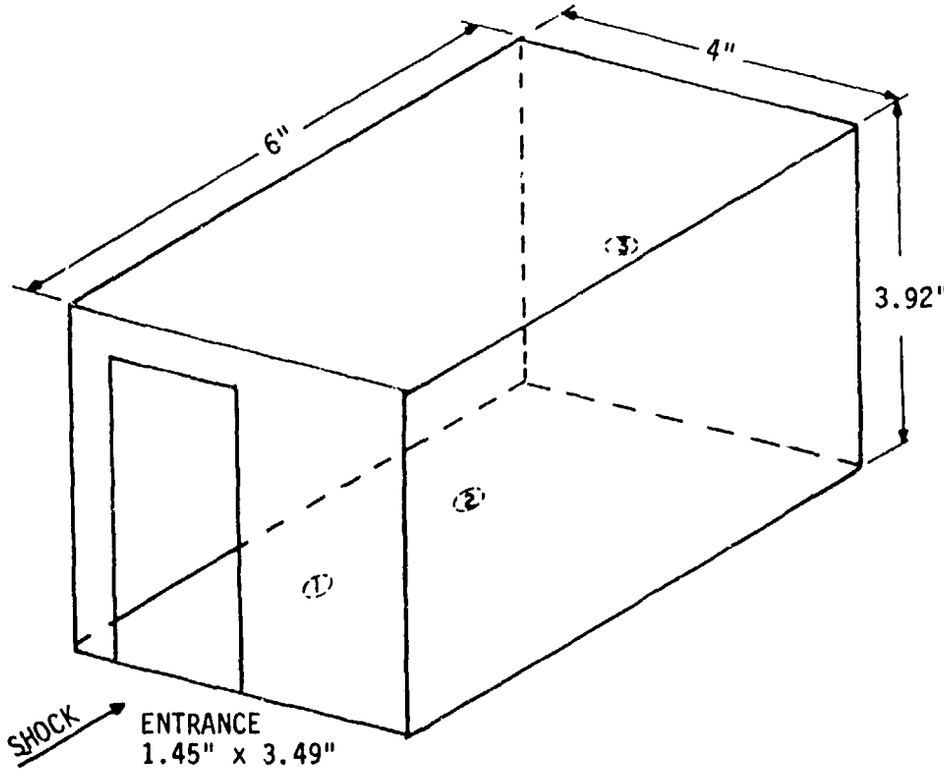

B. Model of Field Structure Tested in a Shock Tube.

Fig. 16. Structures Exposed to Blast Waves in the Field and in a Shock Tube.

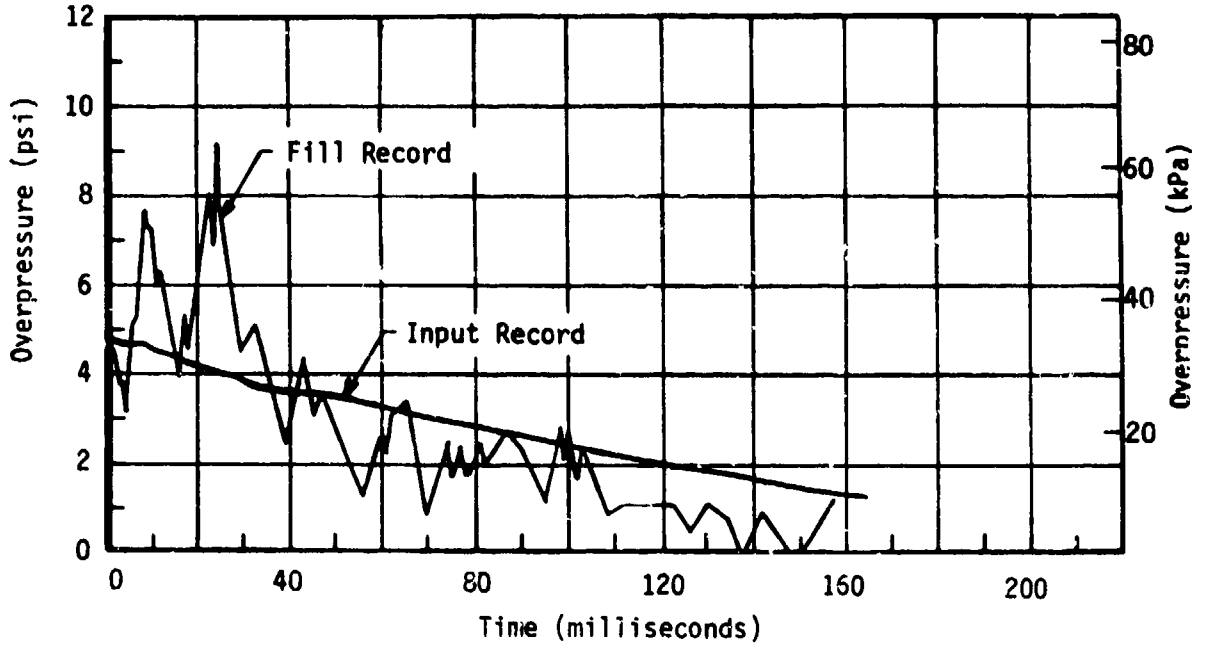

A. Field Record.

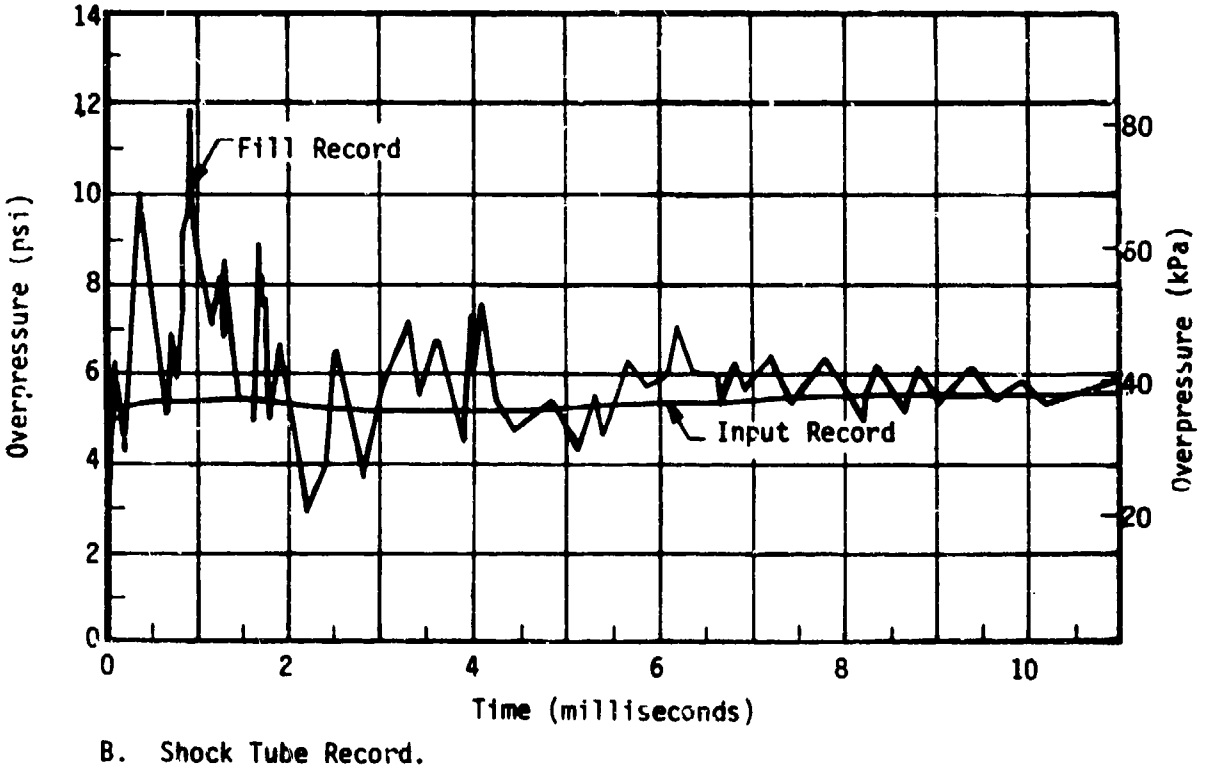

B. Shock Tube Record.

Fig. 17. Pressure Records from Interior Back Wall Gauges.

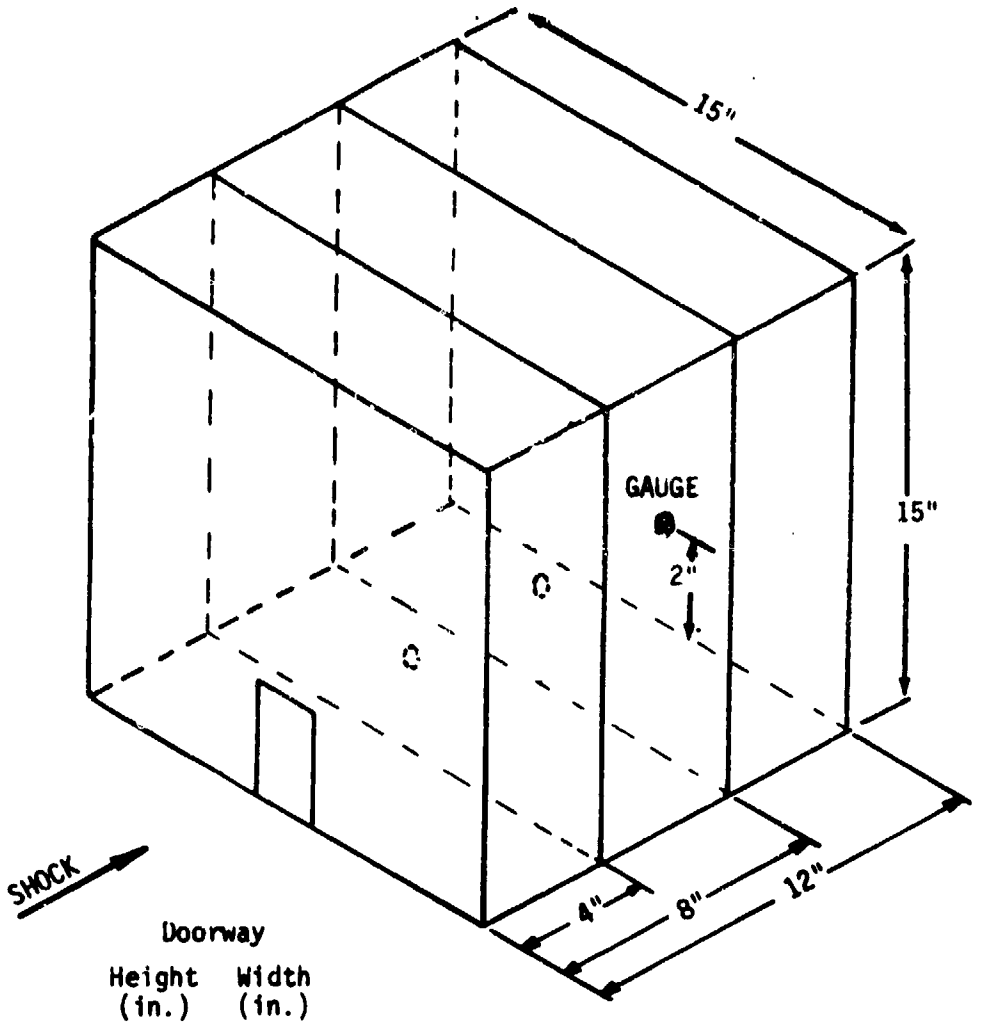

Doorway

Height (in.)	Width (in.)
4	2
2	1
1	½

Fig. 18. Models with Variable Lengths Tested in a Shock Tube.

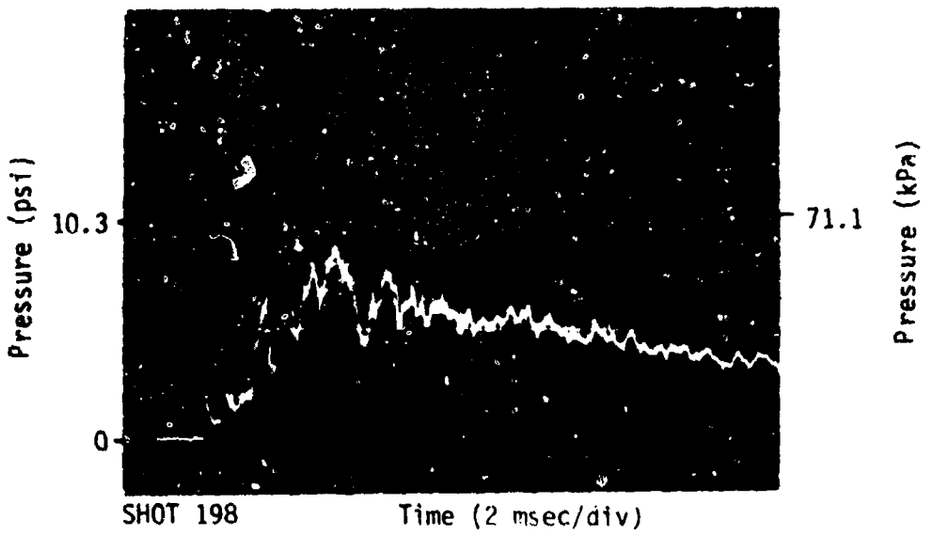

A. Normal Sweep Speed.

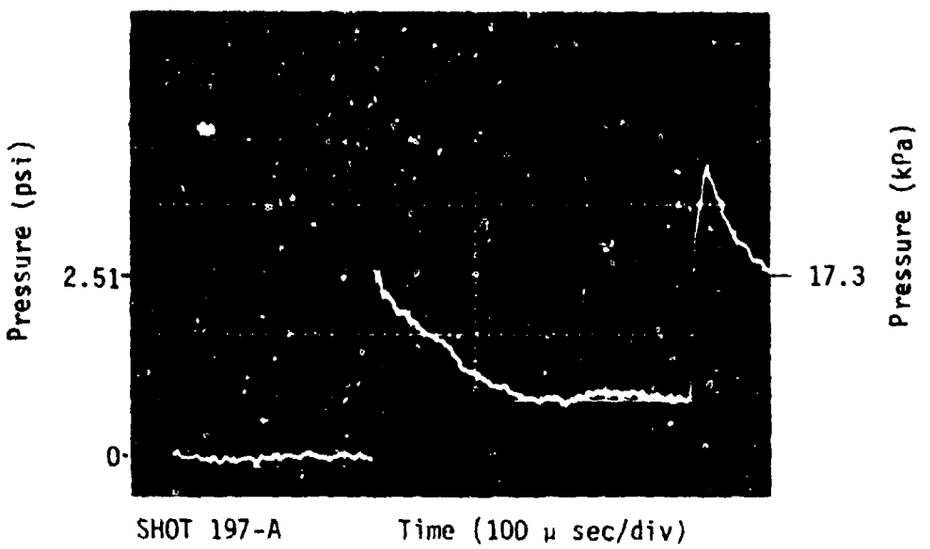

B. Fast Sweep Speed.

Fig. 19. Pressure Records from an Interior Back Wall Gauge in a Model Tested in a Shock Tube. (See Fig. 18.)

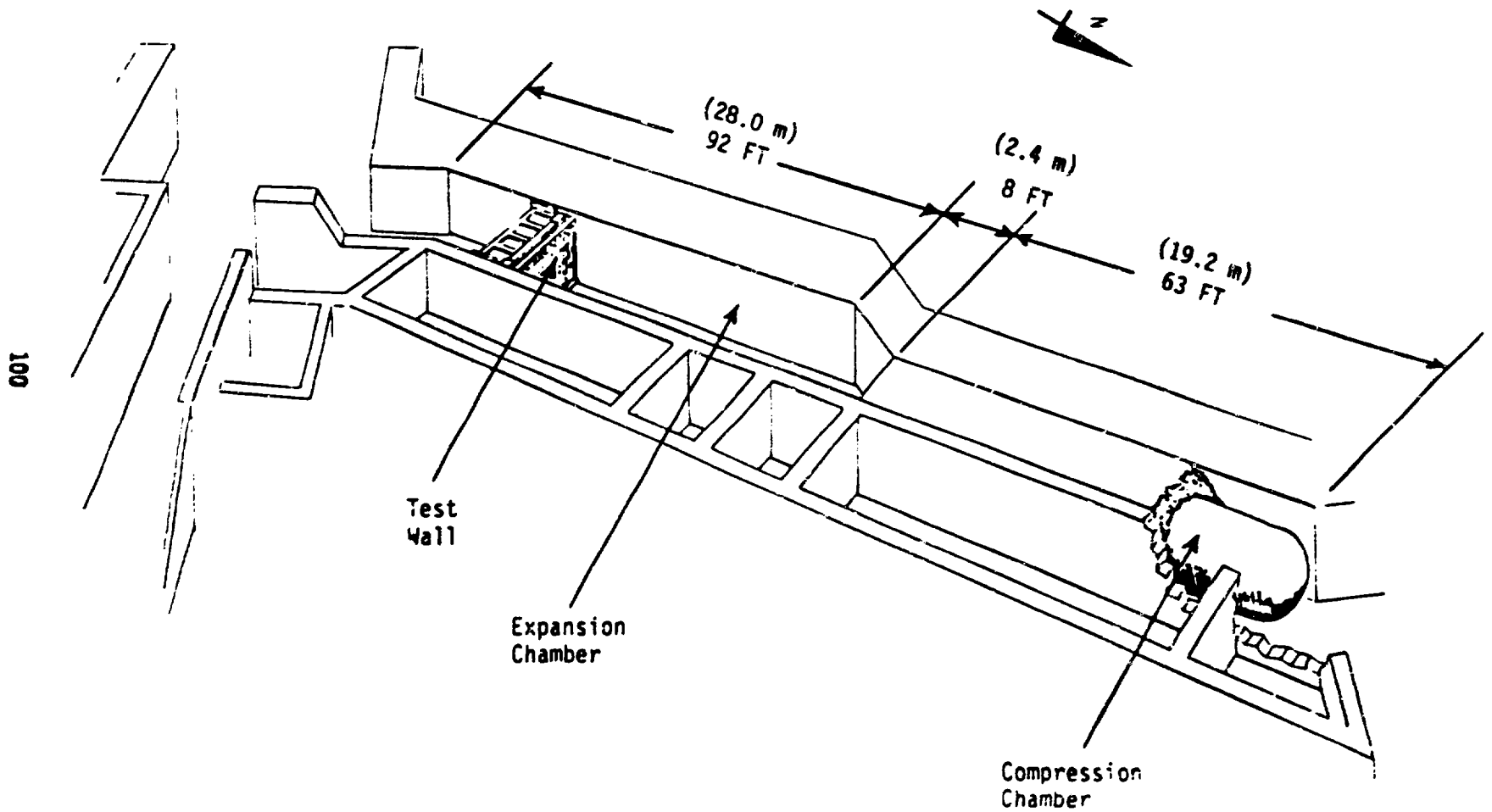

Fig. 20. Cutaway View of Shock Tunnel Showing Wall in Place.

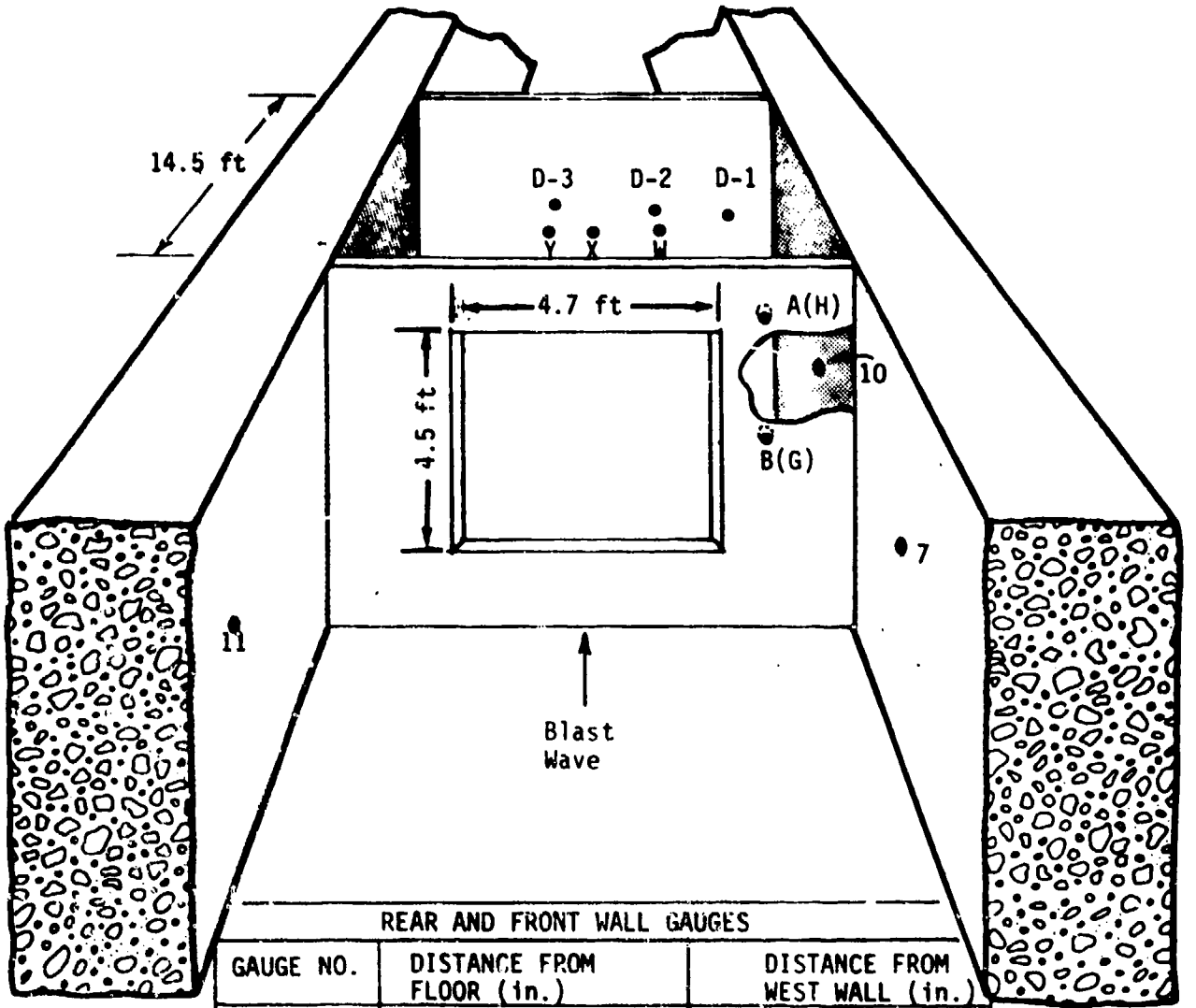

REAR AND FRONT WALL GAUGES

GAUGE NO.	DISTANCE FROM FLOOR (in.)	DISTANCE FROM WEST WALL (in.)
D-1	46	17
D-2	46-⅛	48-3/4
D-3	46-3/4	95-3/4
W	46	46-3/4
X	42-1/8	84-3/4
Y	42-⅛	96-3/4
A(H)	83-½	30
B(G)	51	28-½

SIDE WALL GAUGES

GAUGE NO.	DISTANCE FROM FLOOR (in.)	DISTANCE FROM FRONT WALL (in.)
7	45	21
11	49	38
10 (in room)	49	67-1/8

Fig. 21. Room with a Window Test Configuration in the Shock Tunnel.

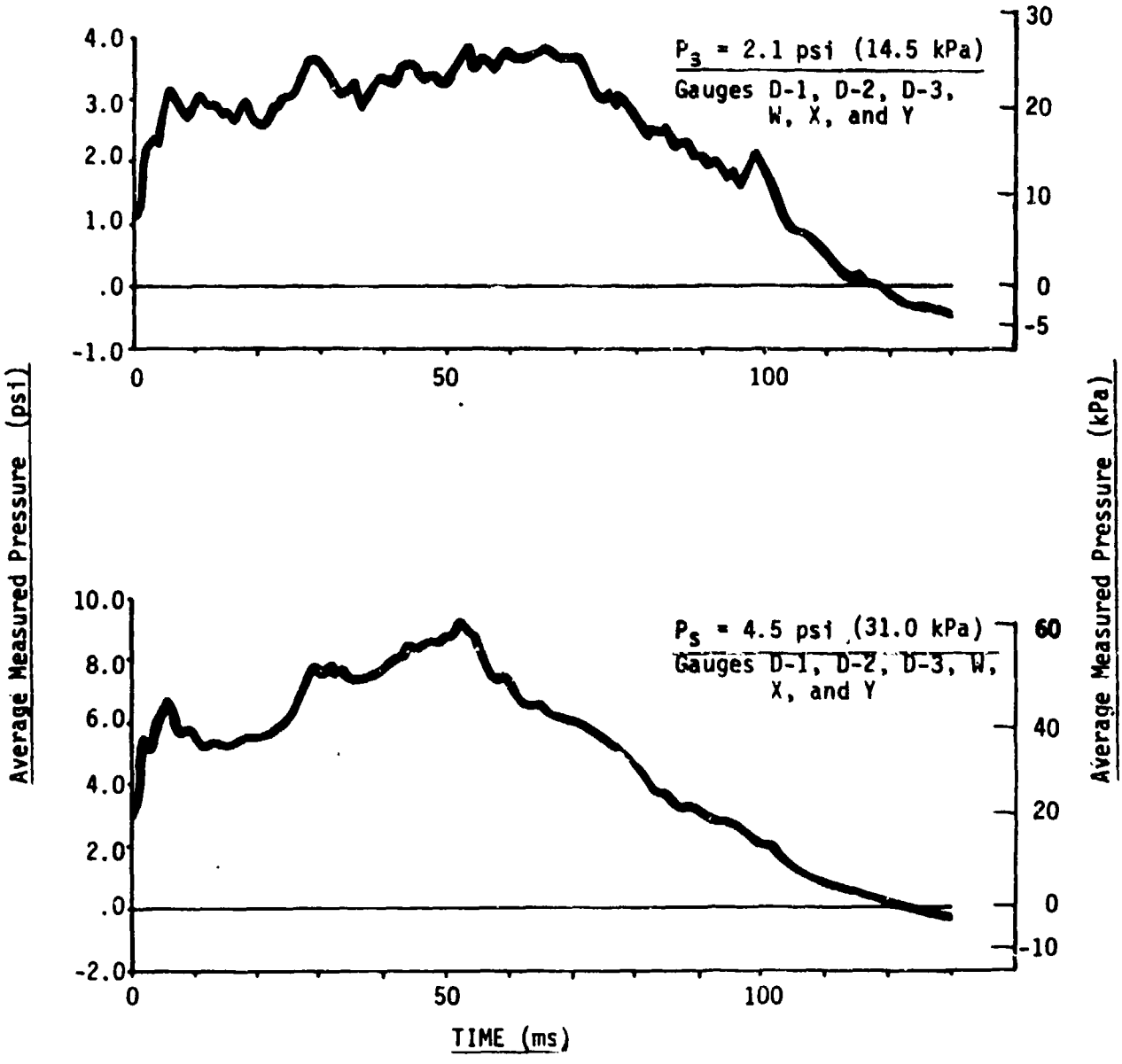

Fig. 22. Average Pressure vs Time on the Rear Wall of a Room with a "20%" Window (See also Fig. 21.)

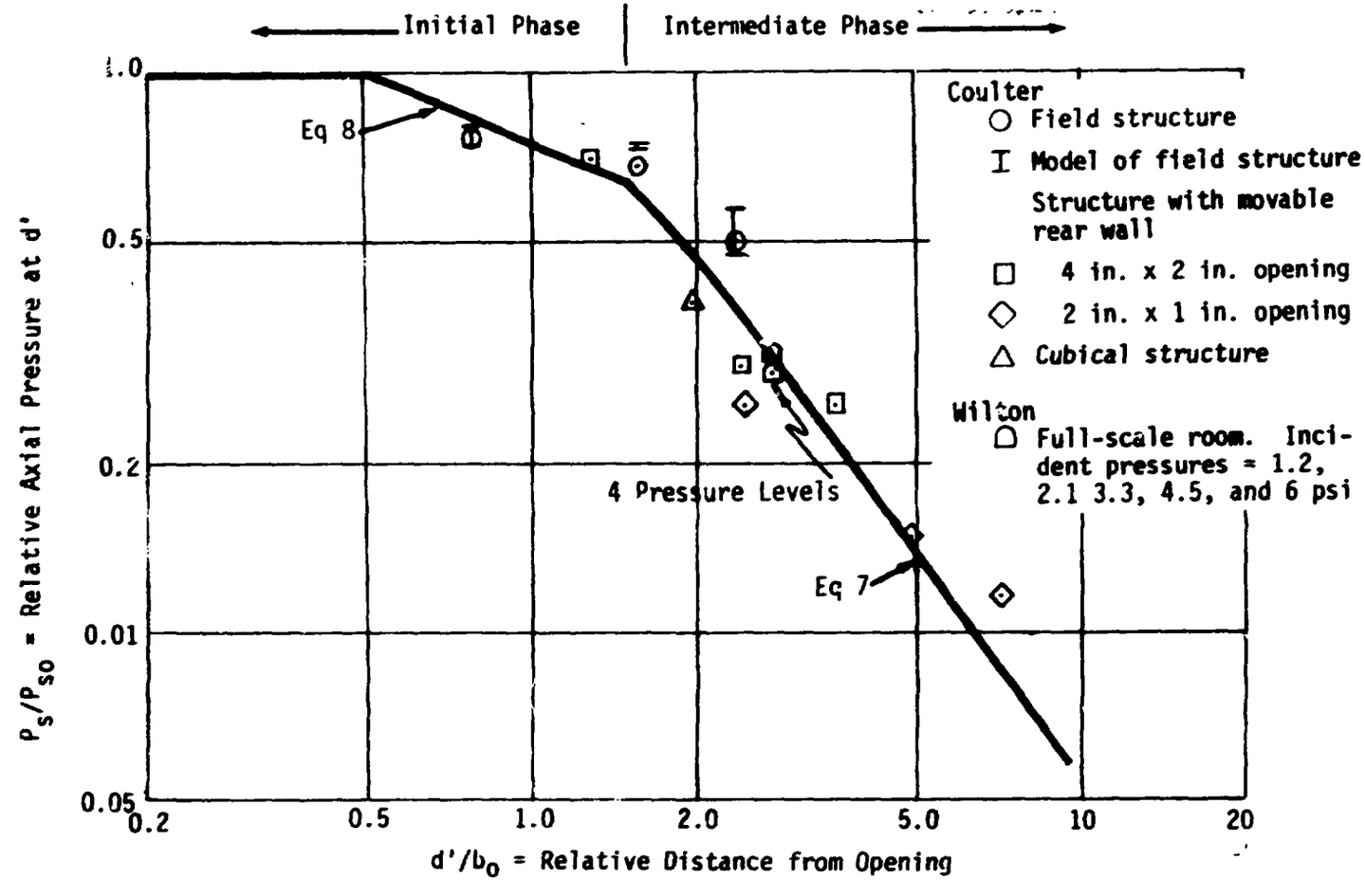

Fig. 23. Comparison of Predicted and Experimental Axial Shock Front Pressures — Initial and Intermediate Phases. Opening Width = b_o; Distance from Opening = d'; Pressure at Opening = P_{so}, Axial Pressure at d' = P_s.

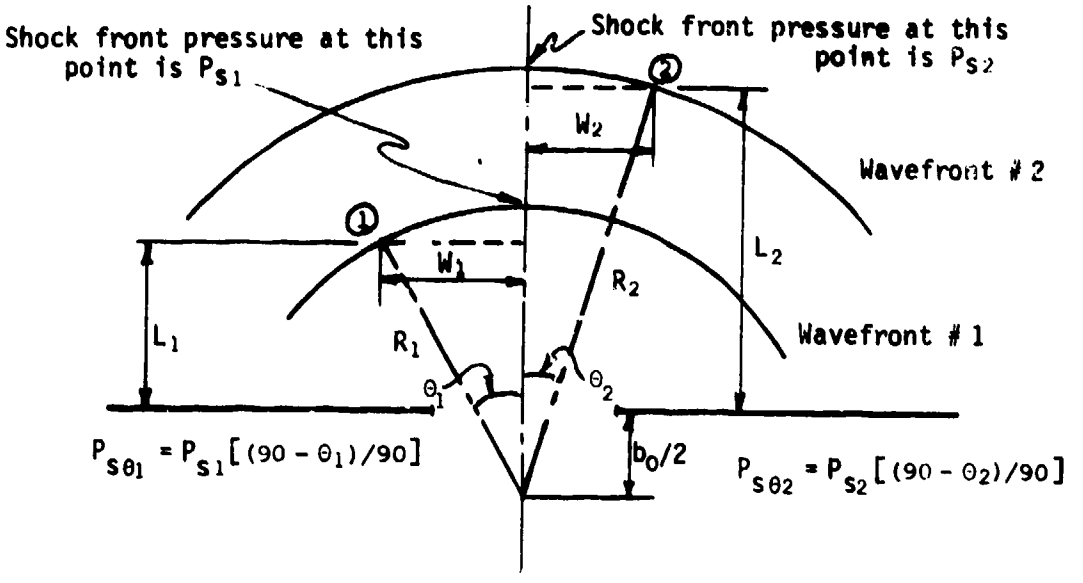

Fig. 24. Sketch Showing Method of Calculating Pressures Along a Wave Front

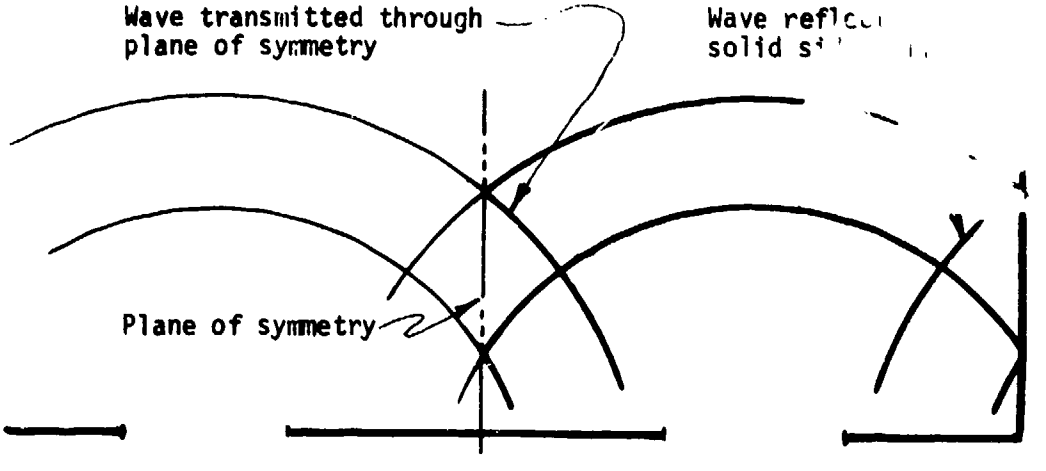

Fig. 25. Sketch Showing Equivalence of a Plane of Symmetry with a Solid Wall

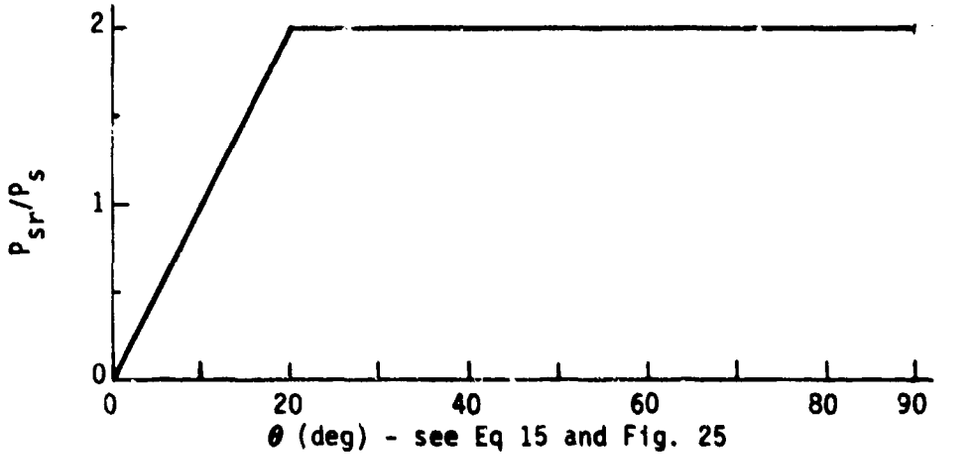

Fig. 26. Reflected Pressure Coefficient P_{sr}/P_s

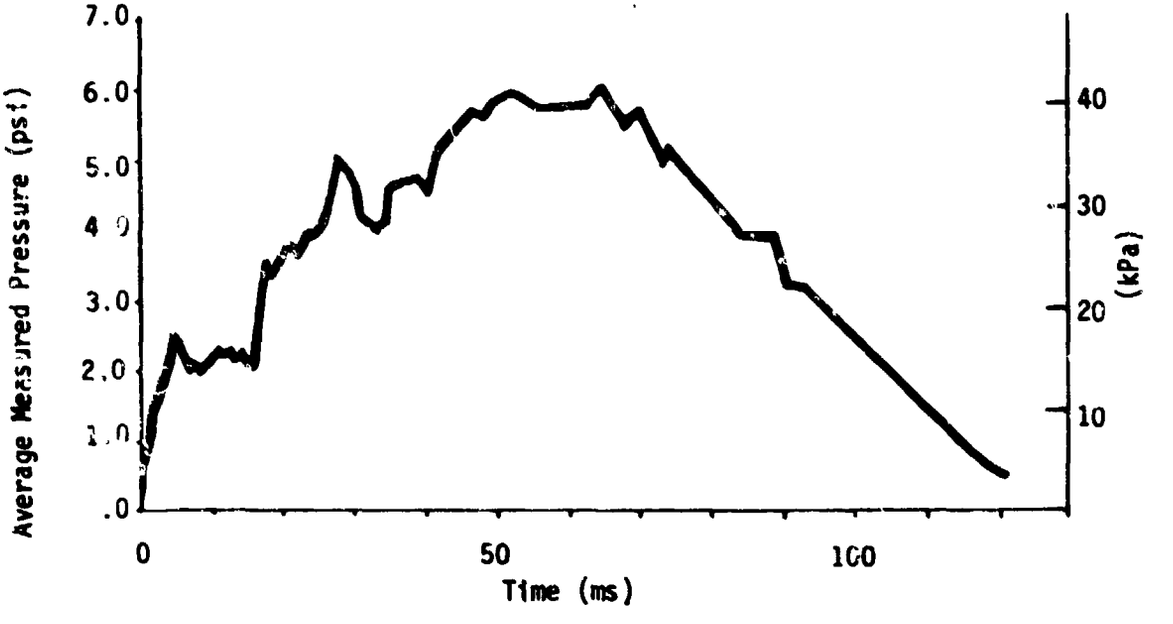

Fig. 27. Average Pressure at a Gauge in the Side Wall of a Room with a "20%" Window. (See also Fig. 21.)

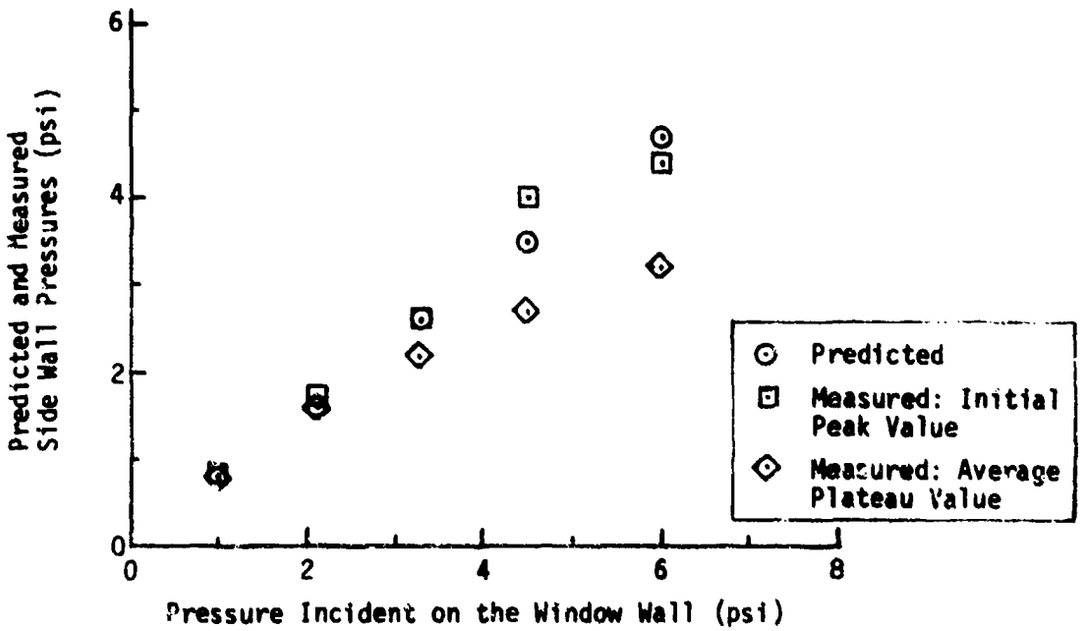

Fig. 28. Predicted and Measured Side Wall Pressures

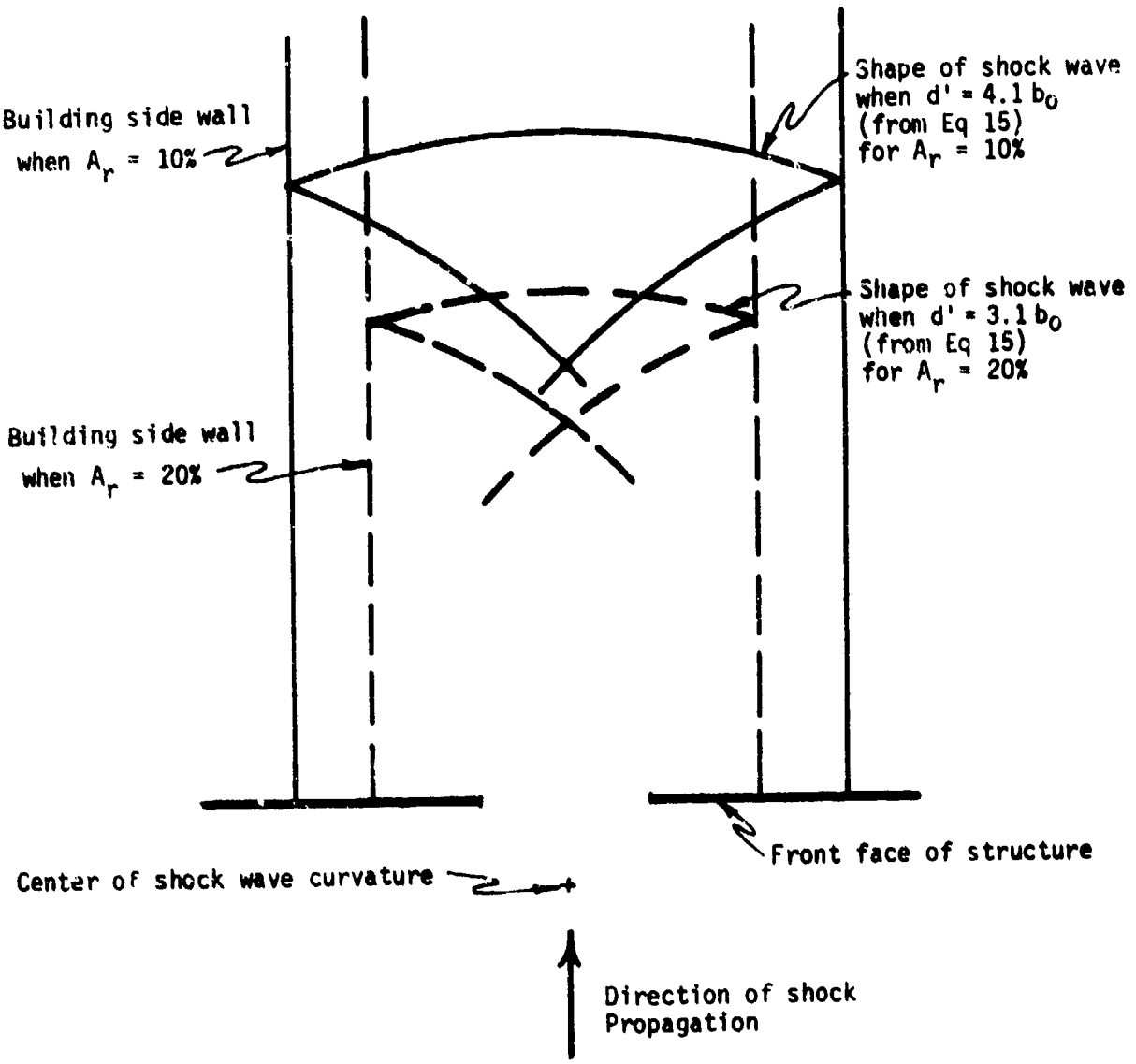

Fig. 29. Shape of Shock Wave at the Predicted Limits for Curved Wave Propagation. Both the opening and the interiors of the structures are assumed to be rectangular.

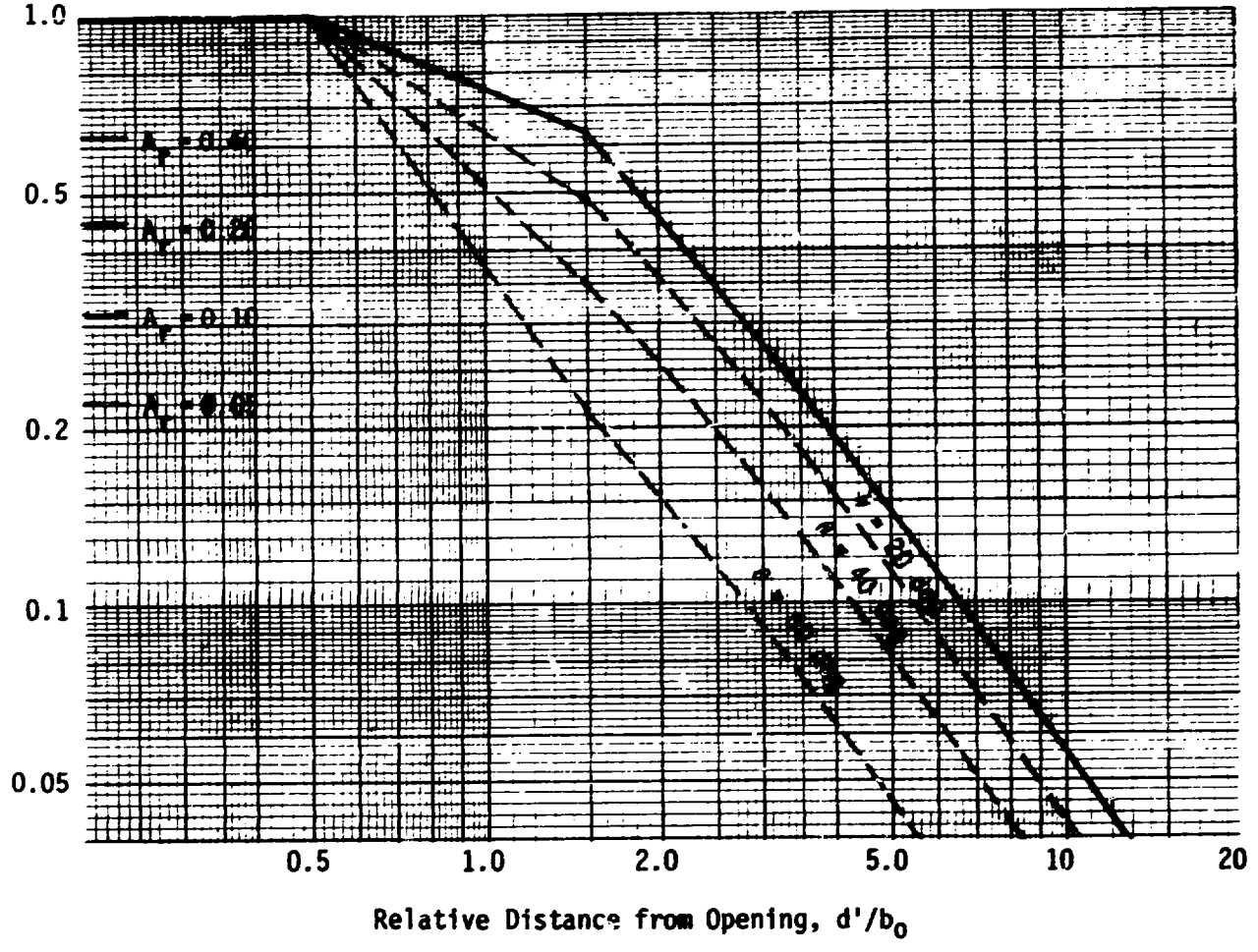

Fig. 30. Prediction Curve for Axial Shock Front Pressures (see instructions for use).

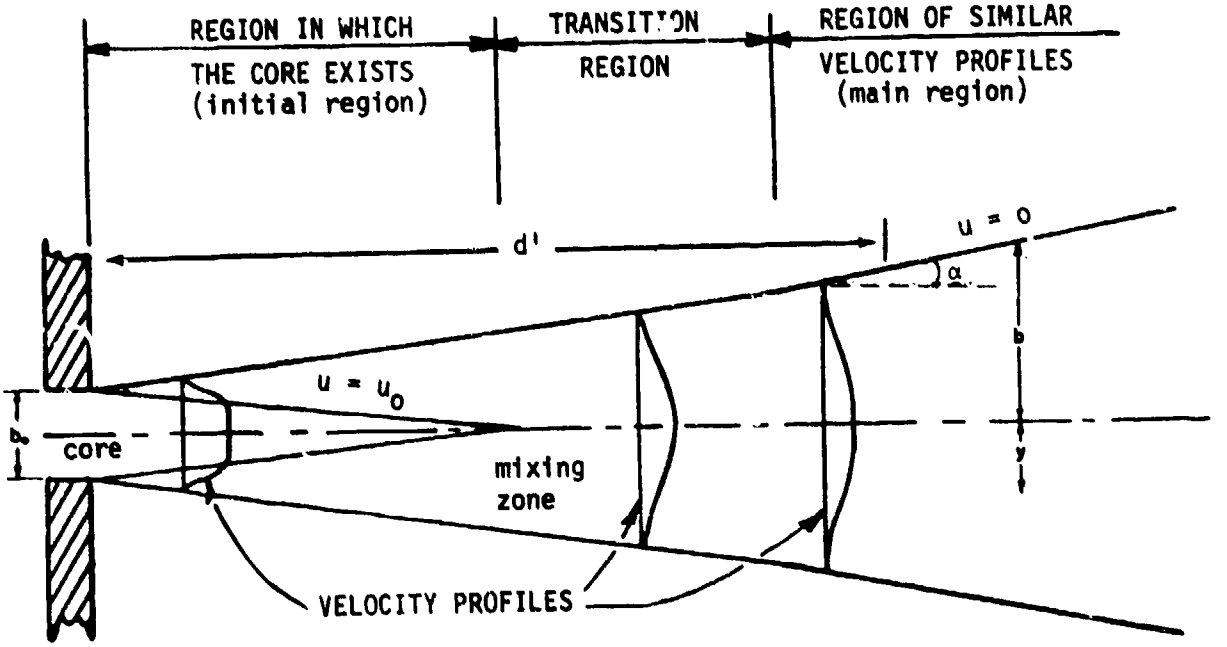

Fig. 31. Jet Flow Characteristics

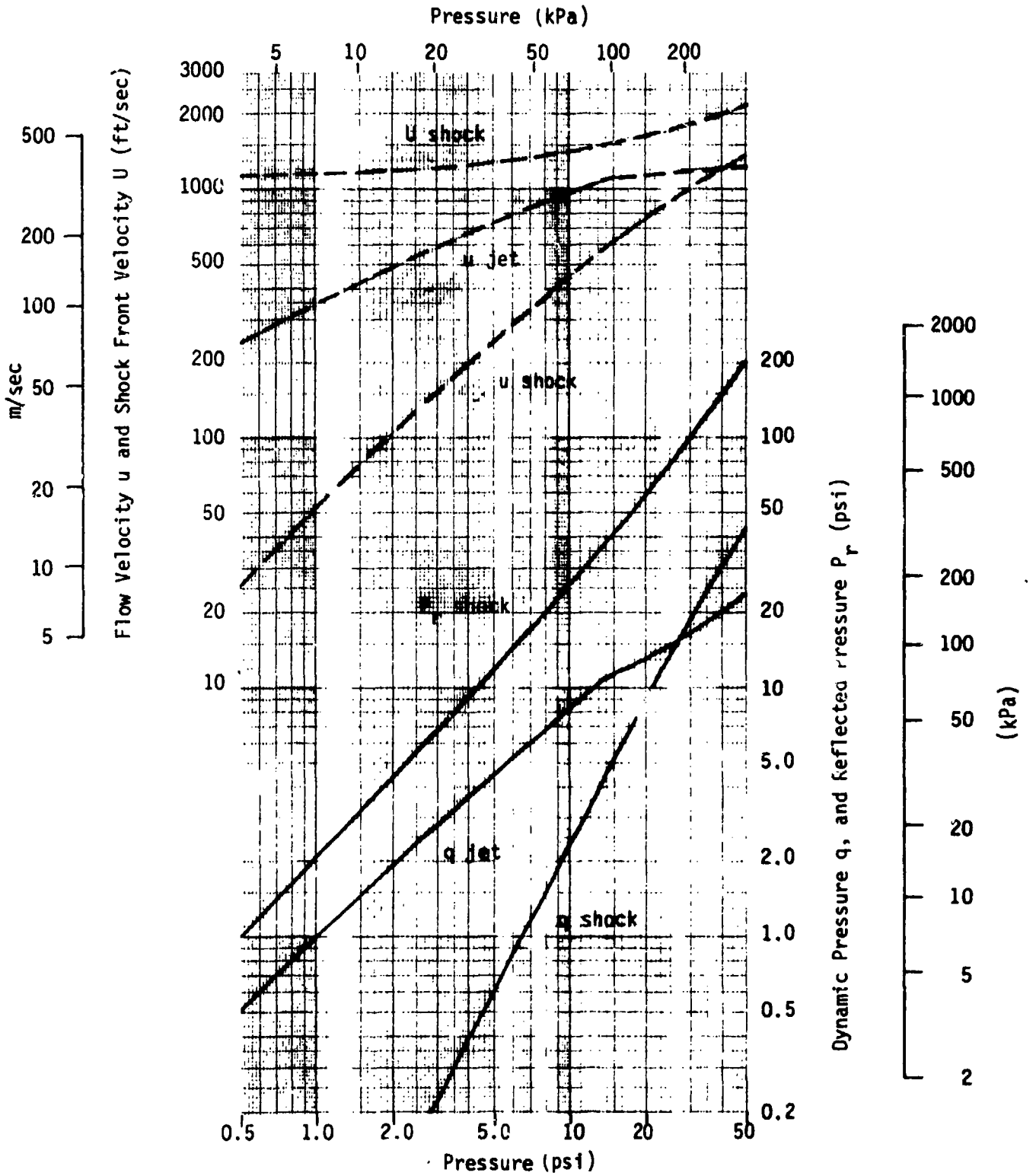

Fig. 32. Shock Wave and Jet Parameters: Dynamic Pressure q, Flow Velocity u, Shock Front Velocity U, Reflected Shock Pressure P_r.

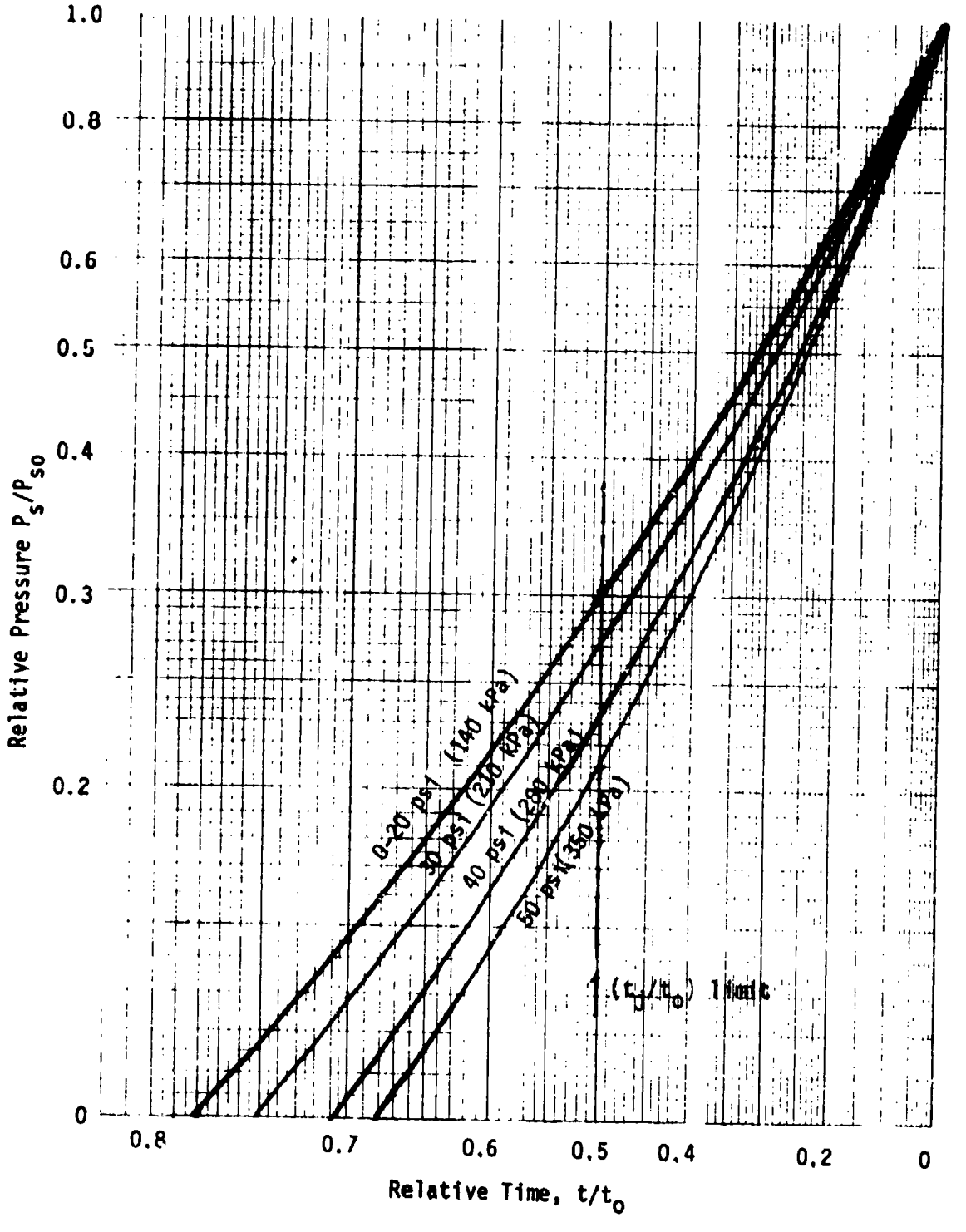

Fig. 33. Details of the Shock Wave from Explosions of TNT. (Eq 1). t_o = shock duration, P_{so} = peak (zero time) pressure.

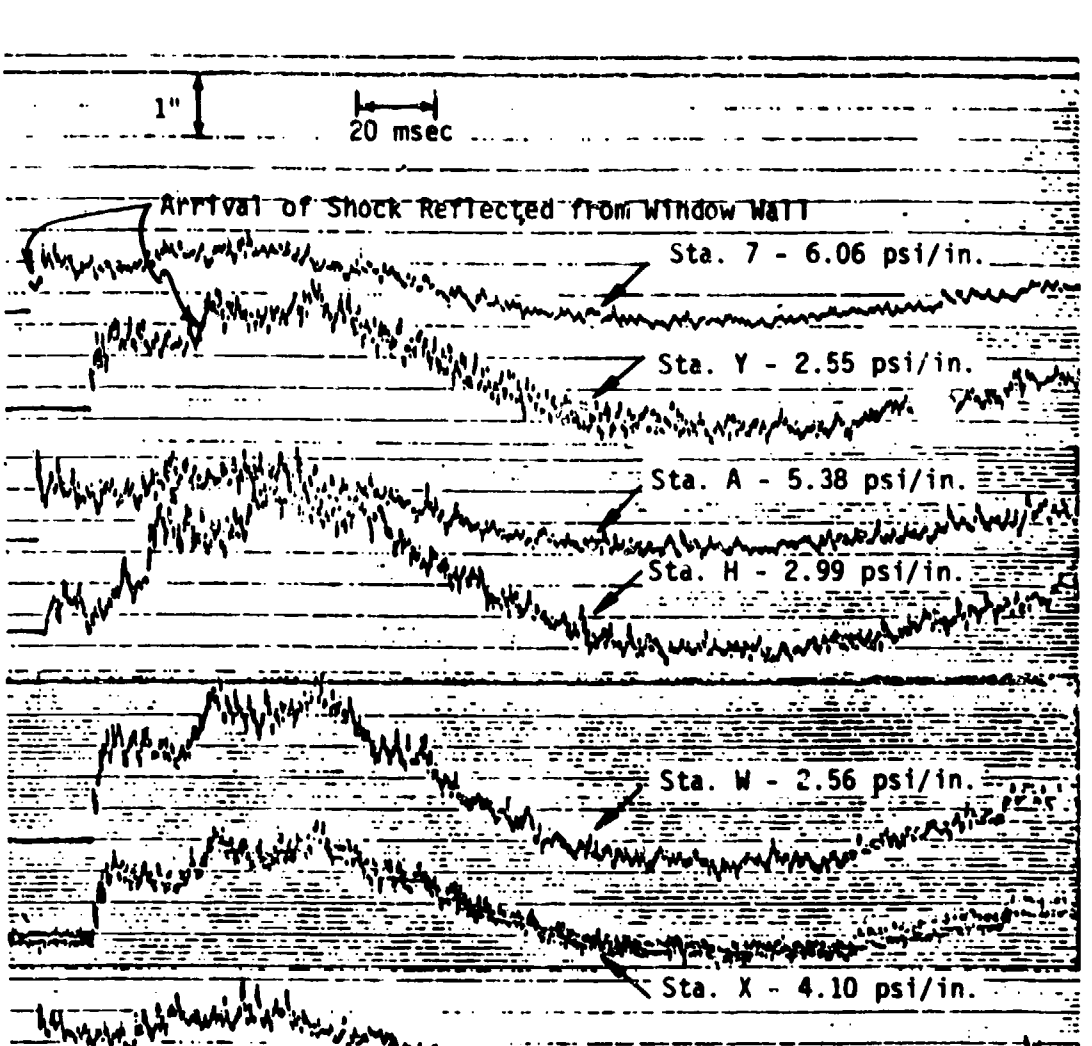

Fig. 34. Pressure vs Time Traces from a Test on a Room with a Window at an Incident Pressure Level of 3.3 psi. Sta 7 is in the Shock Tunnel Side Wall Upstream from the Front (Window) Wall; Sta W, X, and Y are on the Rear Wall; Sta A-H and B-G are Upstream and Downstream Paired Gauges on the Front Wall (see Fig. 21).

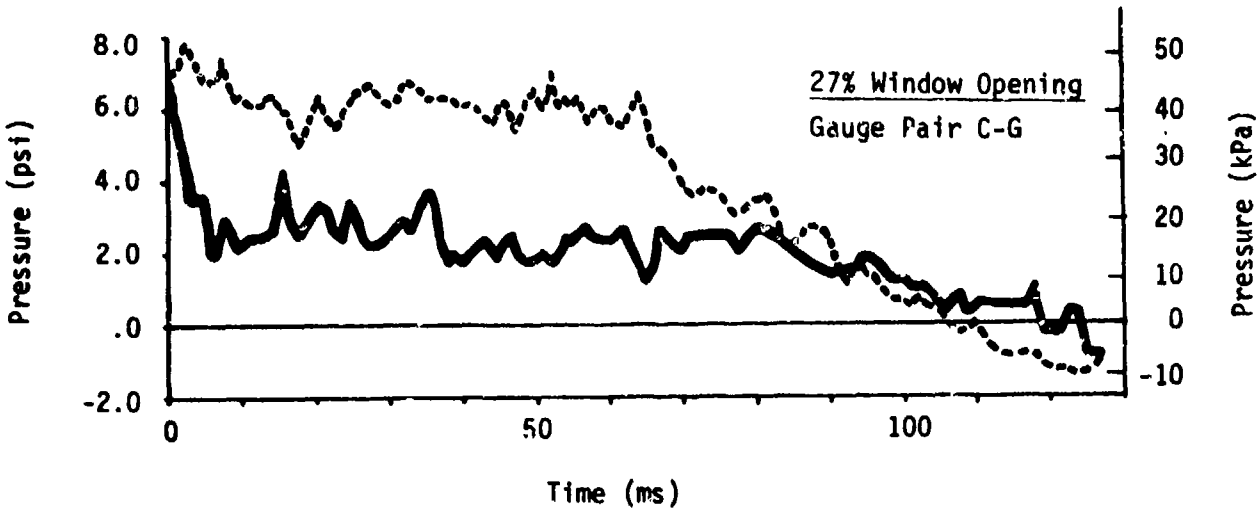

Fig. 35A. Localized Net Pressure vs Time from Paired Gauges. Solid Curve is for a Wall with a Window, Dashed Curve is for a Solid Wall. For Gauge Locations see Fig. 21.

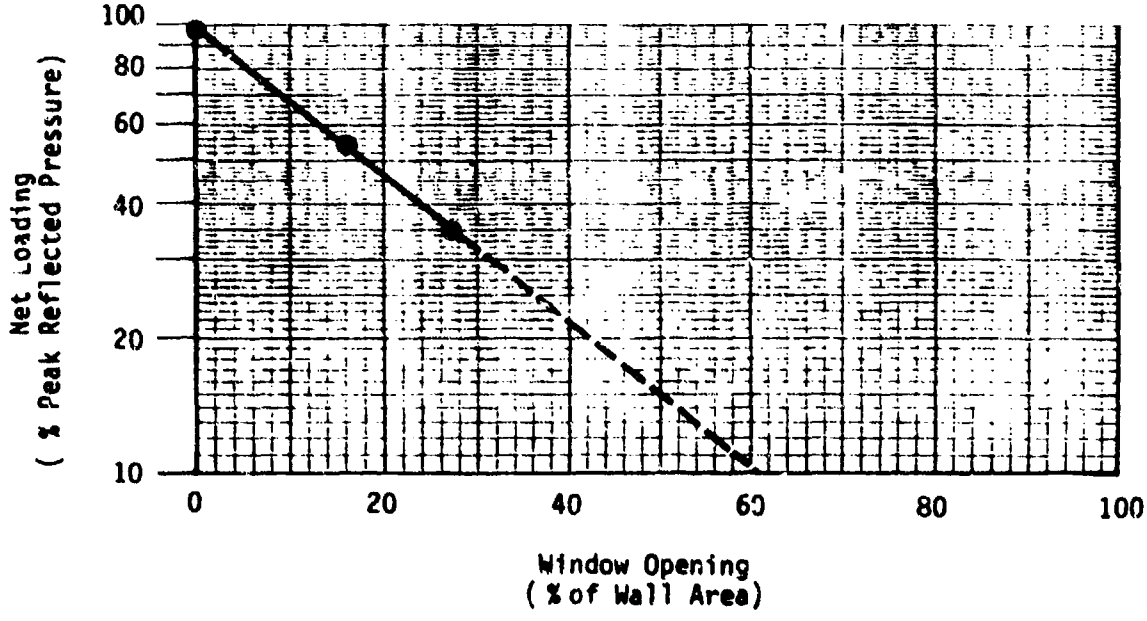

Fig. 35B. Net Loading on a Wall with a Window as a Function of Window Opening Area.

REFERENCES

1. TM 5-1300/NAVFAC P-397/AFM 88-22: Structures to Resist the Effects of Accidental Explosions, Departments of the Army, the Navy and the Air Force, Washington, D.C. June 1969.

2. Kinney, G.F., Explosive Shocks in Air, MacMillan Company, New York, New York, 1962.

3. Brode, H.L., "A Calculation of the Blast Wave from a Spherical Charge of TNT", U.S. Air Force Project Rand Research Memorandum RM-1965, 21 August 1957.

4. Sachs, R.G., "The Dependence of Blast on Ambient Pressure and Temperature", BRL Report No. 466, Ballistics Research Laboratories, Aberdeen Proving Ground, Maryland, 15 May 1944.

5. Patterson, A.M. et al., "Fireball and Shock Wave Anomalies Observed in Chemical Explosions", Combustion and Flame 19, The Combustion Institute, 1972, pp.25-32.

6. DOD 5154-4S: DOD Ammunition and Explosives Safety Standards, Department of Defense, Washington, D.C., March 1976.

7. Engineering Design Handbook: Explosive Series: Properties of Explosives of Military Interest, AMCP 706-177, U.S. Army Materiel Command, Washington, D.C., March 1967.

8. Sullivan, T.J., "Characteristics of Aqueous Gelled Slurry Explosives", Minutes of the Twelfth Explosives Safety Seminar, conducted by the Armed Services Explosives Safety Board, Memphis, Tennessee, 22-25 August 1970, pp. 69-107.

9. Wilton, C., "Study of the Effects of Explosive Density and Geometry on the Characteristics of Blast Waves", Scientific Service, Inc., Redwood City, California (unpublished).

10. Petes, J. "Watch Your Equivalent Weight", Minutes of the Twelfth Explosives Safety Seminar, conducted by the Armed Services Explosives Safety Board, Memphis, Tennessee, 22-25 August, 1970, pp. 371-381.

11. Strehlow, R.A., "Non-Ideal Explosions: The Blast Wave from Low Energy Density Explosion Sources", Minutes of the Seventeenth Annual Explosives Seminar, Vol. II, conducted by the Armed Services Explosives Safety Board, Denver, Colorado, 14-16 September, 1976, pp. 1721-1741.

12. Strehlow, R.A., "Unconfined Vapor Cloud Explosions - An Overview", University of Illinois, Urbana-Champaign.

13. Filler, W.S., J.M. Rossi, and H.R.J. Walsh, Barricade Effectiveness Evaluated from Records of Accidental Explosions, Armed Services Explosives Safety Board, Washington, D.C., July 1966.

14. Kaplan, K. and V.W. Davis, "Effectiveness of Barricades: Review of Basic Information", Final Report, DASA 2014, URS 677-4R, URS Systems Corporation, San Mateo, California, prepared for the Defense Atomic Support Agency, June, 1968.

15. Schleicher, A.R. et al., and A.B. Wenzel, "Influence of a Barricade Upon Blast Wave Parameters, Part I: Background and Analytical Tests, Part II: Experimental Work", Minutes of the Eleventh Explosives Safety Seminar, Vol. I , conducted by the Armed Services Explosives Safety Board, Memphis Tennessee, 9-10 September 1969, pp. 45-49.

16. Zaker, T.A., "Eskimo 2 Summary of Results and Damage Observations", Minutes of the Fifteenth Annual Explosives Safety Seminar, Vol. I, conducted by the Armed Services Explosives Safety Board, San Francisco California, 18-20 September, 1973, pp. 139-148.

17. Sound, A.R., "Summary Report of Earth-Covered Steel-Arch Magazine Tests", NOTS TP 3843, July 1965.

18. Kingery, C.N., and G.A. Coulter, "Blast Parameters from Explosions in Model Earth-Covered Magazines", Minutes of the Seventeenth Annual Explosives Safety Seminar, Vol. II, conducted by the Armed Services Explosives Safety Board, Denver, Colorado, 14-16 September 1976, pp. 1763-1819.

19. Kaplan, K., "The Meaning of Simultaneity of Detonation with Respect to the Application of Quantity-Distance Regulations", Minutes of the Ninth Explosives Safety Seminar,conducted by the Armed Services Explosives Safety Board, San Diego, California 15-17 August, 1967, pp. 273-287.

20. Wilton, C., "Evaluation of Explosion Simultaneity Tests", NWC TP 4720, Naval Weapons Center, May 1969.

21. Swatosh, J.J.Jr,"Sequential Explosion Studies", Minutes of the 13th Annual Explosives Safety Seminar, conducted by the Armed Services Explosives Safety Board, San Diego, California 14-16 September 1971, pp. 77-92.

22. Brinkley, S.R., and J.G. Kirkwood, The Blast Wave in Air Produced by Line Charges, NDRC Report No. A-343, OSRD Report No. 5659.

23. The Port Chicago, California Ship Explosion of 17 July 1944, Army-Navy Explosives Safety Board, Washington, D.C., March 1948.

References (contd)

24. Bleakney, W., The Diffraction of Shock Waves Around Obstacles and the Transient Loading of Structures, Princeton University, March 1950, published and distributed by the Armed Forces Special Weapons Project.

25. Kaplan, K., K.S. Lewis and P.J. Morris, "Blast Loading and Response of Military Equipment", Draft Final Report URS 7339-6, URS Research Company, San Mateo, California, prepared for Ballistic Research Laboratories, December 1973.

26. The Effects of Nuclear Weapons, S. Glasstone,ed., U.S. Atomic Energy Commission, Washington, D.C., (revised edition) 1964.

27. Coulter, G.A., "Air Shock Filling of Model Rooms", BRL Memorandum Report No. 1916, Ballistic Research Laboratories, Aberdeen Proving Ground, Maryland, March 1968.

28. Price, P., S. Weissman and N. Dobbs, Tests of Blast Resistant Acceptor Structures and Components, Picatinny Arsenal.

29. Warnecke, C.H., "Data Report: Support Test Evaluation of a Pre-Engineered Building", TECOM Project No. 2-CO-160-PIC-004, U.S. Army Dugway Proving Ground, Dugway, Utah, June 1977.

30. Newmark, N.M., "An Engineering Approach to Blast Resistant Design", Trans. American Society of Civil Engineers 121, 1956, p.45

31. Iwanski, E.C., et al., "Blast Effects on Buildings and Structures Operation of 6-Foot and 2-Foot Shock Tubes: High Pressure Tests on Simple Shapes" Report No. 54, Final Test Report No. 10, ARF Project D037, Armour Research Foundation of Illinois Institute of Technology.

32. Melichar, J.F., "The Propagation of Blast Waves into Chambers", BRL Memorandum Report 1920, Ballistic Research Laboratories, Aberdeen Proving Ground, Maryland, March 1968.

33. Coulter, G.A., "Air Shock and Flow in Model Rooms", BRL Memorandum Report No. 1987, Ballistic Research Laboratories, Aberdeen Proving Ground, Maryland, June 1969.

34. Coulter, G.A. and R.L. Peterson, "Blast Fill Time of a One-Room Structure", Operation Prairie Flat Project Officers Report - Project LN 111 POR-2102, BRL, November 1964.

35. Wilton, C. and B.L. Gabrielsen, "Shock Tunnel Tests of Preloaded and Arched Wall Panels", Final Report URS 7030-10, prepared for Defense Civil Preparedness Agency, URS Research Company, San Mateo, California June 1973.

36. Wilton, C., K. Kaplan and B.L. Gabrielsen, "The Shock Tunnel: History and Results", Volume II - Loading Studies, Final Report SSI 7618-1, prepared for Defense Civil Preparedness Agency, Scientific Service, Inc. Redwood City, California, March 1978.

37. Courant, R. and K.O. Friedrichs, Supersonic Flow and Shock Waves, Interscience Publishers, Inc., New York, N.Y., 1948.

38. Lampson, C.W., "Resume of the Theory of Plane Shock and Adiabiatic Waves with Applications to the Theory of the Shock Tube", BRL Technical Note No. 139, Ballistic Research Laboratories, Aberdeen Proving Ground, Maryland, March 1950.

39. Abramovich, G.N., The Theory of Turbulent Jets, MIT Press, 1963.

40. Rempel, J.R., Room Filling from Air Blast, Appendix E to the report "Slanting for Combined Nuclear Weapons Effects: Examples with Estimates and Air Blast Room Filling", by H.L. Murphy and J.E. Beck, Stanford Research Institute, Menlo Park, California, June 1973.

41. Bowen, I.G., R.W. Albright, E.R. Fletcher and C.S. White, "A Model Designed to Predict the Motion of Objects Translated by Classical Blast Waves", Lovelace Foundation for Medical Education and Research, Albuquerque, N.M., U.S. Atomic Energy Commission Report CEX 58.9, June 1961.

42. Fletcher, E.R., and I.G. Bowen, "Blast Induced Translational Effects", Prevention of and Protection Against Accidental Explosions of Munitions, Fuels and Other Hazardous Mixtures, Annals of the New York Academy of Sciences, Volume 152, Art. 1, October 1968.

43. Lapple, C.E., et al., Fluid and Particle Mechanics, University of Delaware, Newark, Delaware, March 1956.

44. Kriebel, A.R., "Air Blast in Tunnels and Chambers", Final Report DASA 1200-11, Supplement 1, prepared for Defense Civil Preparedness Agency, URS Research Company, San Mateo, California, Sept. 1372.

45. Wilton, C. and B.L. Gabrielsen, "Shock Tunnel Tests of Wall Panels", Technical Report, Vol. 1, Test Information and Analysis, URS 7030-7, prepared for Defense Civil Preparedness Agency, URS Research Company, San Mateo, California, Jan. 1972.

APPENDIX. EXAMPLES

This Appendix contains examples which employ most of the techniques for determining various effects of openings in structures.

The first example, in which front, side, and rear wall design loadings on a structure are calculated, is the most comprehensive. It involves a structure with multiple openings exposed to a shock wave with relatively low peak pressure from a large explosive source.

The remaining four examples illustrate particular aspects of effects of openings in structures; viz

2. Acceleration of objects in jet flow
3. Filling of small chambers
4. Forces on ductwork behind a vent (high pressure)
5. Forces behind small openings (very high pressures).

EXAMPLE 1
NET STRUCTURAL DESIGN LOADINGS*

TO BE DERIVED: Design Loadings on Front, Rear, and Side Walls.

INPUT INFORMATION

Structural (see Fig. A-1)

Dimensions: Height = 9 ft, Width = 17 ft, Length = 30 ft.

Openings: Front Wall: Two windows, 3 ft H x 3 ft W, two ft from side walls and four ft from ground.
One doorway, 8 ft H x 3 ft W, centered.

Side Walls: One window, 3 ft H x 3 ft W, four ft from ground, centered front to rear.

Rear Wall: none.

Explosive

Weight of Explosive: W = 10,000 lb

Distance to Structure: d = 340 ft

DERIVED QUANTITIES

Symbol	Description	Value
Blast Characteristics		
$W^{1/3}$	Cube root of charge weight	21.54 $lb^{1/3}$
$d/W^{1/3}$	Scaled distance	16 $ft/lb^{1/3}$
P_{so}	Peak pressure, from Fig. 3	4 psi
$t_o/W^{1/3}$	Scaled duration, from Fig. 3	3.0 $ms/lb^{1/3}$
$i_s/W^{1/3}$	Scaled impulse, from Fig. 3	5.2 $psi\text{-}ms/lb^{1/3}$
t_o	Duration	65 ms
i_s	Impulse	112 psi-ms
t_{of}	Fictitious duration = $2 i_s/P$	56 ms

* See comments at end of example.

Symbol	Description	Value
Structural Parameters		
A_o	Area of front wall opening (add all opening areas together)	42 ft^2
A_f	Area of front wall (= A_i, area of interior)	153 ft^2
A_r	(A_o/A_i) = 0.274	0.274
b_o	Characteristic dimension of opening $=(4A_o/\pi)^{\frac{1}{2}}$	7.3 ft
S	Closed structure front and rear face clearing distance. (The lesser of S_H = 9 ft, or $S_{W/2}$ = 8.5 ft)	8.5 ft
S'	Open structure front and rear face clearing distance. (The lesser of $S'_H = 153[1 - (42/153)]/17 = 6.5$ ft or $S'_{W/2} = [153/2][1 - (42/153)]/9 = 6.2$ ft	6.2 ft
S"	Interior clearing distance (for single opening = distance to nearest reflecting surface. For multiple openings, use b_o, and average distances to side wall and roof)	2.9 ft
d'_ℓ	Distance required for plane wave formation, Eq 15 (Note: since d'_ℓ is less than structure length, a plane wave forms)	18.8 ft
Important Times and Interior Conditions		
t_L	Time for single passage of shock = 30/U	≈26 ms
t_j	Time for jet formation = $4\,b_o/c$. (Since each of the multiple openings can clear independently, use average of b_o for each opening. $b_o\,(av)=[2(4x9/\pi)^{\frac{1}{2}} + (4x24/\pi)^{\frac{1}{2}}]/3 = 4.1$ ft Note: since $t_j < t_o/2$, jet effects must be considered in design.)	14.5 ms
t_f	Time for filling = V/2A. (If filling from front face only, t_j = 54.6 ms; if filling from front and side openings all the time, t_j = 38.2 ms. But shock wave takes ≈12 ms to get to side openings. Therefore use average t_j.)	46.4 ms
P_{sp}	Pressure of plane wave = $P_{so}A_r^{\frac{1}{2}}$	2.1 psi
R_p	Distance correction before plane wave forms = $[1 + (d'/d)]^{-1.5}$	-

Symbol	Description	Value
$P_s(15)$*	Pressure of expanding wave 15 ft from opening. From Fig. 30 with $d'/b_o = 2.1$ and including distance correction $= [(0.44)(1 + 15/340)^{-1.5}]P_{so} = (0.44)(0.94)P_{so}$	1.6 psi*
$P_{s\theta}(15, 30)$*	Pressure 30° off-axis accompanying $P_s(15)$. From Fig. 30, with $d'/b_o = 2.1$, and including distance correction $= (0.29)(0.94)P_{so}$	1.1 psi*
q_j	Dynamic pressure in the jet core at time t_j. From Fig. 32	2.4 psi

* Not needed for design calculations.

Symbol	Description	Value
Front Wall Design Loading Diagrams. See Fig. A-2		
	Initial Loadings	
P_{sr}(front)	Zero time peak from Fig. 32	9.0 psi
t_c	Closed structure clearing time = 3S/U	20.4 ms
t'_c	Clearing time for exterior loadings only = 3S'/U	15.6 ms
t''_c	Initial clearing time for net loadings	
	$\Delta t = (3S'/U) - (S''/U) = 15.6 - 2.6 =$	13.0 ms
	$S_r = (S''/S) = 2.9/8.5 =$	0.34
	$t''_c = (3S'/U) - (\Delta t)(S_r)^{\frac{1}{2}} =$	8.0 ms
P_s(red.)	Reduction of net loadings from closed structure values - from Fig. 35B	35%
	Reflected Loadings (all outward)	
	Pressure in incident shock $\left[1 - (\text{side wall open area} / \text{shock front area})\right] P_{sp}$ $= [1 - (18/153)]\ P_{sp} = (0.88)(2.1) =$	1.8 psi
	Pressure in reflected shock. From Fig. 32	3.9 psi
	Clearing time = time of arrvial + 3S'/U	68 ms
	End of reflected pulse = $2t_L + t_{of}$	108 ms

Symbol	Description	Value
Rear Wall Design Loading Diagram (see Fig. A-3)		
	Initial Loadings	
P_s(rear)	= Incident pressure at rear wall = P_{sp}	2.1 psi
P_{sr}(rear)	= Reflected pressure at rear wall from Fig. 32	4.6 psi
t_p	= Time of arrival of exterior and interior shocks at wall	26 ms
P_{so}(rear)	Peak exterior pressure at pos[illegible] rear wall = $P_{so}[1 + (30/340)$	3.5 psi
t_c(rear)	Rear wall clearing time for exterior loadings = S/U	7 ms
	Jet Loadings (flow reversal)	
t_j/t_o	Relative jet clearing time	0.22
P_j/P_o	Relative incident pressure at time t_j. From Fig. 32	0.63
P_j	Incident pressure at time t_j	2.5 psi
q_j	Dynamic pressure at time t_j. From Fig. 32	2.4 psi
P_j(rear)	Pressure on rear wall from jet = $(4q_jA_o)/A_i$	2.6 psi
u_j	Jet core velocity. From Fig. 32	520 ft/sec
t_j(rear)	Time of arrival at rear wall =30/u	58 ms
$t_{of} - t_j$	Nominal duration of jet forces	41 ms
	Reflected Loadings (all outward)	
	Pressure in incident shock including two reductions due to side wall openings, and one reduction due to front face reflection = $[1 - (18/153)]^2[1 - (42/153)]P_{sp} = 0.56\ P_{sp}$	1.2 psi
	Pressure in reflected shock. From Fig. 32	2.5 psi
	Time of arrival = $3\ t_L$	78 ms
	End of reflected pulse = $3\ t_L + t_{of}$	134 ms

Symbol	Description	Value
	Side Wall Design Loading Diagram (see Fig. A-4)	
	(Span parallel to shock front; center 10 ft from front wall; span length L = 4 ft)	
	Initial Loadings	
P_s(ext)	Exterior peak pressure at center of span, including distance correction $= [1 + (10/340)]^{-1.5} P_{so} = 0.96\ P_{so}$	3.8 psi
P_s(int)	Interior peak pressure at center of span $= P_{sp}$	2.1 psi
t_f	Time of shock arrival at leading edge of span $= 8/U$	6.7 ms
t_d	Time to pressure maximum $= 12/U$	10.0 ms
$t_f + (t_d/2)$	Time of shock arrival at span center $= 10/U$	8.3 ms
t_s	Time to end of initial pulse $= t_f + (t_d/2) + t_{of}$	64.3 ms
	Reflected Loadings (all outward)	
	First pressure peak (reflected from rear wall) at center of span, including reduction due to side wall opening $= [1 - 18/153]\, P_{sp} = (0.88)(2.1)$	1.9 psi
	Second pressure peak (reflected from front wall) at center of span, including reduction for reflection from front wall $= [1 - (18/153)][1 - (42/153)]\, P_{so} = (0.88)(0.73)(2.1)$	1.3 psi
	Time of arrival of first peak $= 50/U$	43 ms
	Time of arrival of second peak $= 70/U$	61 ms
	End of reflected pulse $= 70/U + t_{of}$	117 ms

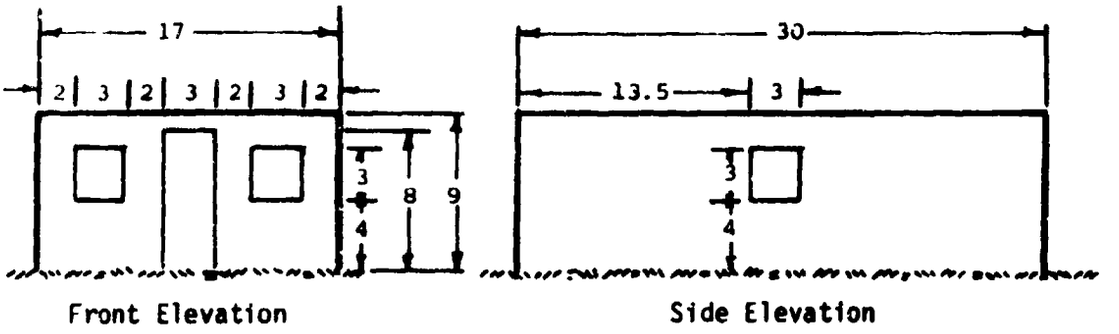

Fig. A-1. Structure Used in Example No. 1. All dimensions are in ft.

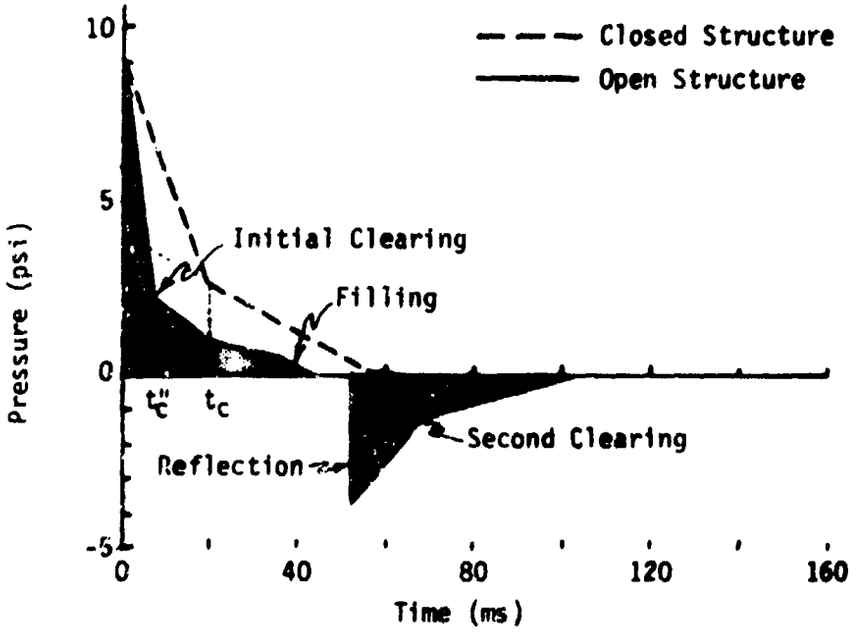

Fig. A-2. Front Wall: Net Loadings for Closed and Open Structure Shown in Fig. A-1.

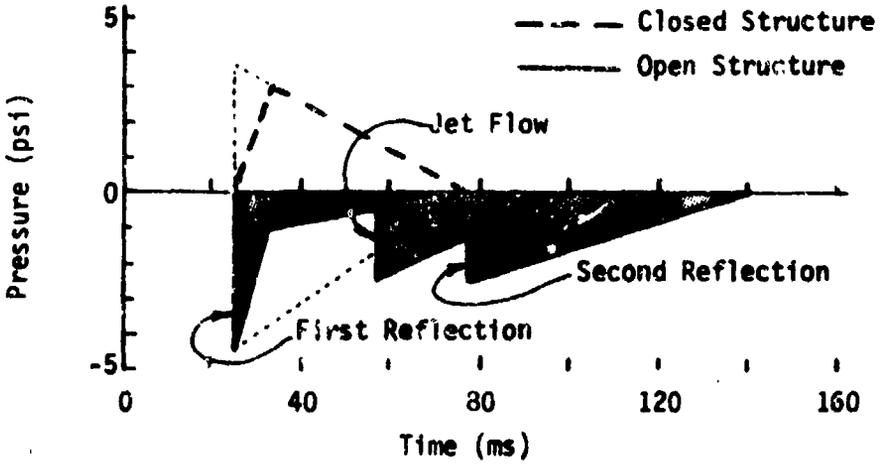

Fig. A-3. Rear Wall: Net Loadings for Closed and Open Structure Shown in Fig. A-1.

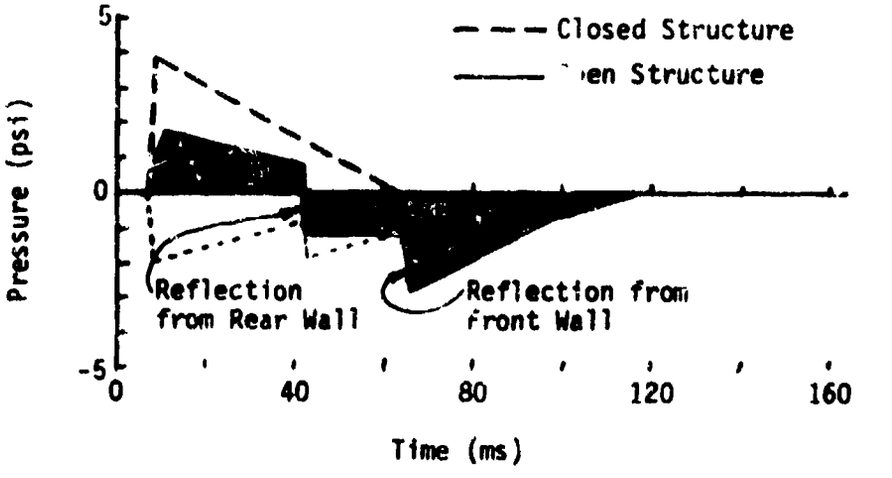

Fig. A-4. Side Wall: Net Loadings for Closed and Open Structure Shown in Fig. A-1.

COMMENTARY

While the example was designed—and calculations carried out—specifically to illustrate many of the concepts discussed in the report, it does serve to illustrate the potential importance of openings in structures on design loadings. Specifically—even without considering jet flow effects, and reflections—front wall and side wall loading impulses were reduced by more than half, and rear wall loadings were reversed in direction. When jet and reflection effects are considered, outward-directed front face impulses are virtually equal to inward-directed initial impulses, and in cases of rear and side walls, they are greater than initial impulses. Similar effects can be expected in most buildings with large openings where the principle of "net loadings" applies (that is, where the exterior and interior faces of a single wall are loaded by the same shock wave).

Some comments on individual calculations follow

1) Front Wall, Filling. Although fill times were calculated, the filling time occurred so late in the pulse (46 ms) that the reduction of net front face loadings to zero could have been ignored. This will generally be true unless openings occupy a very large percent of wall area (A_r is 27% in the example) or unless design explosions are very large (10,000 lb in the example).

2) Rear Wall, Jet . An abrupt increase in force is shown though the increase will actually be more gradual. Nominal jet loading duration is used to determine slope of jet loading curve. Note that jet forces were actually smaller than shock wave forces, but they occurred much later.

3) Rear Wall, Second Reflection. These pressures were not added to jet pressures though they could well have been. Interactions between jet and reflected waves is an extremely complex process (see Fig. 22). Reductions were made in the reflected pulse because of interactions with side window and front wall openings (11% and 19% respectively). For simplicity, both could have been ignored.

4) Side Wall, Both Reflections. Reflected pressures were added to shock wave pressures already present at the various times.

5) Exterior Loadings Only. Since only net loadings were required, these loadings (associated with clearing distance S', and described in detail in Section II-2) are not shown in Fig. A-2 through A-4. They must be considered, however, when an opening does not permit pressures to be applied to the interior face of a wall, as when a doorway leads to a corridor instead of directly to a room.

EXAMPLE 2
ACCELERATION OF OBJECTS IN JET FLOW

TO BE DERIVED: Change in Velocity of Objects

INPUT CONDITIONS

Structural

Opening: Small window, 2 ft high x 3 ft wide

Objects: are subject to core flow

Explosive

Weight of Explosive: W = 7,000 lb

Distance to Structure: d = 270 ft

DERIVED QUANTITIES

Symbol	Description	Value
A_o	Area of opening	6 ft^2
b_o	Width of opening = $(4A_o/\pi)^{1/2}$	2.76 ft
$d/W^{1/3}$	Scaled distance	14.1 $ft/lb^{1/3}$
P_s	Peak incident pressure, from Fig. 3	5.0 psi
$t_o/W^{1/3}$	Scaled duration, from Fig. 3	2.8 $ms/lb^{1/3}$
t_o	Duration	53.6 ms
t_j	Jet clearing time, from Eq 18 (= $4\,b_o/c$)	9.8 ms
t_j/t_o	Relative clearing time	0.18
P_j/P_s	Relative pressure at time t_j, from Fig. 33	0.69
P_j	Pressure at time t_j	3.45 psi
q_j	Jet dynamic pressure, from Fig. 32	3.3 psi
Δv (general)	Change in velocity, from Eq 35	8.3 C_A ft/sec
Δv man crouching	From Table 5	4.6-5.6 ft/sec
Δv concrete block	"	7 ft/sec
Δv ½-in. steel sphere	"	9.3 ft/sec
Δv 10-g stone	"	40 ft/sec
Δv 10-g window glass	"	90-200 ft/sec

EXAMPLE 3
FILLING OF SMALL CHAMBER *

TO BE DERIVED: Filling Pressure in Chamber

INPUT CONDITIONS

Structural

Plenum Chamber is 2 ft x 2 ft x 3 ft

Vent Diameter is 8 in. = b_o

Vent Location is in center of 2 ft x 3 ft side

Explosive

Weight of Explosive: W = 3,000 lb

Incident Pressure: P_s = 5 psi

DERIVED QUANTITIES

Symbol	Description	Value
$i_s/W^{1/3}$	Scaled impulse, from Fig. 3 with P_s = 5 psi	6 psi-ms/lb$^{1/3}$
$t_{of}/W^{1/3}$	Scaled fictitious pulse duration	2.4 ms/lb$^{1/3}$
t_{of}	Fictitious pulse duration	34.6 ms
V	Volume of chamber	12 ft^3
A	Area of vent	0.35 ft^2
t_f	Filling time = V/2 A	17.1 ms
t_f/t_{of}	Relative filling time	0.49
P_f/P_s	Relative filling pressure = $[1 - (t_f/t_{of})]$	0.51
P_f	Fill pressure	2.5 psi

* Chamber must be designed to withstand jet forces.

EXAMPLE 4

FORCES ON DUCTWORK BEHIND A VENT (High Pressure)

TO BE DERIVED: Forces and Impulse Due to Jet

INPUT CONDITIONS

Structural

Structure is equipped with a 16-in. diameter vent on roof. All covering equipment has been carried away by blast.

Vent leads to an initial portion of a duct 33 in. high and 18 in. wide. Duct runs parallel to roof.

Explosive

Weight of Explosive: W = 3,500 lb

Distance to Structure: d = 110 ft

DERIVED QUANTITIES

Symbol	Description	Value
$d/W^{1/3}$	Scaled distance	7.2 $ft/lb^{1/3}$
P_s	Peak incident pressure, from Fig. 3	18 psi
$i_s/W^{1/3}$	Scaled impulse, from Fig. 3	10.8 $psi\text{-}ms/lb^{1/3}$
t_{of}	Duration of fictitious pulse = $(2\,i_s/P_s)$	18.2 ms
b_o	Diameter of vent	16 in.
t_j	Jet clearing time = $4\,b_o/c$	4.7 sec
t_j/t_{of}	Relative jet clearing time	0.26
P_j/P_s	Relative pressure at time t_j = $[1-(t_j/t_{of})]$	0.74
P_j	Pressure at time t_j	13.3 psi
q_j	Jet dynamic pressure at time t_j, from Fig. 32	10.5 psi
A_o	Area of opening = $(\pi b_o^2/4)$	12.6 $in.^2$
F_j	Force on duct at time t_j = $2A_oq_j$	264 lb
I	Impulse on duct due to jet = $A_oq_j(t_{of}-t_j)$*	1,782 lb-ms

* Triangular pulse used rather than modified exponential of Eq 42.

EXAMPLE 5

FORCES BEHIND SMALL OPENINGS (Very High Pressures)

TO BE DERIVED: Maximum force and impulse on ducts located inside structure, 3 ft from vents

INPUT CONDITIONS

Structural

Control structure is equipped with 8-in. square uncovered vents in wall furthest from test cell

Explosive

Explosive Weight: W = 5,000 lb

Distance to Wall with vents: d = 80 ft

DERIVED QUANTITIES

Symbol	Description	Value
$d/W^{1/3}$	Scaled distance	4.7 ft/lb$^{1/3}$
P_{so}	Peak incident pressure, from Fig. 3	48 psi
$i_s/W^{1/3}$	Scaled impulse, from Fig. 3	16 psi-ms/lb$^{1/3}$
$t_{of}/W^{1/3}$	Scaled fictitious duration = $2(i_s/W^{1/3})/P$	0.67 ms/lb$^{1/3}$
t_{of}	Fictitious duration	11.4 ms
A_o	Area of opening	64 in.^{2}
b_o	Characteristic dimension of vent = $(4A_o/\pi)^{1/2}$	9.0 in.
t_j	Jet clearing time = $4b_o/c$	2.7 ms
t_j/t_{of}	Relative jet clearing time	0.23
P_j/P_{so}	Relative pressure at time t_j = $[1 - (t_j/t_{of})]$	0.77
P_j	Pressure at time t_j	36.8 psi
q_j	Dynamic pressure in jet at time t_j, (Fig. 32)	18 psi
q_{cr} *	Dynamic pressure in jet at critical pressure P_{cr} = 13.1	11 psi
t_{cr}	Time at which P_{cr} = 13.1 = $\left[1 - (P_{cr}/P_{so})\right] t_{of}$	8.3 ms

* Initial jet flow is choked. Unchoked flow begins when $P < P_{cr}$ = 13.1 psi

Symbol	Description	Value
F_j	Force on flat surface at time $t_j = 2A_oq_j$	2,304 lb
F_{cr}	Force on flat surface at time $t_{cr} = 2A_oq_{cr}$	1,408 lb
t_{ch}	Time of choked jet flow = $t_{cr} - t_j$ = 8.3 - 2.7 =	5.6 ms
t_u	Time of unchoked jet flow = $t_{of} - t_{cr}$ = 11.4 - 8.3 =	3.1 ms
I	Impulse from jet, sum of: choked (2304 - 1408)(5.6/2) + (1408)(5.6) = 10394 unchoked (1408)(3.1/2) = 2182	12,576 lb-ms
d_i	Diameter of area over which impulse is applied = 0.22 x 36	16 in.
I_{av}	Average impulsive pressure over $(\pi d_i)^2$	15.6 psi-ms

TABLE OF EQUIVALENTS

ft	m
1	.305
2	.610
2.76	.84
2.9	.88
3	.91
4	1.22
4.5	1.37
4.7	1.43
5	1.52
5.1	1.55
5.2	1.58
5.6	1.71
6	1.83
6.2	1.89
7	2.13
7 3	2.22
8	2.44
8.5	2.59
9	2.74
10	3.05
12	3.66
13.5	4.11
14.5	4.42
15	4.57
17	5.18
18.8	5.73
30	9.14
100	30.5
270	82.3
340	103.6

in	m
.5	.0127
.625	.0159
1	.0254
1.245	.0316
1.25	.0317
1.45	.0368
2	.051
2.54	.065
3.2	.081
3.49	.089
3.92	.010
4	.102
6	.152
8	.203
9	.229
12	.305
15	.381
16	.406
17	.432
21	.533
28.5	.724
30	.762
33	.838
38	.965
42.25	1.07
42.375	1.08
44	1.12
45	1.14
46	1.17
46.25	1.17
46.75	1.18
48.75	1.24
49	1.24
51	1.30
67.375	1.7
83.5	2.1
84.75	2.2
95.75	2.4
96.75	2.5

psi	kPa
.29	2.0
.3	2.1
.39	2.7
.50	3.45
.57	3.9
.58	4.0
.60	4.1
.74	5.1
.9	6.2
.95	6.6
1	6.9
1.1	7.6
1.2	8.3
1.3	9.0
1.4	9.6
1.5	10.3
1.6	11.0
1.8	12.4
1.9	13.1
2	13.8
2.1	14.5
2.2	15.2
2.4	16.5
2.5	17.2
2.55	17.6
2.56	17.7
2.6	17.9
2.7	18.6
2.8	19.3
2.9	20.0
2.99	20.6
3	20.7
3.1	21.4
3.2	22.1
3.3	22.8
3.45	23.8
3.5	24.1
3.6	24.8
3.8	26.2
3.9	26.9
4	27.6
4.1	28.3

psi	kPa
4.2	29.0
4.4	30.3
4.5	31.0
4.6	31.7
4.7	32.4
5	34.5
5.1	35.2
5.2	35.9
5.3	36.5
5.38	37.1
5.5	37.9
5.54	38.2
5.6	28.6
5.7	39.3
6	41.4
6.06	41.8
6.1	42.0
6.4	44.1
7	48.3
7.3	50.3
8	55.2
9	62.0
10	68.9
10.5	72.4
10.7	73.8
11	75.8
13.1	90.3
13.13	90.5
13.3	91.7
15	103.4
18	124
20	137.9
26	179.3
27.38	188.8
27.83	191.9
36.8	253.7
43	296.5
48	331
50	345

lb	kg
2	.91
4	1.8
16	7.3
72	32.6
100	45.4
168	76.2
200	90.8
264	119.7
700	317.5
850	385.6
1000	453.6
1408	639
1700	771
2304	1045
3000	1361
10,000	4536

$ft^2/slug$	m^2/kg
.2	.00127
.203	.0013
.5	.0032
.6	.0038
.676	.0043
.75	.0048
.85	.0054
.966	.0062
1.12	.0071
1.67	.0106
2.24	.0143
3.36	.0214
4.83	.0308
10.3	.0657
10.9	.0695

ft/sec	m/sec
4.6	.14
5.6	1.7
7	2.1
8.3	2.5
9.3	2.8
40	12.2
90	27.4
200	61.0
230	70.1
520	158.5
720	219.4
1000	304.8

ft^2	m^2
.35	.033
6	.56
42	3.9
153	14.2

ton	kg
100	90,718
500	453,592

$slug/ft^3$	kg/m^3
.0025	1.29

$lb^{1/3}$	$kg^{1/3}$
16	12.3
21.54	16.6

in/ms	m/ms
13.6	.345

in^2	m^2
12.6	.008
64	.041

ft/ms	m/ms
1.13	.344

ft^3	m^3
12	.34
800	22.7

lb-ms	kg-ms
1782	808
12,576	5704

$\frac{psi\text{-}ms}{lb^{1/3}}$	$\frac{kPa\text{-}ms}{kg^{1/3}}$
5.2	46.6
6	53.8
10.8	96.8
16	143.4

psi-ms	kPa-ms
15.6	107.5
112	772.2

$ft/lb^{1/3}$	$m/kg^{1/3}$
4.7	1.87
7.2	2.86
14.1	5.60

$ms/lb^{1/3}$	$ms/kg^{1/3}$
.67	.87
2.4	3.1
2.8	3.6
3	3.9

DISTRIBUTION LIST

Commander
U.S. Army Armament Research & Development Command
ATTN: DRDAR-CG
DRDAR-LCM-E
DRDAR-LCM-S (25)
DRDAR-SF
DRDAR-TSS (5)
Dover, NJ 07801

Chairman
Dept of Defense Explosives Safety Board (2)
Room 856C, Hoffman Building I
2461 Eisenhower Ave
Alexandria, VA 22331

Administrator
Defense Documentation Center
ATTN: Accessions Division (12)
Cameron Station
Alexandria, VA 22314

Commander
Department of the Army
Office, Chief, Research, Development & Acquisition
ATTN: DAMA-CSM-P
Washington, DC 20310

Office, Chief of Engineers
ATTN: DAEN-MCZ
Washington, DC 20314

Commander
U.S. Army Materiel Development & Readiness Command
ATTN: DRCSF
DRCDE
DRCIS
DRCMT
DRCRP
5001 Eisenhower Avenue
Alexandria, VA 22333

Commander
DARCOM Installations & Services Agency
ATTN: DRCIS-RI
Rock Island, IL 61299

Director
Industrial Base Engineering Activity
ATTN: DRXIB-MT & EN
Rock Island, IL 61299

Commander
U.S. Army Materiel Development & Readiness Command
ATTN: DRCPM-PBM
DRCPM-PBM-T
DRCPM-PBM-L (2)
DRCPM-PBM-E (2)
DRCPM-PBM-LN-CE
Dover, NJ 07801

Commander
U.S. Army Armament Materiel Readiness Command
ATTN: DRSAR-SF (3)
DRSAR-SC
DRSAR-EN
DRSAR-LEP-L
DRSAR-IRC
DRSAR-RD
DRSAR-IS
DRSAR-ASF
Rock Island, IL 61299

Director
DARCOM Field Safety Activity
ATTN: DRXOS-ES (2)
Charlestown, IN 47111

Commander
Volunteer Army Ammunition Plant
Chattanooga, TN 37401

Commander
Kansas Army Ammunition Plant
Parsons, KS 67357

Commander
Newport Army Ammunition Plant
Newport, IN 47966

Commander
Badger Army Ammunition Plant
Baraboo, WI 53913

Commander
Indiana Army Ammunition Plant
Charlestown, IN 47111

Commander
Holston Army Ammunition Plant
Kingsport, TN 37660

Commander
Lone Star Army Ammunition Plant
Texarkana, TX 75501

Commander
Milan Army Ammunition Plant
Milan, TN 38358

Commander
Iowa Army Ammunition Plant
Middletown, IA 52638

Commander
Joliet Army Ammunition Plant
Joliet, IL 60436

Commander
Longhorn Army Ammunition Plant
Marshall, TX 75760

Commander
Louisiana Army Ammunition Plant
Shreveport, LA 71130

Commander
Ravenna Army Ammunition Plant
Ravenna, OH 44266

Commander
Newport Army Ammunition Plant
Newport, IN 47966

Commander
Radford Army Ammunition Plant
Radford, VA 24141

Division Engineer
U.S. Army Engineer Division, Huntsville
ATTN: HNDCD
P.O. Box 1600, West Station
Huntsville, AL 35809

Division Engineer
U.S. Army Engineer Division, Southwestern
ATTN: SWDCD
1200 Main Street
Dallas, TX 75202

Division Engineer
U.S. Army Engineer Division, Missouri River
ATTN: MRDCD
P.O. Box 103 Downtown Station
Omaha, NE 68101

Division Engineer
U.S. Army Engineer Division, North Atlantic
ATTN: NADCD
90 Church Street
New York, NY 10007

Division Engineer
U.S. Army Engineer Division, South Atlantic
30 Pryor Street, S.W.
Atlanta, GA 30303

District Engineer
U.S. Army Engineer District, Norfolk
803 Front Street
Norfolk, VA 23510

District Engineer
U.S. Army Engineer District, Baltimore
P.O. Box 1715
Baltimore, MD 21203

District Engineer
U.S. Army Engineer District, Omaha
215 N. 17th Street
Omaha, NE 68102

District Engineer
U.S. Army Engineer District, Philadelphia
Custom House
2nd & Chestnut Street
Philadelphia, PA 19106

District Engineer
U.S. Army Engineer District, Fort Worth
P.O. Box 17300
Fort Worth, TX 76102

District Engineer
U.S. Army Engineer District, Kansas
601 E. 12th Street
Kansas City, MO 64106

District Engineer
U.S. Army Engineer District, Sacramento
650 Capitol Mall
Sacramento, CA 95814

District Engineer
U.S. Army Engineer District, Mobile
P.O. Box 2288
Mobile, AL 36628

Commander
U.S. Army Construction Engr Research Laboratory
Champaign, IL 61820

Commander
Dugway Proving Ground
ATTN: STEDP-MT-DA-HD (2)
Dugway, UT 84022

Civil Engineering Laboratory
Naval Construction Battalion Center
ATTN: L51
Port Hueneme, CA 93043

Commander
Naval Facilities Engineering Command
(Code 04, J. Tyrell)
200 Stovall Street
Alexandria, VA 22322

Commander
Atlantic Division
Naval Facilities Engineering Command
Norfolk, VA 23511

Commander
Chesapeake Division
Naval Facilities Engineering Command
Building 57
Washington Navy Yard
Washington, DC 20374

Commander
Northern Division
Naval Facilities Engineering Command
Building 77-L
U.S. Naval Base
Philadelphia, PA 19112

Commander
Southern Division
Naval Facilities Engineering Command
PO Box 10068
Charleston, SC 29411

Commander
Western Division
Naval Facilities Engineering Command
San Bruno, CA 94066

Commander
Naval Ammunition Depot
Naval Ammunition Production Engineering Center
Crane, IN 47522

Technical Library
ATTN: DRDAR-CLJ-L
Aberdeen Proving Ground, MD 21010

Technical Library
ATTN: DRDAR-TSB-S
Aberdeen Proving Ground, MD 21005

Benet Weapons Laboratory
Technical Library
ATTN: DRDAR-LCB-TL
Watervliet, NY 12189

Ammann & Whitney (10)
2 World Trade Center
New York, NY 10048

Scientific Service, Inc. (10)
1536 Maple Street
Redwood City, CA 94063

Weapon System Concept Team/CSL
ATTN: DRDAR-ACW
Aberdeen Proving Ground, MD 21010

Commander
U.S. Army Armament Materiel Readiness Command
ATTN: DRSAR-LEP-L
Rock Island, IL 61299

Director
U.S. Army TRADOC Systems Analysis Activity
ATTN: ATAA-SL (Tech Lib)
White Sands Missile Range, NM 88002

U.S. Army Materiel Systems Analysis Activity
ATTN: DRXSY-MP
Aberdeen Proving Ground, MD 21005